Università degli studi di Napoli
"Federico II"

Facoltà di Ingegneria

Doctorate Thesis in Electrical Engineering

Nonlinear Magnetization Dynamics in Thin-films and Nanoparticles

Massimiliano d'Aquino

Tutors:
Prof. Giovanni Miano
Prof. Claudio Serpico

December 2004

To my parents, Eduardo and Livia,
to my brother Mauro
and my love Marianna

Acknowledgments

It is a great pleasure to have the possibility to thank the people, to whom I will be forever grateful, who have introduced me to the study of magnetism.

First of all, I would like to thank very much my supervisor Claudio Serpico for his precious teachings, spreading from advanced mathematics to electromagnetism and micromagnetics, but, above all, for his strong support in every moment, fine or less fine, of my research activity in these three years. It has been always challenging, but also funny, working together. I hope that this is only the starting point of future collaborations in magnetics.

I am also very grateful to my supervisor Giovanni Miano, who always supported me with interesting scientific discussions about electromagnetism, thermodynamics, numerical models and many other remarkable subjects. Moreover, I would like to thank again both my supervisors for giving me the possibility to attend various conferences and workshops on magnetism.

Special thanks go to Giorgio Bertotti, from the Istituto Elettrotecnico Nazionale "Galileo Ferraris", and Isaak Mayergoyz, from University of Maryland, who gave me the possibility to join their working group and give my contribution to the investigation of dynamical magnetic phenomena.

I am grateful to Thomas Schrefl and Josef Fidler for the possibility to stay three months with their group in Vienna last year. It was a great time there, I learned many things about computational micromagnetics, but also I had the possibility to meet wonderful guys like Dieter Suess, Werner Scholz, Rok Dittrich, Markus Kirschner and Gino Hrkac, who I would like to thank for the scientific discussions, collaborations and the very pleasant evenings drinking beer, during conferences around the world.

Special thanks go to Ciro Visone and Daniele Davino, from Università del Sannio, for wonderful discussions and collaborations in the topic of magnetic hysteresis.

Last but not least, I would like to thank my doctorate colleagues Alessandro D'Elia, Daniela Proto, Rosario Schiano Lo Moriello and Walter Zamboni. During these three years, we really supported one another in every moment.

Finally, I would like to thank my institution, namely Dipartimento di Ingegneria Elettrica, University of Napoli, and I would like to acknowledge the financial support of the Italian MIUR-FIRB (contract No. RBAU01B2T8).

Contents

Introduction

The study of magnetization processes in magnetic materials has been in the last fifty years the focus of considerable research for its application to magnetic recording technology. In fact, the design of nowadays widespread magnetic storage devices, such as the hard-disks which are within computers on our desktops, requires the knowledge of the "microscopic" phenomena occurring within magnetic media. In this respect, it is known that some materials, referred to as *ferromagnetic materials*, present spontaneous magnetization at room temperature, which is the result of "spontaneous" alignment of the elementary magnetic moments that constitute the medium. Roughly speaking, from a phenomenological point of view, one has a medium whose magnetization state can be changed by means of appropriate external magnetic fields. The magnetic recording technology exploits the magnetization of ferromagnetic media to store information.

The first example of magnetic storage device was the magnetic core memory prototype, realized by IBM in 1952, and used in the IBM 405 Alphabetical Accounting Machine. The working principle of magnetic core memories is very simple. One can think about several cores placed at the nodal positions of an array-type structure made with horizontal and vertical wired lines, as sketched in Fig. 1. Each core is basically a bistable unit, capable of storing one bit (binary digit), which is the smallest piece of binary-coded information (can be let's say "0" or "1"). In Figure 1, on the right, it is illustrated the writing mechanism of the IBM 2361 Core Storage Module. Basically, the target magnetic core can be "switched", from 0 to 1 or viceversa, by addressing it with the horizontal and vertical current lines which pass through the core. The currents flowing in the addressing wires generate a magnetic field that can change the magnetic state of the core. Nevertheless, the magnetic field produced by the single current line is designed to be not sufficient to switch a core. Therefore, the only core that switches is the only one traversed by two currents, namely the one addressed by the horizontal and the vertical current lines. It turns out that a collection of magnetic cores can store a sequence of bits, namely can record a piece of information. After magnetic core memories, magnetic tapes (or, equivalently, floppy disks)

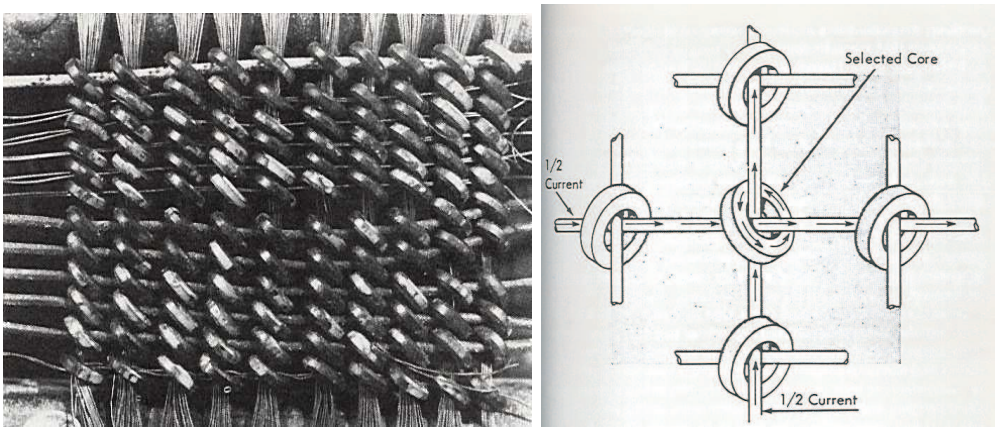

Figure 1: (left) The first magnetic core memory, from the IBM 405 Alphabetical Accounting Machine. The photo shows the single drive lines through the cores in the long direction and fifty turns in the short direction. The cores are 150 mm inside diameter, 240 mm outside, 45 mm high. This experimental system was tested successfully in April 1952. (right) Writing mechanism of magnetic cores memory.

have been used, but the most widespread magnetic storage device is certainly the *hard-disk*.

In this respect, it is evident from the photography in Fig. 1 that the first prototypes of magnetic storage devices had dimensions in the order of meters. The progress made by research activity performed worldwide in this subject has led to exponential decay of magnetic device dimensions. In fact, modern recording technology deals with magnetic media whose characteristic dimensions are in the order of microns and submultiples. It is sufficient to mention that commercial hard disks are capable of storing more that 100 Gbit (gigabit $\sim 10^9$ bits) per square inch!

Recently the possibility to realize magnetic random access memories (from now on MRAMs), similar in principle to magnetic core memories, has been investigated, but, at the moment no commercial realization of MRAMs is present on the market. However, both hard disks and MRAMs rely on flat pieces of magnetic materials having the shape of thin-films. Typically, the information, coded as bit sequences, is connected to the magnetic orientation of these films, which have dimensions in the order of microns and submultiples.

Let us now consider the simple scheme of principle of hard disk, depicted in Fig. 2. The recording medium is a flat magnetic material that is thin-film shaped. The read and write heads are separate in modern realizations, since they use different mechanisms. In fact, as far as the writing process is concerned, one can see that the writing head is constituted by a couple of polar expansions made of

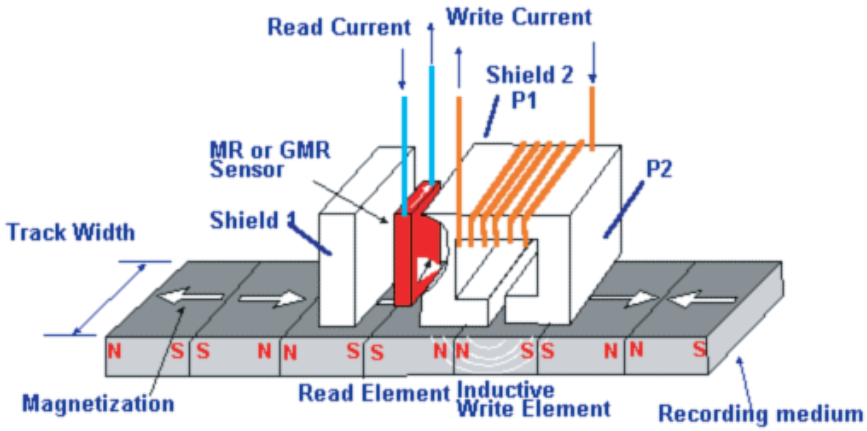

Figure 2: Simple representation of Read/Write magnetic recording device present in hard disks realizations.

soft materials, excited by the current flowing in the writing coil. The fringing field generated by the polar expansions is capable to change the magnetization state of the recording medium. Generally the recording medium is made with magnetic materials that have privileged magnetization directions. This means that the recording medium tends to be naturally magnetized either in one direction (let's say '1' direction) or in the opposite ('0' direction). In this sense, pieces of the material can behave like bistable elements. The bit-coded information can be therefore stored by magnetizing pieces of the recording medium along directions 0 or 1. The size of the magnetized bit is a critical design parameter for hard disks. In addition, for the actual data rates, magnetization dynamics cannot be neglected in the writing process.

The reading mechanism currently relies on a magnetic sensor, called *spin valve*, which exploits the *giant magneto-resistive* (GMR) effect. Basically, the spin valve is constituted by a multi-layers structure. Typically two layers are made with ferromagnetic material. One is called free layer since its magnetization can change freely. The other layer, called pinned layer, has fixed magnetization. If suitable electric current passes through the multi-layers, significant changes in the measured electric resistance can be observed depending on the mutual orientation of the magnetization in the free and pinned layer. Let us see how this can be applied to read data magnetically stored on the recording medium.

Basically, the spin valve is placed in the read head almost in contact with the recording medium [1]. Then, when the head moves over the recording medium, the magnetization orientation in the free layer is influenced by the magnetic field produced by magnetized bits on the recording medium. More specifically, when

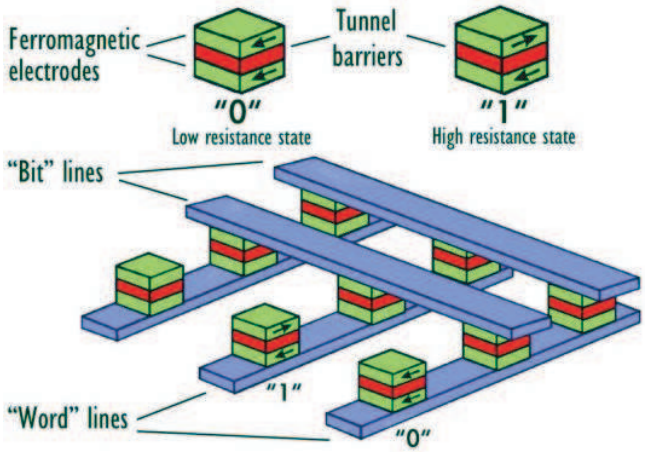

Figure 3: Typical array structure for magnetic random access memories (MRAMs).

magnetization in the free layer and magnetization in the pinned layer are parallel, the electrical resistance has the lowest value. Conversely, the antiparallel configuration of magnetization in the free layer and pinned layer yields the highest value of the resistance. Thus, by observing the variation in time of the electrical resistance (that is, the variation of the read current passing trough the multilayers) of the GMR head, the bit sequence stored on the recording medium can be recognized.

It is possible to say something also about MRAMs prototypes. The magnetic random access memories follow a working principle very similar to the older magnetic core memories. In fact, they present the same cell array structure as their predecessors, but each cell is constituted by a magnetic multi-layers structure rather than a magnetic core (see Fig. 3). The reading mechanism is based on GMR effect, whereas the writing process is conceptually analogous to the one seen for magnetic core memories. Thus, an MRAM cell can be switched by addressing it with the current lines (bit lines in Fig. 3). The switching is realized by means of the magnetic field pulse produced by the sum of horizontal and vertical current. This magnetic field pulse can be thought as applied in the film plane at 45° off the direction of the magnetization. In this situation, the magnetic torque, whose strength depends on the angle between field and magnetization, permits the switching of the cell. This behavior is simple in principle, but it is very hard to realize in practice on a nanometric scale. In fact, the array structure must be designed such that the magnetic field produced by only one current line cannot switch the cells. Conversely, the field produced by two currents must be

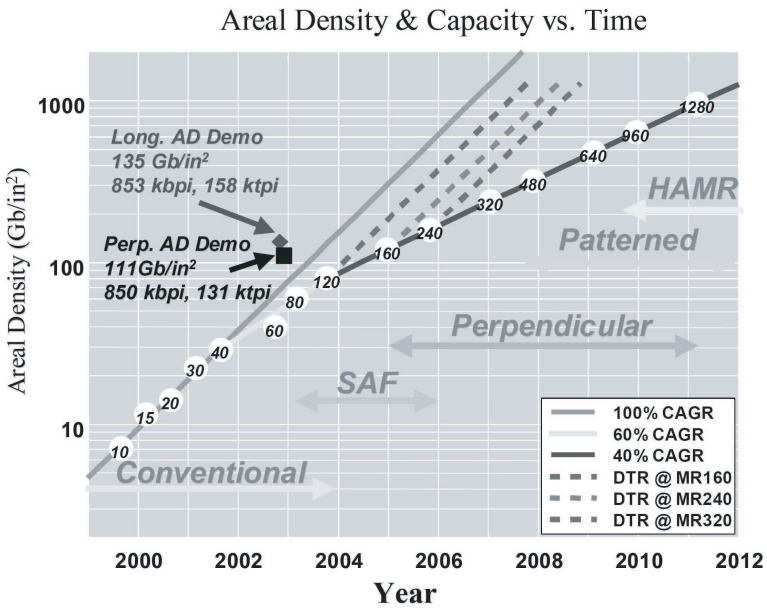

Figure 4: Magnetic Recording Disk Technology: Practical Challenges in Delivering the Areal Density Performance [2].

such that it switches only the target cell.

Recently, to circumvent the problems of switching MRAMs cells with magnetic field, the possibility of using spin-polarized currents, injected directly in the magnetic free layer with the purpose to switch its magnetization, has been investigated. In particular, this possibility has been first predicted by the theory developed by J. Slonczewski in 1996 (see Ref. [44]) and then observed experimentally [45, 46, 48]. The interaction between spin-polarized currents and the magnetization of the free layer is permitted by suitable quantum effects. From a "macroscopic" point of view, these effects produce a torque acting on the magnetization of the free layer. The resulting dynamics may indeed exhibit very complicated behaviors.

The above situations are only few examples of technological problems which require to be investigated by means of theoretical models. Now, referring to hard disk technology, at the present time the main challenges and issues can be summarized as follows:

1. Higher areal density.

2. Improved thermal stability of magnetized bits.

3. Increasing read/write speed in recording devices (< 1 ns)

The first two points are strongly connected, since the smaller is the size of the bit, the stronger are the thermal fluctuations which tend to destabilize the configuration of the "magnetized bit". For this reasons, as far as the bit size decreases, it has been recognized that the use of perpendicular media, constituted of grains in which the bit is magnetized in the direction normal to the film plane, leads to better thermal stability. In fact, by looking at Fig. 4, the future perspectives in hard disk design show that the use of perpendicular media, patterned media and heat-assisted magnetic recording technology will possibly yield [2] areal densities towards 1 Terabit/in^2 by the year 2011. Thus, being the spatial scale of magnetic media in the order of, more or less, hundred nanometers, magnetic phenomena has to be analyzed by theoretical models with appropriate resolution. This is the case of micromagnetics, which is a continuum theory that stands between quantum theory and macroscopic theories like mathematical hysteresis models (Preisach, etc.).

Moreover, as far as the read/write speed increases (frequencies in the order of GHz and more), dynamic effects cannot be neglected. Therefore, as a result, the design of modern ultra-fast magnetic recording devices cannot be done out of the framework of magnetization dynamics. This is the motivation for the research activity that will be illustrated in the following chapters.

In chapter 1 the micromagnetic model and the Landau-Lifshitz-Gilbert (LLG) equation will be introduced to describe magnetization phenomena in ferromagnetic bodies. First, an approach in terms of the free energy associated with the magnetic body will be presented to derive the static equilibrium conditions for magnetization vector field. Then, the dynamic effects due to the gyromagnetic precession will be introduced. Both Landau-Lifshitz and Landau-Lifshitz-Gilbert equation will be presented. Phenomenological Gilbert damping will be analyzed in terms of Rayleigh dissipation function.

In chapter 2 the study of magnetization dynamics in uniformly magnetized particles will be addressed. In particular, first the static Stoner-Wohlfarth model and then magnetization switching processes will be analyzed. In addition, novel analytical techniques to study magnetization dynamics under circularly polarized external fields and magnetization dynamics driven by spin-polarized currents will be introduced and deeply discussed. In this respect, it will be shown how some behaviors indeed observed in experiments, can be explained in terms of bifurcations of fixed points and limit cycles of the LLG dynamical system.

As a further step, in chapter 3, the assumption of magnetization spatial uniformity will be removed and the problem of studying thin-films reversal processes

of technological interest will be addressed. In this respect, as preliminary step, the issue of the computation of magnetostatic fields, which is still the bottleneck of micromagnetic simulations, will be illustrated together with the mostly used methods at this time. Then, a comparison of damping and precessional switching processes in thin-films will be performed, showing that fast precessional switching can be considered spatially quasi-uniform and, therefore, its crucial aspects can be analyzed by means of uniform mode theory discussed in chapter 2. Finally, a uniform mode analysis will be applied to the fast switching of granular tilted media which represents one of the most promising solutions for high density magnetic storage in future hard disks.

In chapter 4, the problem of the geometrical numerical integration of LLG equation will be considered. In particular, mid-point rule time-stepping will be applied to the LLG equation. In fact, it will be shown that the fundamental properties of magnetization dynamics, embedded in the continuous model, are reproduced by the mid-point discretized LLG equation regardless of the time step. In addition, since the resulting numerical scheme is implicit, special and reasonably fast quasi-Newton technique will be developed to solve the nonlinear system of equations arising at each time step. The proposed mid-point technique will be validated on the micromagnetic standard problem no. 4 which concerns with thin-films reversal processes. Finally, discussion on numerical results and computational cost will be performed.

In the end, some conclusions about the results obtained and the possible future work will be drawn.

Chapter 1

The Micromagnetic Model and The Dynamic Equation

In this chapter a brief overview of the micromagnetic model [3, 4] is presented. The discussion starts with the introduction of the different interactions that occur within ferromagnetic bodies at different spatial scales. The expressions of the energies related to each analyzed interaction are reported. As second step, the *Brown's equations* are derived by imposing micromagnetic equilibrium as a 'stationary point' of the free energy functional. As a further step, the semi-classical dynamic model for damped gyromagnetic precession, described by the *Landau-Lifshitz* and *Landau-Lifshitz-Gilbert* equations [3, 18], is introduced on the basis of physical considerations on spin magnetic momentum of electrons and the well-known relationship with angular momentum through the *gyromagnetic ratio*. The dimensionless form of the free energy and Landau-Lifshitz-Gilbert equation is presented. The fundamental properties of magnetization dynamics, magnetization magnitude conservation and energy balance, are derived. General introduction of the phenomenological Gilbert damping is also explained.

1.1 Micromagnetic Free Energy

In this section we introduce a continuum model, in terms of magnetic polarization per unit volume, and characterize the state of a generic ferromagnetic body by means of its free energy.

1.1.1 Continuum Hypothesis

Let us consider a region Ω occupied by a magnetic body. Let us now focus on a 'small' region $dV_{\mathbf{r}}$ within the body, denoted by the position vector $\mathbf{r} \in \Omega$. The word 'small' here indicates that the volume $dV_{\mathbf{r}}$ is large enough to contain a huge number N of elementary magnetic moments $\boldsymbol{\mu}_j$, $j = 1, \ldots, N$, but small enough in order that the average magnetic moment varies smoothly. In this respect,

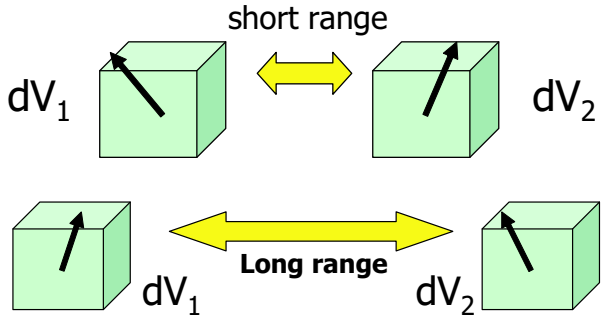

Figure 1.1: Different kinds of magnetic interactions depending on the distance between dipoles.

we define the magnetization vector field $\mathbf{M}(\mathbf{r})$, such that the product $\mathbf{M}(\mathbf{r})\, dV_{\mathbf{r}}$ represent the net magnetic moment of the elementary volume $dV_{\mathbf{r}}$:

$$\mathbf{M}(\mathbf{r}) = \frac{\sum_j^N \boldsymbol{\mu}_j}{dV_{\mathbf{r}}} \quad . \tag{1.1}$$

Moreover, we assume that the magnetization is also a function of time t:

$$\mathbf{M} = \mathbf{M}(\mathbf{r}, t) \quad . \tag{1.2}$$

First of all, it is important to recall that the micromagnetic model [3, 4, 5] is interested in magnetic phenomena which arise in a wide spatial scale, going from few nanometers (nm) to few microns (μm). The micromagnetic framework includes short and long-range (maxwellian) interactions between magnetic moments. In this respect, we shall start the discussion from the short-range exchange and anisotropy interactions introduced with phenomenological approach. Finally, we will introduce the long-range magnetostatic interactions due to 'maxwellian' magnetic fields. All the these interactions can be described in terms of the *free energy* of the body. In the next section a brief overview of basic thermodynamic laws and definitions is reported before each contribution to the micromagnetic free energy is analyzed in some details.

1.1.2 BASIC THERMODYNAMICS FOR MAGNETIZED MEDIA. THERMODYNAMIC POTENTIALS

We consider now a small volume dV of magnetic material which is subject to an external magnetic field $\mathbf{H}_{\mathrm{a}}$ and is in contact with a thermal bath at constant temperature T. We introduce the quantity $\mathcal{M} = \mathbf{M}dV$ such that $\mu_0\mathcal{M}$ is the net magnetic moment present in the volume dV. We assume that no volume changes due to thermal expansion and magnetostriction occur. The First Law

of thermodynamics states that for any transformation between two equilibrium states A and B, it happens that:

$$\Delta U = U_B - U_A = \Delta L + \Delta Q \quad , \tag{1.3}$$

where ΔU is the variation of the *internal energy* U, ΔL is the work performed on the system and ΔQ is the heat absorbed by the system. The magnetic work, under constant external magnetic field $\mathbf{H}_\mathrm{a}$, has the following form:

$$\Delta L = \mu_0 \mathbf{H}_\mathrm{a} \cdot \Delta \mathcal{M} \quad . \tag{1.4}$$

The Second Law of thermodynamics for isolated systems states that, for any transformation between equilibrium states A and B, the following inequality is satisfied [7]:

$$\Delta S = S_B - S_A \geq 0 \quad , \tag{1.5}$$

where S is the *entropy*. In Eq. (1.5) the equal sign holds in case of reversible transformations. In this respect, reversible transformations occur when the system passes through a sequence of thermodynamic equilibrium states. The second law (1.5) has to be interpreted as follows. Referring to our magnetic body, let us imagine that it is prepared in a certain initial state A by using appropriate constraints which allow to keep fixed, for instance, the magnetic moment of the body. Then, the constraints are partially or totally removed and the system is left isolated (no work, no heat is exchanged with the system). In this situation, the system relaxes toward a new equilibrium state B, and therefore the magnetic moment approaches a new value too. The remarkable fact is that the new equilibrium state B will be necessarily characterized by a value of the entropy S_B greater than S_A.

The Second Law of thermodynamics can be also written for non-isolated systems in the following way [7]:

$$\Delta S \geq \frac{\Delta Q}{T} \quad . \tag{1.6}$$

where the equal sign still holds in case of reversible transformations. Moreover, to study transformations occurring at constant temperature, appropriate thermodynamic potentials can be introduced. For instance, the *Helmholtz free energy* $F(\mathcal{M}, T)$ can be defined by means of suitable Legendre transformation [6]:

$$F = \min_S [U - TS] \quad . \tag{1.7}$$

The inequality (1.6) leads to suitable inequality involving the Helmholtz free energy F. In fact, for constant temperature, the variation of F between two

equilibrium states A and B can be written as:

$$\Delta F = \Delta U - T\,\Delta S \quad . \tag{1.8}$$

Now, by taking into account that $T\Delta S \geq \Delta Q$, according to the second law (1.6), and the first law (1.3), one obtains:

$$\Delta F \leq \Delta L \quad . \tag{1.9}$$

where the equal sign holds for reversible transformations. In addition, if no work is done on the system, the latter equation becomes

$$\Delta F = F_B - F_A \leq 0 \quad , \tag{1.10}$$

meaning that, if the system is prepared in a certain equilibrium state with certain constraints, the removal of constraints implies that the Helmholtz free energy has to decrease towards a minimum.

Another thermodynamic potential is the *Gibbs free energy* $G(\mathbf{H}_\mathrm{a}, T)$, which, for constant temperature and constant external field $\mathbf{H}_\mathrm{a}$ can be written as [6]:

$$G = \min_{\mathcal{M}}[F - \mu_0 \mathcal{M} \cdot \mathbf{H}_\mathrm{a}] \quad . \tag{1.11}$$

By following very similar line of reasoning to the one done for the Helmholtz free energy, one can easily derive that, for constant external field and temperature, the transformation between equilibria A and B, induced by the removal of the constraints, satisfies the following inequality:

$$\Delta G = G_B - G_A \leq 0 \quad , \tag{1.12}$$

meaning that also the Gibbs free energy has to decrease towards a minimum. The Gibbs free energy is very useful as far as experiments are considered where one can somehow control the external field, since it is instead very difficult controlling the magnetic moment $\mu_0\mathcal{M}$.

In addition, for reversible transformations at constant temperature, one can easily derive that:

$$dF = \delta L = \mu_0 \mathbf{H}_\mathrm{a} \cdot \delta\mathcal{M} \quad , \tag{1.13}$$

$$dG = -\mu_0 \mathcal{M} \cdot d\mathbf{H}_\mathrm{a} \quad . \tag{1.14}$$

This leads to the following relationship holding for equilibrium states:

$$\frac{1}{\mu_0}\left[\frac{\partial F}{\partial \mathcal{M}}\right]_T = \mathbf{H}_\mathrm{a} \quad , \quad \left[\frac{\partial G}{\partial \mathbf{H}_\mathrm{a}}\right]_T = -\mu_0 \mathcal{M} \quad . \tag{1.15}$$

We observe that the Gibbs free energy (1.11) depends by definition only on $(\mathbf{H}_\mathrm{a}, T)$. This means that the value of $\mathcal{M}$ has to be expressed through the equation of state:

$$\mathcal{M} = \mathcal{M}(\mathbf{H}_\mathrm{a}, T) \quad , \tag{1.16}$$

which is well-defined at thermodynamic equilibrium. In other words, at thermodynamic equilibrium, for given $(\mathbf{H}_\mathrm{a}, T)$, the state variable $\mathcal{M}$ is uniquely determined.

If we consider now the case of a ferromagnetic body, this property is not fulfilled anymore, that is, a given value of $(\mathbf{H}_\mathrm{a}, T)$, is not sufficient to determine uniquely the state variable $\mathcal{M}$. In fact, we deal with a system whose free energy has many local minima corresponding to *metastable equilibria* [20]. This framework is known as *non-equilibrium thermodynamics* and is not yet well-established from theoretical point of view. Nevertheless, many contributions in this sense have been developed. In this respect, the presence of many metastable state can be taken into account, as result of a deeper analysis in the framework of non-equilibrium thermodynamics, by the following generalized Gibbs[1] free energy

$$G(\mathbf{H}_\mathrm{a}, T, \mathcal{M}) = F(\mathcal{M}, T) - \mu_0 \mathbf{H}_\mathrm{a} \cdot \mathcal{M} \quad . \tag{1.17}$$

We observe that the free energy (1.17) coincides with the Gibbs free energy (1.11) at thermodynamic equilibrium. The explicit dependance on $\mathcal{M}$ expresses somehow the distance of the system from thermodynamic equilibrium when the state variable assumes the particular value $\mathcal{M}$, as if it were an external constraint. In this framework, one can determine the (metastable) equilibrium condition by imposing that the free energy (1.17) is stationary[2] with respect to $\mathcal{M}$:

$$\left[\frac{\partial G}{\partial \mathcal{M}}\right]_{\mathbf{H}_\mathrm{a}, T} = \left[\frac{\partial F}{\partial \mathcal{M}}\right]_{T} - \mu_0 \mathbf{H}_\mathrm{a} = 0 \quad . \tag{1.18}$$

In the latter equation, the first of Eqs. (1.15) has been used. It is important to underline that, from this analysis, one cannot say which metastable state the system will reach, given an initial state. The only way to determine this information is to introduce dynamics. Therefore, an appropriate dynamic equation must be considered to describe the evolution of the system.

The above considerations can be extended to the case of an inhomogeneous system, where the state variables and the thermodynamic potentials are also

[1] In Ref. [20] this free energy is called *Landau free energy* G_L to distinguish from the Gibbs free energy G. Here we perform an abuse of notation.

[2] It can be shown that metastable equilibria are minima of the free energy (1.17). In this sense the minimization of the free energy (1.17) generalizes the minimization of the Gibbs free energy that holds in equilibrium thermodynamics.

space-dependent functions, under the hypothesis that the body is in *local thermodynamic equilibrium*[3]. Therefore, the state functions can be well-defined within each elementary volume and thermodynamic relations which are valid for homogeneous bodies, can be written point-wise as balance equations. Moreover, the thermodynamic potentials become functionals of the state variables which, in turn, are space functions.

In the following sections we analyze the contributions to the free energy functional for ferromagnetic bodies. In this respect, the role of the state variable will be played by the magnetization vector field $\mathbf{M}$ and the equilibrium condition will be computed by imposing that the variational derivative of the free energy functional $G(\mathbf{M}, \mathbf{H}_\mathrm{a})$, with respect to $\mathbf{M}$, vanishes according to Eq. (1.18). Finally, in section 1.3 we shall introduce the appropriate dynamic equation which is necessary to describe the evolution of the system, as seen before.

1.1.3 EXCHANGE INTERACTION AND ENERGY

Now we will discuss the exchange interactions in ferromagnetic bodies. This interaction should be analyzed by means of quantum theory, since it strongly concerns with spin-spin interactions. More specifically, on a scale in the order of the atomic scale, the exchange interaction tends to align neighbor spins. In view of a continuum average analysis in terms of magnetization vector field, we expect that the exchange interactions tends to produce small uniformly magnetized regions, indeed observed experimentally and called *magnetic domains*. In this respect, the existence of domains [8] was postulated by Weiss in the early 1900s to explain the inverse temperature dependance of susceptibility for ferromagnetic materials investigated by Curie. This theory was partially validated by the work of Barkhausen (1915), in which the emergence of irreversible jumps in magnetization reversal was connected to the Weiss domains. Successively, experimental observations [9] based on Faraday and Kerr effect measurements, definitely stated the existence of magnetic domains. However, in 1931 Heisenberg [10] described ferromagnetic bodies in terms of exchange interactions, justifying the Weiss theory on molecular field. In the following sections a brief summary of paramagnetism and classical Weiss molecular field is presented before deriving the phenomenological expression of exchange free energy used in micromagnetics.

[3] although the whole body is not in equilibrium, one assumes that each elementary volume is in equilibrium

Paramagnetism

It is well known that most of the materials, subject to magnetic fields, exhibits either *diamagnetic* or *paramagnetic* behavior [5]. This reflects in a value of the magnetic permeability slightly different from the vacuum permeability μ_0. Conversely, few materials, like Fe, Ni, and Co behaves differently and are referred to as *ferromagnetic* materials. In the following, we will briefly explain the paramagnetism, since it is helpful for describing ferromagnetic materials.

Thus, let us consider a medium whose elementary particles possess magnetic moment. Let us suppose that no external field is applied, and that the body is in thermodynamic equilibrium. Due to the random orientation of the elementary magnets, the magnetization vector $\mathbf{M}$ is zero everywhere in the medium. When an external field $\mathbf{H}_\mathrm{a}$ is applied, an equilibrium between the tendency of dipoles to align with the field and the thermal agitation establishes. This produces the magnetization of the body in the same direction and orientation as the external field. If we call $\mathbf{m}_0$ the permanent magnetic moment of the generic dipole and θ the angle between $\mathbf{m}_0$ and $\mathbf{H}_\mathrm{a}$, the contribution dM to the total magnetic moment of the body, given by the single dipole, is the component of $\mathbf{m}_0$ along the field direction

$$dM = m_0 \cos\theta \quad . \tag{1.19}$$

Now we have to determine the distribution of the dipoles with respect to the angle θ and then to compute the average value of $m_0 \cos\theta$. To this end, we can use Boltzmann statistic which gives the probability $p(E)$ for a dipole to have suitable potential energy E as:

$$p = \exp\left(-\frac{E}{k_B T}\right) \quad , \tag{1.20}$$

where k_B is the Boltzmann constant and T is the temperature. The potential energy of a dipole subject to the field $\mathbf{H}_\mathrm{a}$ is:

$$E = -\mu_0 \mathbf{m}_0 \cdot \mathbf{H}_\mathrm{a} \quad . \tag{1.21}$$

If N is the number of dipoles per unit volume, the total magnetic moment M per unit volume can be expressed as the following statistical average:

$$\begin{aligned} M &= \int_{E_\mathrm{min}}^{E_\mathrm{max}} N m_0 \cos\theta \, p(E) \, dE = \\ &= \int_{E_\mathrm{min}}^{E_\mathrm{max}} N m_0 \cos\theta \, \exp\left(\frac{\mu_0 m_0 H_\mathrm{a} \cos\theta}{k_B T}\right) d(-\mu_0 m_0 H_\mathrm{a} \cos\theta) \quad . \end{aligned} \tag{1.22}$$

With the positions

$$x = \cos\theta \quad , \quad \beta = \frac{\mu_0 m_0 H_\mathrm{a}}{k_B T} \quad , \tag{1.23}$$

Eq. (1.22) becomes:

$$M = M_s \left(\coth \beta - \frac{1}{\beta} \right) = M_s \, \mathcal{L}(\beta) \quad , \tag{1.24}$$

where $M_s = N m_0$ is the saturation magnetization, corresponding to the case in which all the dipoles are aligned, and $\mathcal{L}(\beta)$ is the Langevin function. Generally, in experiments on paramagnetic substances, typical temperatures and fields are such that

$$\beta = \frac{\mu_0 m_0 H_\mathrm{a}}{k_B T} \ll 1 \quad . \tag{1.25}$$

Since the Langevin function can be developed in Taylor series

$$\mathcal{L}(\beta) = \frac{\beta}{3} + \mathcal{O}(\beta^2) \quad , \tag{1.26}$$

for small β we can take the first order expansion and rewrite Eq. (1.24) as

$$M = \frac{\mu_0 M_s m_0}{3 k_B T} H_\mathrm{a} = \chi H_\mathrm{a} \quad . \tag{1.27}$$

where the magnetic susceptibility χ is in the order of 10^{-4} for typical values of the parameters. One can clearly see that Eq. (1.27) explains the inverse dependance of the susceptibility on the temperature observed experimentally by Curie.

Ferromagnetism. Weiss molecular field

Some materials present very strong magnetization, typically in the order of the saturation magnetization, also in absence of external field, i.e. they present spontaneous magnetization. This kind of materials are referred to as *ferromagnetic materials* (Fe, Co, Ni, Gd, alloys, etc.). Typical properties of some ferromagnetic materials can be found in Appendix A. The behavior of very small regions of ferromagnetic materials can be treated by following the same line of reasoning used for paramagnetism. With respect to the continuum model introduced in section 1.1.1, we are now dealing with phenomena occurring inside our elementary volume $dV_\mathbf{r}$, which involve the interactions between single spins. Here we report the theory developed by Weiss which is very similar to the one used for paramagnetism. In fact, the main difference stays in the postulation of an additional magnetic field H_w whose non magnetic (Maxwellian) origin is not investigated. This field was called *molecular field* by Weiss [8]; by adding the field $H_\mathrm{w} = N_\mathrm{w} M$ (N_w is characteristic of the material) to the external field in Eq. (1.24), one ends up with the following equation:

$$M = M_s \, \mathcal{L} \left(\frac{\mu_0 m_0 (H_\mathrm{a} + N_\mathrm{w} M)}{kT} \right) \quad . \tag{1.28}$$

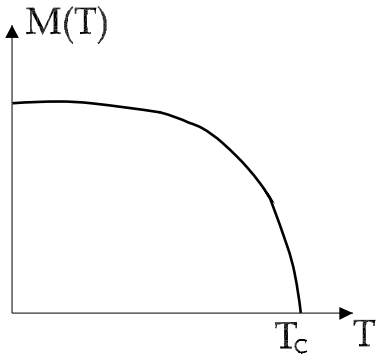

Figure 1.2: Typical behavior of spontaneous magnetization as function of temperature.

The latter equation can be linearized for high temperatures, which corresponds to small β as seen before. Then, one can find the well-known *Curie-Weiss law* that once again expresses the dependance of the susceptibility on the temperature

$$\chi \propto \frac{1}{T - T_c} \quad , \quad T_c = \frac{\mu_0 M_s m_0 N_\mathrm{w}}{3k} \quad , \tag{1.29}$$

where T_c is the Curie temperature, characteristic of the material. Thus, for temperatures $T > T_c$ the ferromagnetic materials behave like paramagnetic. For temperature $T < T_c$, one can use Eq. (1.28) to derive the relationship between the saturation magnetization M_s and the temperature T. The resulting relationship $M_s = M_s(T)$ behaves like in Fig. 1.2. This behavior qualitatively matches with experimental observations [5]. In addition, the phenomenological approach of molecular field was theoretically justified when Heisenberg introduced the exchange interaction on the basis of quantum theory (1931).

Nevertheless, the Weiss theory gives information about the magnitude of magnetization, but nothing can be said about the direction. In this respect micromagnetics has the purpose to find the direction of magnetization at every location within the magnetic body. In this respect, for constant temperature, the magnetization vector field $\mathbf{M}(\mathbf{r}, t)$ can be written as

$$\mathbf{M}(\mathbf{r}, t) = M_s \, \mathbf{m}(\mathbf{r}, t) \quad , \tag{1.30}$$

where $\mathbf{m}(\mathbf{r}, t)$ is the magnetization unit-vector field.

Microscopic model

Now we have to investigate how the exchange interactions play on a larger spatial scale, namely how the elementary magnetic moments $\mathbf{M}\, dV_\mathbf{r}$ exchange-interact with one another. We follow the derivation proposed by Landau and Lifshitz in

1935, reported by W.F. Brown Jr. in Ref [12]. In this respect, an energy term which penalizes magnetization disuniformities is introduced in the free energy. This term, in the isotropic case (i.e. cubic cell) is consisted of an expansion in even power series of the gradients of magnetization components [11]. If one stops the expansion to the first term, the disuniformity penalization assumes the form:

$$f_{\rm ex} = A[(\nabla m_x)^2 + (\nabla m_y)^2 + (\nabla m_z)^2] \quad , \tag{1.31}$$

where the constant A, having dimension of [J/m], has to be somehow determined. One way is to identify the exchange constant from experiments, but it is also possible to estimate it with a theoretical approach. In fact, let us consider a cubic lattice of spins, with interaction energy given by the Heisenberg Hamiltonian:

$$W = -2J \sum \mathbf{S}_i \cdot \mathbf{S}_j \quad , \tag{1.32}$$

where the sum is extended to the *nearest neighbors only* and $\mathbf{S}_i$, $\mathbf{S}_j$ are the spin angular momenta, expressed in units of $\hbar$, associated to sites i and j, and J is the nearest neighbor exchange integral. We assume that the forces between spins are sufficiently strong to keep the neighbor spins almost parallel. Thus, if $\mathbf{m}_i$ is the unit-vector in the direction $-\mathbf{S}_i$, such that $\mathbf{S}_i = -S\mathbf{m}_i$ (S is the spin magnitude), and if $\theta_{i,j}$ is the small angle between the directions $\mathbf{m}_i$ and $\mathbf{m}_j$, one can rewrite Eq. (1.32) as

$$\begin{aligned} W &= -2JS^2 \sum \cos\theta_{i,j} \simeq -2JS^2 \sum \left(1 - \frac{1}{2}\theta_{i,j}^2\right) = \\ &= \text{const.} + JS^2 \sum \theta_{i,j}^2 \simeq \text{const.} + JS^2 \sum (\mathbf{m}_j - \mathbf{m}_i)^2 \quad , \end{aligned} \tag{1.33}$$

since for small $\theta_{i,j}$, $|\theta_{i,j}| = |\mathbf{m}_j - \mathbf{m}_i|$. We now assume that the displacement vector $\mathbf{m}_j - \mathbf{m}_i$ can be written in terms of a continuous function $\mathbf{m}$ such that:

$$\mathbf{m}_j - \mathbf{m}_i = \Delta\mathbf{r}_j \cdot \nabla\mathbf{m} \quad , \tag{1.34}$$

where $\Delta\mathbf{r}_j = \mathbf{r}_j - \mathbf{r}_i$ is the position vector of neighbor j with respect to site i. Then, if $\mathbf{m} = m_x\mathbf{e}_x + m_y\mathbf{e}_y + m_z\mathbf{e}_z$,

$$\begin{aligned} W &= \text{const.} + JS^2 \sum (\Delta\mathbf{r}_j \cdot \nabla\mathbf{m})^2 = \\ &= \text{const.} + JS^2 \sum [(\Delta\mathbf{r}_j \cdot \nabla m_x)^2 + (\Delta\mathbf{r}_j \cdot \nabla m_y)^2 + (\Delta\mathbf{r}_j \cdot \nabla m_z)^2] \quad . \end{aligned} \tag{1.35}$$

Now we sum over j and multiply by the number of spins per unit volume n in order to obtain the energy per unit volume $f_{\rm ex}$. It is important to notice that, if $\Delta\mathbf{r}_j = x_j\mathbf{e}_x + y_j\mathbf{e}_y + z_j\mathbf{e}_z$, due to the cubic symmetry it happens that $\sum_j x_j y_j = 0$, and $\sum_j x_j^2 = \frac{1}{3}\sum_j \Delta\mathbf{r}_j^2$. By using these properties and neglecting the constant term, one ends up with:

$$f_{\rm ex} = A[(\nabla m_x)^2 + (\nabla m_y)^2 + (\nabla m_z)^2] \quad , \tag{1.36}$$

where A is the exchange constant:

$$A = \frac{1}{6} nJS^2 \sum \Delta \mathbf{r}_j^2 \quad , \tag{1.37}$$

which can be particularized for different lattice geometries (body-centered, face-centered cubic crystals). Typical values of A are in the order of 10^{-11} J/m.

Finally, one can write the contribution of exchange interactions to the free energy of the whole magnetic body by integrating Eq. (1.36) over the region Ω:

$$F_{\text{ex}} = \int_{\Omega} A[(\nabla m_x)^2 + (\nabla m_y)^2 + (\nabla m_z)^2]\, dV \quad . \tag{1.38}$$

It is important to notice that, in this case, the exchange interaction is isotropic in space, meaning that the exchange energy of a given volume ΔV is the same for any orientation of the magnetization vector, provided that its strength remains the same. In this respect, the expression (1.38) for the exchange energy puts this consideration into evidence.

1.1.4 Anisotropy

In ferromagnetic bodies it is very frequent to deal with anisotropic effects, due to the structure of the lattice and to the particular symmetries that can arise in certain crystals. In fact, in most experiments one can generally observe that certain energy-favored directions exist for a given material, i.e. certain ferromagnetic materials, in absence of external field, tend to be magnetized along precise directions, which in literature are referred to as *easy directions*. The fact that there is a "force" which tends to align magnetization along easy directions can be taken into account, in micromagnetic framework, by means of an additional phenomenological term in the free energy functional.

To this end, let us refer to an elementary volume ΔV, uniformly magnetized and characterized by magnetization unit-vector $\mathbf{m} = \mathbf{M}/M_s$. The magnetization unit-vector $\mathbf{m} = m_x \mathbf{e}_x + m_y \mathbf{e}_y + m_z \mathbf{e}_z$ can be expressed in spherical coordinates by means of the angles θ and ϕ such that:

$$\begin{aligned} m_x &= \sin\theta \cos\phi \\ m_y &= \sin\theta \sin\phi \\ m_z &= \cos\theta \quad . \end{aligned} \tag{1.39}$$

The anisotropy energy density $f_{\text{an}}(\mathbf{m})$ can be seen as a function of the spherical angles θ and ϕ, and the anisotropy energy as

$$F_{\text{an}}(\mathbf{m}) = \int_{\Omega} f_{\text{an}}(\mathbf{m})\, dV \quad . \tag{1.40}$$

In this phenomenological analysis, it turns out that the easy directions correspond to the minima of the anisotropy energy density, whereas saddle-points and maxima of $f_{\text{an}}(\mathbf{m})$ determine the medium-hard axes and the hard axes respectively.

Uniaxial anisotropy

The most common anisotropy effect is connected to the existence of one only easy direction, and in literature it is referred to as uniaxial anisotropy. Thus, the anisotropy free energy density $f_{\text{an}}(\mathbf{m})$ will be rotationally-symmetric with respect to the easy axis and will depend only on the relative orientation of $\mathbf{m}$ with respect to this axis. We suppose, for sake of simplicity, that the easy direction coincides with the cartesian axis z. Therefore, we can write the expression of $f_{\text{an}}(\mathbf{m})$ as an even function of $m_z = \cos\theta$, or equivalently using as independent variable $m_x^2 + m_y^2 = 1 - m_z^2 = \sin\theta$. This expression, developed in series assumes the following form:

$$f_{\text{an}}(\mathbf{m}) = K_0 + K_1 \sin^2\theta + K_2 \sin^4\theta + K_3 \sin^6\theta + \dots \tag{1.41}$$

where K_1, K_2, $K_3, \dots$, are the *anisotropy constants* having the dimensions of energy per unit volume [J/m^3].

Here we will limit our analysis to the case in which the expansion (1.41) is truncated after the $\sin^2\theta$ term:

$$f_{\text{an}}(\mathbf{m}) = K_0 + K_1 \sin^2\theta \quad . \tag{1.42}$$

In the latter case, the anisotropic behavior depends on the sign of the constant K_1. When $K_1 > 0$, the anisotropy energy admits two minima at $\theta = 0$ and $\theta = \pi$, that is when the magnetization lies along the positive or negative z direction with no preferential orientation. This case is often referred to as *easy axis anisotropy* (see Fig. 1.3). Conversely, when $K_1 < 0$ the energy is minimized for $\theta = \pi/2$, meaning that any direction in $x - y$ plane corresponds to an easy direction. For this reason, this case is often referred to as *easy plane anisotropy.* In the sequel, referring to uniaxial anisotropy, we will intend to use the following anisotropy free energy, derived from the integration over the whole body of the energy density Eq. (1.42):

$$G_{\text{an}}(\mathbf{m}) = \int_\Omega K_1[1 - (\mathbf{e}_{\text{an}}(\mathbf{r}) \cdot \mathbf{m}(\mathbf{r}))^2]\, dV \quad , \tag{1.43}$$

where $\mathbf{e}_{\text{an}}(\mathbf{r})$ is the easy axis unit-vector at the location $\mathbf{r}$ and the constant part connected to K_0 has been neglected.

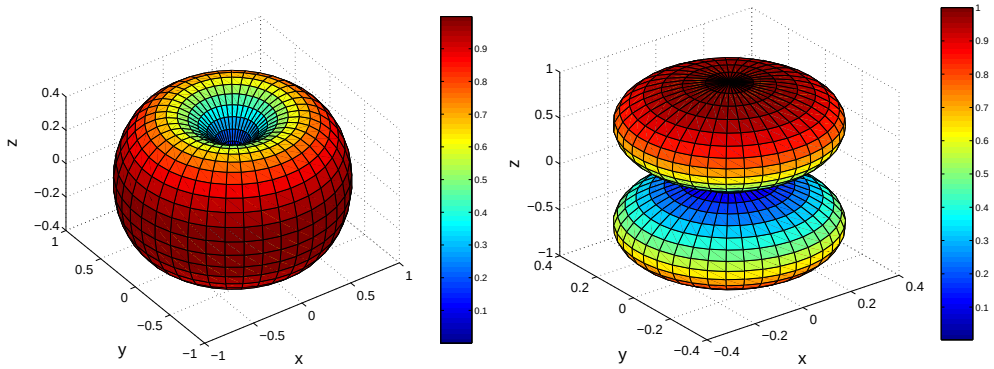

Figure 1.3: Uniaxial anisotropy energy density. (left) easy axis anisotropy ($K_1 > 0$). (right) easy plane anisotropy ($K_1 < 0$).

Cubic anisotropy

This is the case when the anisotropy energy density has cubic symmetry, mostly due to spin-lattice coupling in cubic crystals. Basically it happens that three privileged directions exist. A typical expansion of the anisotropy energy density in this case is, in cartesian coordinates:

$$f_{\text{an}}(\mathbf{m}) = K_0 + K_1(m_x^2 m_y^2 + m_y^2 m_z^2 + m_z^2 m_x^2) + K_2 m_x^2 m_y^2 m_z^2 + \dots \qquad (1.44)$$

As before, let us neglect terms of order grater than fourth (i.e. $K_2 = 0$, etc.). When $K_1 > 0$, there are six equivalent energy minima corresponding to the directions x, y, z, both positive and negative (see Fig. 1.4). Conversely, when $K_1 < 0$ a more complex situation arises. In fact, there are eight equivalent minima along the directions pointing the vertices of the cube (e.g. the direction [1,1,1]) and the coordinate axes directions become now hard axes. This case has been inserted for sake of completeness, but in the sequel cubic anisotropy will be not considered anymore. It is important to underline that the character of anisotropy interaction is local, that is, the anisotropy energy related to an elementary volume $dV_{\mathbf{r}'}$ depends only on the magnetization $\mathbf{M}(\mathbf{r}')$.

1.1.5 Magnetostatic interactions

Magnetostatic interactions represent the way the elementary magnetic moments interact over 'long' distances within the body. In fact, the magnetostatic field at a given location within the body depends on the contributions from the whole magnetization vector field, as we will see below. Magnetostatic interactions can be taken into account by introducing the appropriate magnetostatic field $\mathbf{H}_{\text{m}}$

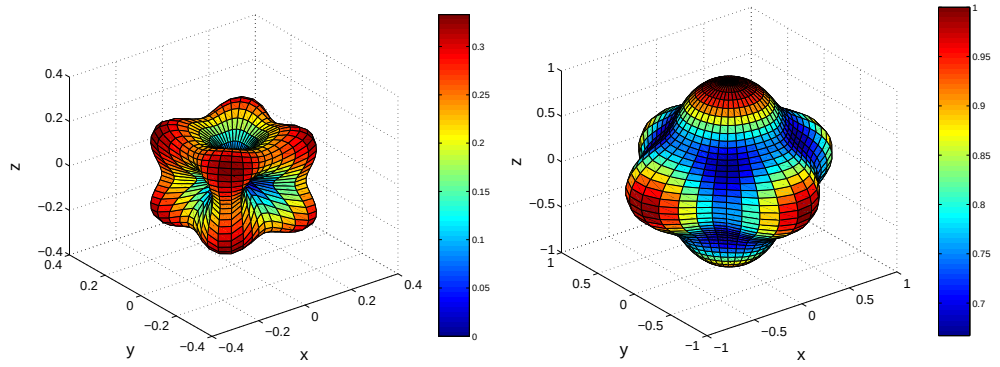

Figure 1.4: Cubic Anisotropy energy density. (left) coordinate axes are easy axes ($K_2 > 0$). (right) coordinate axes are easy axes ($K_2 < 0$).

according to Maxwell equations for magnetized media:

$$\begin{cases} \nabla \cdot \mathbf{H}_\mathrm{m} = -\nabla \cdot \mathbf{M} & \text{in } \Omega \\ \nabla \cdot \mathbf{H}_\mathrm{m} = 0 & \text{in } \Omega^c \\ \nabla \times \mathbf{H}_\mathrm{m} = \mathbf{0} \end{cases} , \tag{1.45}$$

with the following conditions at the body discontinuity surface $\partial\Omega$

$$\begin{cases} \mathbf{n} \cdot [\mathbf{H}_\mathrm{m}]_{\partial\Omega} = \mathbf{n} \cdot \mathbf{M} \\ \mathbf{n} \times [\mathbf{H}_\mathrm{m}]_{\partial\Omega} = \mathbf{0} \end{cases} . \tag{1.46}$$

In Eqs. (1.45)-(1.46), we have denoted with $\mathbf{n}$ the outward normal to the boundary $\partial\Omega$ of the magnetic body, and with $[\mathbf{H}_\mathrm{m}]_{\partial\Omega}$ the jump of the vector field $\mathbf{H}_\mathrm{m}$ across $\partial\Omega$.

Magnetostatic energy

Now we will provide the expression for the contribution of magnetostatic interactions to the free energy of the system. The derivation of such expression is quite straightforward if one assumes that the energy density [14] of magnetostatic field is given by:

$$U_\mathrm{m} = \int_{\Omega_\infty} \frac{1}{2}\mu_0 {\mathbf{H}_\mathrm{m}}^2 \, dV \quad , \tag{1.47}$$

where Ω_∞ is the whole space. In fact, by expressing the magnetostatic field as

$$\mathbf{H}_\mathrm{m} = \frac{\mathbf{B}_\mathrm{m}}{\mu_0} - \mathbf{M} \quad , \tag{1.48}$$

Eq. (1.47) becomes:

$$U_\mathrm{m} = \int_{\Omega_\infty} \frac{1}{2}\mu_0 \mathbf{H}_\mathrm{m} \cdot \left(\frac{\mathbf{B}_\mathrm{m}}{\mu_0} - \mathbf{M} \right) dV \quad . \tag{1.49}$$

The first term in Eq. (1.49) vanishes owing to the integral orthogonality of the solenoidal field $\mathbf{B}_\mathrm{m}$ and the conservative field $\mathbf{H}_\mathrm{m}$ over the whole space [14]. The remaining part, remembering that $\mathbf{M}$ is nonzero only within the region Ω, is the magnetostatic free energy:

$$F_\mathrm{m} = -\int_\Omega \frac{1}{2}\mu_0 \mathbf{M}\cdot\mathbf{H}_\mathrm{m}\, dV \quad . \tag{1.50}$$

We observe that magnetostatic energy expresses a nonlocal interaction, since the magnetostatic field functionally depends, through the boundary value problem (1.45), on the whole magnetization vector field, as we anticipated in the beginning of the section. The latter equation has the physical meaning of an interaction energy of an assigned continuous magnetic moments distribution, namely it can be obtained by computing the work, made against the magnetic field generated by the continuous distribution, to bring an elementary magnetic moment $\mu_0\mathbf{M}\,dV$ from infinity to its actual position within the distribution [15]. Discussion on the choice of the magnetostatic field energy density can be found in Ref. [14] and references therein.

1.1.6 The External Field. Zeeman Energy

Until now, we have treated the case of magnetic body not subject to external field. Therefore, all the energy terms introduced in the previous sections can be regarded as parts of the Helmholtz free energy functional. When the external field is considered, it is convenient to introduce the Gibbs free energy functional. In this respect, the additional term (see Eq. (1.17)) related to the external field $\mathbf{H}_\mathrm{a}$, is itself a long-range contribution too. In fact, it can be seen as the potential energy of a continuous magnetic moments distribution [15] subject to external field $\mathbf{H}_\mathrm{a}$:

$$G_\mathrm{a} = -\int_\Omega \mu_0 \mathbf{M}\cdot\mathbf{H}_\mathrm{a} \quad . \tag{1.51}$$

This energy term is referred in literature to as *Zeeman energy*.

1.1.7 Magnetoelastic interactions

Ferromagnetic bodies are also sensible to mechanical stress and deformations. This means that when they are subject to an external field, mechanical stresses, due to the interaction with the field, arise within the bodies and consequent deformations of the bodies themselves can be observed (magnetostrictive materials). Viceversa, if one deforms a ferromagnetic body, the consequent mechanical stress affects the state of magnetization of the body. In other words, there is interaction between magnetic and elastic processes. Therefore, in our framework

based on energy aspects, an additional term to describe this magneto-mechanical coupling should be inserted in the free energy (see Ref. [19] for details). Here we neglect magnetoelastic interaction, for sake of simplicity, but in principle it can be treated, apart from mathematical complications, in the same way as the other free energy terms, as we will see in the following sections.

1.1.8 The Free Energy Functional

Now we are able to write the complete expression for the free energy of the ferromagnetic body. In fact, by collecting Eqs. (1.38), (1.40), (1.50) and (1.51), one has:

$$\begin{aligned} G(\mathbf{M},\mathbf{H}_\mathrm{a}) &= F_\mathrm{ex} + F_\mathrm{an} + F_\mathrm{m} + G_\mathrm{a} = \\ &= \int_\Omega \Big\{ A[(\nabla m_x)^2 + (\nabla m_y)^2 + (\nabla m_z)^2] + f_\mathrm{an} + \\ &- \frac{1}{2}\mu_0 \mathbf{M}\cdot\mathbf{H}_\mathrm{m} - \mu_0 \mathbf{M}\cdot\mathbf{H}_\mathrm{a} \Big\}\, dV \quad , \end{aligned} \tag{1.52}$$

which can be put in the compact form by expressing the exchange interaction energy density as $A(\nabla\mathbf{m})^2$:

$$G(\mathbf{M},\mathbf{H}_\mathrm{a}) = \int_\Omega \left[A(\nabla\mathbf{m})^2 + f_\mathrm{an} + -\frac{1}{2}\mu_0 \mathbf{M}\cdot\mathbf{H}_\mathrm{m} - \mu_0 \mathbf{M}\cdot\mathbf{H}_\mathrm{a} \right] dV \quad , \tag{1.53}$$

1.2 Micromagnetic Equilibrium

In section 1.1.2 we recalled the fact that, for constant external field and temperature, the equilibria (i.e. metastable states) are given by the minima of the free energy (1.53). Remembering that $\mathbf{M} = M_s\mathbf{m}$, the unknown will be the magnetization unit-vector field $\mathbf{m}$.

1.2.1 First-order Variation of the Free Energy

In the following we impose that the first-order variation δG vanishes for any variation $\delta\mathbf{m}$ of the vector field $\mathbf{m}$, compatible with the constraint $|\mathbf{m}+\delta\mathbf{m}| = 1$ (which in turn corresponds to $|\mathbf{M}+\delta\mathbf{M}| = M_s$). This will allow us to derive the equilibrium condition [4] and, therefore, the equilibrium configuration for magnetization within the body. We approach separately each term of the free energy (1.53).

Exchange

Let us take the first-order variation of Eq. (1.38):

$$\delta F_\mathrm{ex} = F_\mathrm{ex}(\mathbf{m}+\delta\mathbf{m}) - F_\mathrm{ex}(\mathbf{m}) = \int_\Omega 2A\nabla\mathbf{m}\cdot\nabla\delta\mathbf{m}\, dV \quad , \tag{1.54}$$

where $\nabla\mathbf{m}\cdot\nabla\delta\mathbf{m}$ is a compact notation for $\nabla m_x\cdot\nabla\delta m_x+\nabla m_y\cdot\nabla\delta m_y+\nabla m_z\cdot\nabla\delta m_z$. Now we proceed in the derivation for the x component, the remaining y,z can be treated analogously. By applying the vector identity

$$\mathbf{v}\cdot\nabla f=\nabla\cdot(f\mathbf{v})-f\nabla\cdot\mathbf{v} \quad , \tag{1.55}$$

in which we put $f=\delta m_x$ and $\mathbf{v}=\nabla m_x$, one obtains:

$$\int_\Omega \nabla m_x\cdot\nabla\delta m_x\,dV=\int_\Omega\left[\nabla\cdot(\delta m_x A\nabla m_x)-\delta m_x\nabla\cdot(A\nabla m_x)\right]dV \quad . \tag{1.56}$$

By using the divergence theorem, the first term can be written as surface integral over the boundary $\partial\Omega$

$$\int_\Omega \nabla m_x\cdot\nabla\delta m_x\,dV=\int_{\partial\Omega}\delta m_x A\frac{\partial m_x}{\partial\mathbf{n}}\,dS-\int_\Omega\delta m_x\nabla\cdot(A\nabla m_x)\,dV \quad . \tag{1.57}$$

By substituting the latter equation and the analogous for the y,z components into Eq. (1.54), one ends up with:

$$\delta F_{\mathrm{ex}}=-\int_\Omega\left[2\nabla\cdot(A\nabla\mathbf{m})\cdot\delta\mathbf{m}\right]dV+\int_{\partial\Omega}\left[2A\frac{\partial\mathbf{m}}{\partial\mathbf{n}}\cdot\delta\mathbf{m}\right]dS \quad , \tag{1.58}$$

which is the exchange contribution to the first-order variation of the free energy functional.

Anisotropy

As far as anisotropy is concerned, taking the first-order variation of the energy F_{an} is equivalent to write the following equation:

$$\delta F_{\mathrm{an}}=\int_\Omega\frac{\partial f_{\mathrm{an}}}{\partial\mathbf{m}}\cdot\delta\mathbf{m}\,dV \quad . \tag{1.59}$$

For instance, referring to the case of uniaxial anisotropy and, therefore, to Eq. (1.43), the latter equation becomes

$$\delta F_{\mathrm{an}}=\int_\Omega -2K_1(\mathbf{m}\cdot\mathbf{e}_{\mathrm{an}})\mathbf{e}_{\mathrm{an}}\cdot\delta\mathbf{m}\,dV \quad . \tag{1.60}$$

Magnetostatic energy

By taking the first-order variation of the free energy functional (1.50), one has:

$$\delta F_{\mathrm{m}}=-\int_\Omega\frac{1}{2}\mu_0 M_s\,\delta\mathbf{m}\cdot\mathbf{H}_{\mathrm{m}}\,dV-\int_\Omega\frac{1}{2}\mu_0 M_s\,\mathbf{m}\cdot\delta\mathbf{H}_{\mathrm{m}}\,dV \quad . \tag{1.61}$$

The above two integral term are identical as stated by the reciprocity theorem [4, 5] and then the latter equation can be rewritten in the following form:

$$\delta F_{\mathrm{m}}=-\int_\Omega\mu_0 M_s\,\mathbf{H}_{\mathrm{m}}\cdot\delta\mathbf{m}\,dV \quad . \tag{1.62}$$

Zeeman energy

Since the applied field does not depend on the magnetization, the first-order variation of the Zeeman free energy (1.51) is:

$$\delta G_{\mathrm{a}} = -\int_{\Omega} \mu_0 M_s \mathbf{H}_{\mathrm{a}} \cdot \delta\mathbf{m} \quad . \tag{1.63}$$

1.2.2 Effective Field and Brown's Equations

Thus, to summarize the previously derived results, we can write the expression for the first-order variation of the free energy functional (1.53):

$$\begin{aligned} \delta G = -\int_{\Omega} \left[2\nabla \cdot (A\nabla\mathbf{m}) - \frac{\partial f_{\mathrm{an}}}{\partial \mathbf{m}} + \mu_0 M_s \mathbf{H}_{\mathrm{m}} + \mu_0 M_s \mathbf{H}_{\mathrm{a}} \right] \cdot \delta\mathbf{m}\, dV + \\ + \int_{\partial\Omega} \left[2A \frac{\partial \mathbf{m}}{\partial \mathbf{n}} \cdot \delta\mathbf{m} \right] dS = 0 \quad . \end{aligned} \tag{1.64}$$

Now we claim the fact that the variation $\delta\mathbf{m}$ has to satisfy the constraint $|\mathbf{m} + \delta\mathbf{m}| = 1$. For this reason, it can be easily observed that the most general variation is a rotation of the vector field $\mathbf{m}$, that is

$$\delta\mathbf{m} = \mathbf{m} \times \vec{\delta\theta} \quad , \tag{1.65}$$

where the vector $\vec{\delta\theta}$ represents an elementary rotation of angle $\delta\theta$. By substituting this expression in Eq. (1.64) and remembering that $\mathbf{v} \cdot (\mathbf{w} \times \mathbf{u}) = \mathbf{u} \cdot (\mathbf{v} \times \mathbf{w}) = -\mathbf{u} \cdot (\mathbf{w} \times \mathbf{v})$, one obtains:

$$\begin{aligned} \delta G = \int_{\Omega} \mathbf{m} \times \left[2\nabla \cdot (A\nabla\mathbf{m}) - \frac{\partial f_{\mathrm{an}}}{\partial \mathbf{m}} + \mu_0 M_s \mathbf{H}_{\mathrm{m}} + \mu_0 M_s \mathbf{H}_{\mathrm{a}} \right] \cdot \vec{\delta\theta}\, dV + \\ + \int_{\partial\Omega} \left[2A \frac{\partial \mathbf{m}}{\partial \mathbf{n}} \times \mathbf{m} \right] \cdot \vec{\delta\theta}\, dS = 0 \quad . \end{aligned} \tag{1.66}$$

Since the elementary rotation $\delta\theta$ is arbitrary, Eq. (1.66) can be identically zero if and only if:

$$\begin{cases} \mathbf{m} \times \left[2\nabla \cdot (A\nabla\mathbf{m}) - \dfrac{\partial f_{\mathrm{an}}}{\partial \mathbf{m}} + \mu_0 M_s \mathbf{H}_{\mathrm{m}} + \mu_0 M_s \mathbf{H}_{\mathrm{a}} \right] = \mathbf{0} \\ \left[2A \dfrac{\partial \mathbf{m}}{\partial \mathbf{n}} \times \mathbf{m} \right]_{\partial\Omega} = \mathbf{0} \end{cases} . \tag{1.67}$$

In the second equation the fact that $\frac{\partial \mathbf{m}}{\partial \mathbf{n}} \times \mathbf{m} = \mathbf{0}$ implies that $\frac{\partial \mathbf{m}}{\partial \mathbf{n}} = \mathbf{0}$, as the vectors $\mathbf{m}$ and $\frac{\partial \mathbf{m}}{\partial \mathbf{n}}$ are always orthogonal; in fact, the only way their vector product can vanish is that $\frac{\partial \mathbf{m}}{\partial \mathbf{n}}$ is identically zero. We introduce now the *effective field*

$$\mathbf{H}_{\mathrm{eff}} = \frac{2}{\mu_0 M_s} \nabla \cdot (A\nabla\mathbf{m}) - \frac{1}{\mu_0 M_s} \frac{\partial f_{\mathrm{an}}}{\partial \mathbf{m}} + \mathbf{H}_{\mathrm{m}} + \mathbf{H}_{\mathrm{a}} \quad , \tag{1.68}$$

where the first two terms take into account the exchange and anisotropy interjections. In other words, these interactions effectively act on the magnetization as they were suitable fields:

$$\mathbf{H}_{\text{exc}} = \frac{2}{\mu_0 M_s} \nabla \cdot (A \nabla \mathbf{m}) \quad , \tag{1.69}$$

$$\mathbf{H}_{\text{an}} = \frac{1}{\mu_0 M_s} \frac{\partial f_{\text{an}}}{\partial \mathbf{m}} \quad . \tag{1.70}$$

Eqs. (1.67) can be rewritten as

$$\begin{cases} \mu_0 M_s \, \mathbf{m} \times \mathbf{H}_{\text{eff}} = \mathbf{0} \\ \left. \dfrac{\partial \mathbf{m}}{\partial \mathbf{n}} \right|_{\partial\Omega} = \mathbf{0} \end{cases} \qquad \text{Brown's Equations.} \tag{1.71}$$

The Brown's equations allow one to find the equilibrium configuration of the magnetization within the body. The first equation states that the torque exerted on magnetization by the effective field must vanish at the equilibrium. It is important to notice that Eqs. (1.71) are nonlinear, since the effective field (1.68) has a functional dependance on the whole vector field $\mathbf{m}(\cdot)$. As we will discuss later, the existence of exact analytical solutions is subject to appropriate simplifying assumptions. For this reason, in most cases numerical solution of Eqs. (1.71) is required. In addition, as mentioned in section 1.1.2, the model must be completed with a dynamic equation to properly describe the evolution of the system. This will be done in the following section.

1.3 The Dynamic Equation

Up to now, we have presented a variational method based on the minimization of the free energy of a ferromagnetic body. This method allows one to find the equilibrium configurations for a magnetized body, regardless of describing how magnetization reaches the equilibrium during time. Recently, the challenging requirements of greater speed and areal density in magnetic storage elements, has considerably increased the effort of the researchers in the investigation of magnetization dynamics. Most of the analysis are based on the dynamic model proposed by Landau and Lifshitz [3] in 1935, and successively modified by Gilbert [18] in 1955. In this section we will present both Landau-Lifshitz and Gilbert equations as a model for magnetization 'motion'. The differences between them are emphasized and the properties of magnetization dynamics are shown in view of the discussions and results presented in the following chapters.

1.3.1 GYROMAGNETIC PRECESSION

It is known from quantum mechanics that there is a proportionality relationship between the magnetic spin momentum $\boldsymbol{\mu}$ and angular momentum $\mathbf{L}$ of electrons. This relationship can be expressed as

$$\boldsymbol{\mu} = -\gamma \mathbf{L} \quad , \tag{1.72}$$

where $\gamma = 2.21 \times 10^5$ m A^{-1} s^{-1} is the absolute value of the gyromagnetic ratio

$$\gamma = \frac{g\,|e|}{2m_e\,c} \quad ; \tag{1.73}$$

$g \simeq 2$ is the Landé splitting factor, $e = -1.6 \times 10^{-19}$ C is the electron charge, $m_e = 9.1 \times 10^{-31}$ kg is the electron mass and $c = 3 \times 10^8$ m/s is the speed of light. By applying the momentum theorem one can relate the rate of change of the angular momentum to the torque exerted on the particle by the magnetic field $\mathbf{H}$:

$$\frac{d\mathbf{L}}{dt} = \boldsymbol{\mu} \times \mathbf{H} \quad . \tag{1.74}$$

By using Eq. (1.72), one ends up with a model which describes the precession of the spin magnetic moment around the field:

$$\frac{d\boldsymbol{\mu}}{dt} = -\gamma \boldsymbol{\mu} \times \mathbf{H} \quad . \tag{1.75}$$

The frequency of precession is the *Larmor frequency*

$$f_L = \frac{\gamma\, H}{2\pi} \quad . \tag{1.76}$$

Eq. (1.75) can be written for each spin magnetic moment within the elementary volume $dV_{\mathbf{r}}$:

$$\frac{d\boldsymbol{\mu}_j}{dt} = -\gamma \boldsymbol{\mu}_j \times \mathbf{H} \quad , \tag{1.77}$$

where now the magnetic field $\mathbf{H}$ is intended to be spatially uniform. Now, by taking the volume average of both members of the latter equation, one has:

$$\frac{1}{dV_{\mathbf{r}}} \frac{d\sum_j \boldsymbol{\mu}_j}{dt} = -\gamma \frac{\sum_j \boldsymbol{\mu}_j}{dV_{\mathbf{r}}} \times \mathbf{H} \quad , \tag{1.78}$$

and, therefore, recalling the definition (1.1) of magnetization vector field $\mathbf{M}$, we end up with the following continuum gyromagnetic precession model:

$$\frac{\partial \mathbf{M}}{\partial t} = -\gamma \mathbf{M} \times \mathbf{H} \quad . \tag{1.79}$$

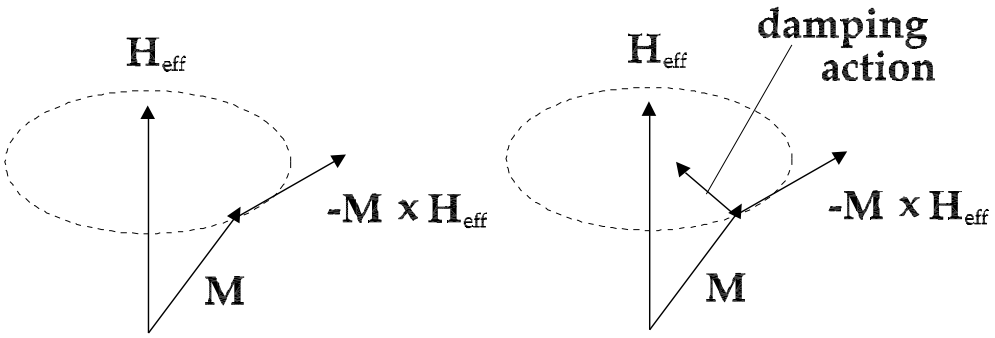

Figure 1.5: (left) Undamped gyromagnetic precession. (right) Damped gyromagnetic precession.

1.3.2 The Landau-Lifshitz equation

The first dynamical model for the precessional motion of the magnetization was proposed by Landau and Lifshitz in 1935. Basically, this model is constituted by a continuum precession equation (1.79), in which the presence of quantum-mechanical effects and anisotropy is phenomenologically taken into account by means of the effective field $\mathbf{H}_{\text{eff}}$ given by Eq. (1.68). Then, the Landau-Lifshitz equation is:

$$\frac{\partial \mathbf{M}}{\partial t} = -\gamma \mathbf{M} \times \mathbf{H}_{\text{eff}} \quad . \tag{1.80}$$

First of all, we observe that if the magnetization rate of change $\partial \mathbf{m}/\partial t$ vanishes, Eq. (1.80) expresses the equilibrium condition given by the first of the Brown's equations (1.71). In addition, since Eq. (1.80) is an integro-partial differential equation, the Neumann boundary condition given by the second Brown's equation is used [4].

We observe that Landau-Lifshitz equation (1.80) is a conservative (hamiltonian) equation.

Nevertheless, dissipative processes take place within dynamic magnetization processes. The microscopic nature of this dissipation is still not clear and is currently the focus of considerable research [16, 17]. The approach followed by Landau and Lifshitz consists of introducing dissipation in a phenomenological way. In fact, they introduce an additional torque term that pushes magnetization in the direction of the effective field (see Fig. 1.5). Then, the *Landau-Lifshitz equation* becomes:

$$\frac{\partial \mathbf{M}}{\partial t} = -\gamma \mathbf{M} \times \mathbf{H}_{\text{eff}} - \frac{\lambda}{M_s} \mathbf{M} \times (\mathbf{M} \times \mathbf{H}_{\text{eff}}) \quad , \tag{1.81}$$

where $\lambda > 0$ is a phenomenological constant characteristic of the material. It is important to observe that the additional term is such that the magnetization

magnitude is preserved according to the micromagnetic constraint $\mathbf{M} = M_s$. This can be seen by scalar multiplying both members of Eq. (1.81) by $\mathbf{M}$.

1.3.3 LANDAU-LIFSHITZ-GILBERT EQUATION

An in principle different approach was proposed by Gilbert [18] in 1955, who observed that since the conservative equation (1.80) can be derived from a Lagrangian formulation where the role of the generalized coordinates is played by the components of magnetization vector M_x, M_y, M_z. In this framework, the most natural way to introduce phenomenological dissipation occurs by introducing a kind of 'viscous' force, whose components are proportional to the time derivatives of the generalized coordinates. More specifically, he introduces the following additional torque term:

$$\frac{\alpha}{M_s}\mathbf{M} \times \frac{\partial \mathbf{M}}{\partial t} \quad , \tag{1.82}$$

which correspond to the torque produced by a field $-\frac{\alpha}{\gamma M_s}\frac{\partial \mathbf{M}}{\partial t}$, where $\alpha > 0$ is the Gilbert damping constant, depending on the material (typical values are in the range $\alpha = 0.001 \div 0.1$). We observe that, similarly to the case of Landau-Lifshitz equation, the additional term introduced by Gilbert preserves the magnetization magnitude[4]. In the following section, when we will analyze the fundamental properties of magnetization dynamics, we will show that the Gilbert damping is connected to the assumption of a suitable Rayleigh dissipation function. Therefore, the precessional equation (1.80), modified according to Gilbert's work, is generally referred to as *Landau-Lifshitz-Gilbert equation*:

$$\frac{\partial \mathbf{M}}{\partial t} = -\gamma \mathbf{M} \times \mathbf{H}_{\text{eff}} + \frac{\alpha}{M_s}\,\mathbf{M} \times \frac{\partial \mathbf{M}}{\partial t} \quad . \tag{1.83}$$

There is substantial difference between Landau-Lifshitz and Landau-Lifshitz-Gilbert equations although they are very similar from mathematical point of view. For instance, Landau-Lifshitz equation (1.81) can be obtained easily from Gilbert equation. In fact, by vector multiplying both members of Eq. (1.83) by $\mathbf{M}$, one obtains:

$$\mathbf{M} \times \frac{\partial \mathbf{M}}{\partial t} = -\gamma \mathbf{M} \times (\mathbf{M} \times \mathbf{H}_{\text{eff}}) + \mathbf{M} \times \left(\frac{\alpha}{M_s}\mathbf{M} \times \frac{\partial \mathbf{M}}{\partial t} \right) \quad ; \tag{1.84}$$

remembering the vector identity $\mathbf{a} \times (\mathbf{b} \times \mathbf{c}) = \mathbf{b}(\mathbf{a} \cdot \mathbf{c}) - \mathbf{c}(\mathbf{a} \cdot \mathbf{b})$ and observing that $\mathbf{M} \cdot \frac{\partial \mathbf{M}}{\partial t} = 0$ (see section 1.3.5), one ends up with:

$$\mathbf{M} \times \frac{\partial \mathbf{M}}{\partial t} = -\gamma \mathbf{M} \times (\mathbf{M} \times \mathbf{H}_{\text{eff}}) - \alpha M_s \frac{\partial \mathbf{M}}{\partial t} \quad . \tag{1.85}$$

[4] We will discuss this aspect in section 1.3.5

By substituting the latter equation in the right hand side of Landau-Lifshitz-Gilbert equation (1.83), one has:

$$\frac{\partial \mathbf{M}}{\partial t} = -\gamma \mathbf{M} \times \mathbf{H}_{\text{eff}} - \frac{\gamma\alpha}{M_s}\mathbf{M} \times (\mathbf{M} \times \mathbf{H}_{\text{eff}}) - \alpha^2 \frac{\partial \mathbf{M}}{\partial t} \quad . \tag{1.86}$$

The latter equation can be appropriately recast to obtain the following expression:

$$\frac{\partial \mathbf{M}}{\partial t} = -\frac{\gamma}{1+\alpha^2}\mathbf{M} \times \mathbf{H}_{\text{eff}} - \frac{\gamma\alpha}{(1+\alpha^2)M_s}\mathbf{M} \times (\mathbf{M} \times \mathbf{H}_{\text{eff}}) \quad , \tag{1.87}$$

which is commonly referred to as Landau-Lifshitz equation in the Gilbert form. One can immediately notice that Eq.(1.87) and Eq. (1.81) are mathematically the same, provided that one assumes:

$$\gamma_L = \frac{\gamma}{1+\alpha^2} \quad , \quad \lambda = \frac{\gamma\alpha}{1+\alpha^2} \quad . \tag{1.88}$$

Moreover, the work of Podio-Guidugli [82] has pointed out that both Landau-Lifshitz and Landau-Lifshitz-Gilbert equations belong to the same family of damped gyromagnetic precession equations. Nevertheless some considerations about the meaning of the quantity γ, which indeed is the ratio between physical characteristics of the electrons like mass and charge, are sufficient to say that Eqs. (1.81) and (1.83) express different physics and are identical only in the limit of vanishing damping. Moreover, first Kikuchi [30] and then Mallinson [29] have pointed out that in the limit of infinite damping ($\lambda \to \infty$ in Eq. (1.81), $\alpha \to \infty$ in Eq. (1.83)), the Landau-Lifshitz equation and the Landau-Lifshitz-Gilbert equation give respectively:

$$\frac{\partial \mathbf{M}}{\partial t} \to \infty \quad , \quad \frac{\partial \mathbf{M}}{\partial t} \to 0 \quad . \tag{1.89}$$

Since the second result is in agreement with the fact that a very large damping should produce a very slow motion while the first is not, one may conclude that the Landau-Lifshitz-Gilbert (1.83) equation is more appropriate to describe magnetization dynamics. In this thesis, from now on, we will use the Landau-Lifshitz-Gilbert equation (1.83).

1.3.4 Normalized equations

It is very useful to write the micromagnetic equations in dimensionless units. This is helpful as soon as one wants to investigate which terms are prevalent in given situations and moreover, the normalization considerably simplifies the expressions. We start our discussion from the expression of the free energy (1.53). By dividing both members of Eq. (1.53) by $\mu_0 M_s^2 V_0$ (V_0 is the volume of the body) one obtains:

$$g(\mathbf{m}, \mathbf{h}_{\text{a}}) = \frac{G(\mathbf{M}, \mathbf{H}_{\text{a}})}{\mu_0 M_s^2 V_0} = \int_\Omega \left[\frac{A}{\mu_0 M_s^2} (\nabla \mathbf{m})^2 + \frac{1}{\mu_0 M_s^2} f_{\text{an}} + -\frac{1}{2}\mathbf{m}\cdot\mathbf{h}_{\text{m}} - \mathbf{m}\cdot\mathbf{h}_{\text{a}} \right] dv \quad , \tag{1.90}$$

where the normalized volume v is measured in units of V_0. In this framework, we can obtain the normalized effective field $\mathbf{h}_{\text{eff}} = \mathbf{H}_{\text{eff}}/M_s$ by taking the variational derivative $\delta g/\delta \mathbf{m}$ of the normalized free energy:

$$\mathbf{h}_{\text{eff}} = \frac{2}{\mu_0 M_s^2}\nabla \cdot (A\nabla \mathbf{m}) - \frac{1}{\mu_0 M_s^2}\frac{\partial f_{\text{an}}}{\partial \mathbf{m}} + \mathbf{h}_{\text{m}} + \mathbf{h}_{\text{a}} \quad . \tag{1.91}$$

It is important to focus on the following quantity with the dimension of a length in Eq. (1.90):

$$l_{\text{ex}} = \sqrt{\frac{2A}{\mu_0 M_s^2}} \quad , \tag{1.92}$$

which is commonly referred to as *exchange length*. The exchange length gives an estimation of the characteristic dimension on which the exchange interaction is prevalent. For typical magnetic recording materials l_{ex} is in the order of $5 \div 10$ nm. Therefore, one expects that on a spatial scale in the order of l_{ex} the magnetization is spatially uniform. This is very important when spatial discretization of micromagnetic equations has to be preformed. In fact, one should be sure that the mesh characteristic dimension is smaller than l_{ex}.

Now let us consider the Landau-Lifshitz-Gilbert equation (1.83). By dividing both members by γM_s^2 one obtains:

$$\frac{1}{\gamma M_s^2}\frac{\partial \mathbf{M}}{\partial t} = -\frac{1}{M_s^2}\mathbf{M} \times \mathbf{H}_{\text{eff}} + \frac{\alpha}{\gamma M_s^2\, M_s}\,\mathbf{M} \times \frac{\partial \mathbf{M}}{\partial t} \quad . \tag{1.93}$$

Now, remembering that

$$\mathbf{m} = \frac{\mathbf{M}}{M_s} \quad , \quad \mathbf{h}_{\text{eff}} = \frac{\mathbf{H}_{\text{eff}}}{M_s} \tag{1.94}$$

and by measuring the time in units of $(\gamma M_s)^{-1}$, Eq. (1.93) can be rewritten in the following dimensionless form:

$$\frac{\partial \mathbf{m}}{\partial t} = -\mathbf{m} \times \mathbf{h}_{\text{eff}} + \alpha \mathbf{m} \times \frac{\partial \mathbf{m}}{\partial t} \quad . \tag{1.95}$$

In the case of $M_s \simeq 796$ kA/m ($\mu_0 M_s = 1$ T), the dimensionless time unit corresponds to $(\gamma M_s)^{-1} \simeq 5.7$ ps.

1.3.5 PROPERTIES OF MAGNETIZATION DYNAMICS

Magnetization magnitude conservation

Let us now briefly recall the fundamental properties of Landau-Lifshitz-Gilbert (LLG) dynamics. By scalar multiplying both members of the LLG equation (1.95) by $\mathbf{m}$ one can easily obtain:

$$\frac{d}{dt}\left(\frac{1}{2}|\mathbf{m}|^2\right) = 0 \quad , \tag{1.96}$$

which implies that, for any t_0, t and $\mathbf{r} \in \Omega$, it happens that:

$$|\mathbf{m}(t, \mathbf{r})| = |\mathbf{m}(t_0, \mathbf{r})| \quad . \tag{1.97}$$

Thus, any magnetization motion, at a given location $\mathbf{r}$, will occur on the unit sphere.

Energy balance equation

It is convenient to recast the normalized Landau-Lifshitz-Gilbert equation (1.95) in the following form:

$$\frac{\partial \mathbf{m}}{\partial t} = -\mathbf{m} \times \left(\mathbf{h}_{\text{eff}} - \alpha \frac{\partial \mathbf{m}}{\partial t} \right) . \tag{1.98}$$

Now by scalar multiplying both members of Eq. (1.98) by $\mathbf{h}_{\text{eff}} - \alpha \frac{\partial \mathbf{m}}{\partial t}$ one ends up with:

$$\frac{\partial \mathbf{m}}{\partial t} \cdot \left(\mathbf{h}_{\text{eff}} - \alpha \frac{\partial \mathbf{m}}{\partial t} \right) = 0 \quad . \tag{1.99}$$

The effective field and the time derivative of the free energy are related by the following relationship:

$$\begin{aligned} \frac{dg}{dt} &= \int_\Omega \left[\frac{\delta g}{\delta \mathbf{m}} \cdot \frac{\partial \mathbf{m}}{\partial t} + \frac{\delta g}{\delta \mathbf{h}_{\text{a}}} \cdot \frac{\partial \mathbf{h}_{\text{a}}}{\partial t} \right] dv = \\ &= \int_\Omega \left[-\mathbf{h}_{\text{eff}} \cdot \frac{\partial \mathbf{m}}{\partial t} - \mathbf{m} \cdot \frac{\partial \mathbf{h}_{\text{a}}}{\partial t} \right] dv \quad . \end{aligned} \tag{1.100}$$

By integrating Eq. (1.99) over the body volume Ω and by using the latter equation, one obtains:

$$\frac{dg}{dt} = -\int_\Omega \alpha \left| \frac{\partial \mathbf{m}}{\partial t} \right|^2 dv - \int_\Omega \mathbf{m} \cdot \frac{\partial \mathbf{h}_{\text{a}}}{\partial t} \, dv \quad . \tag{1.101}$$

Equation (1.101) is the energy balance relationship for magnetization dynamics. An interesting case occurs when the applied field is constant in time and, therefore, $\frac{\partial \mathbf{h}_{\text{a}}}{\partial t} = \mathbf{0}$. The energy balance equation becomes:

$$\frac{dg}{dt} = -\int_\Omega \alpha \left| \frac{\partial \mathbf{m}}{\partial t} \right|^2 dv \quad , \tag{1.102}$$

meaning that the free energy is a non-increasing function of time, since $\alpha \geq 0$. This property is often referred to as *Lyapunov structure* [82] of LLG equation. In particular, for $\alpha = 0$, one can observe that the free energy conservation holds:

$$g(t) = g(t_0) \quad \forall \; t, t_0 \quad . \tag{1.103}$$

The properties expressed by (1.97), (1.101) and (1.103) are very important constraints for magnetization dynamics. Since the solution of LLG equation cannot be obtained in exact analytical form, except some very particular cases, it is fundamental to derive numerical models that can reproduce this properties also in discrete dynamics. This issue will be addressed in detail in chapter 4.

Classical treatment of dissipation

It is possible to give a generalized form for introducing the dissipation in magnetization dynamics, through the so-called *Rayleigh dissipation function*. We focus now the attention on the case when $\frac{\partial \mathbf{h}_a}{\partial t} = \mathbf{0}$, without affecting the generality of the analysis. Let us suppose to assign the following function:

$$\mathcal{R}\left(\frac{\partial \mathbf{m}}{\partial t}\right) = \frac{1}{2}\int_\Omega \frac{\partial \mathbf{m}}{\partial t} \cdot \mathcal{A} \cdot \frac{\partial \mathbf{m}}{\partial t}\, dv \quad , \tag{1.104}$$

where $\mathcal{A}$ is a symmetric positive-definite second order tensor. Now, we can rewrite the Landau-Lifshitz-Gilbert equation (1.98) in the following way:

$$\frac{\partial \mathbf{m}}{\partial t} = -\mathbf{m} \times \left(-\frac{\delta g}{\delta \mathbf{m}} - \frac{\delta \mathcal{R}}{\delta \frac{\partial \mathbf{m}}{\partial t}}\right) , \tag{1.105}$$

where the variational derivative of the Rayleigh function determines the 'viscous force' acting during magnetization motion. The important property of this formulation lies in the fact that equilibrium configurations remain unchanged after the introduction of the dissipation, as one can see from the observation of the Rayleigh function (1.104). Now, if we scalar multiply both members of Eq. (1.105) by $\frac{\delta g}{\delta \mathbf{m}} + \frac{\delta \mathcal{R}}{\delta \frac{\partial \mathbf{m}}{\partial t}}$ and integrate over the volume Ω, we end up with:

$$\frac{dg}{dt} = -\int_\Omega \frac{\delta \mathcal{R}}{\delta \frac{\partial \mathbf{m}}{\partial t}} \cdot \frac{\partial \mathbf{m}}{\partial t}\, dv \quad . \tag{1.106}$$

By applying Euler's theorem on homogeneous functions, the latter equation becomes:

$$\frac{dg}{dt} = -2\mathcal{R} = -\int_\Omega \frac{\partial \mathbf{m}}{\partial t} \cdot \mathcal{A} \cdot \frac{\partial \mathbf{m}}{\partial t}\, dv \quad . \tag{1.107}$$

The choice of Gilbert damping corresponds to assume

$$\mathcal{A} = \alpha \mathcal{I} \quad , \tag{1.108}$$

where $\mathcal{I}$ is the identity tensor and α is the Gilbert damping constant. Such an approach can be generalized if $\mathcal{A}$ is a self-adjoint operator in a suitable function space. An example of this is considered in Ref. [82], where an additional term is considered in the Rayleigh function involving the time derivative of the spatial gradient of magnetization vector field. Moreover, in Ref. [82] the most general gyromagnetic precessional equation is reported, which includes both the cases of Landau-Lifshitz and Landau-Lifshitz-Gilbert equations.

Chapter 2

Uniformly magnetized particles

The purpose of this chapter is to show that some dynamical magnetic phenomena which are connected with technological applications, as for example magnetic storage, can be studied with analytical approach. More specifically, the control parameters, namely the quantities that the experimenter can vary at his will, can be found as analytical expression.

The only assumption of this approach is that no space dependance of the magnetization vector field $\mathbf{m}$ is considered. In other words, we suppose to deal with uniformly magnetized particles.

In this respect, the first model to explain the hysteretic behavior of suitable uniformly magnetized particles was proposed by Stoner and Wohlfarth in 1948. With this model it is possible to derive equilibrium configurations of magnetization, when the particle is subject to an external field. In the following we will describe briefly the basic ideas of the Stoner-Wohlfarth model, which is a static model as well as Brown's equation presented in the previous chapter.

Then, the problem of switching the magnetization in thin-films is analyzed. In this respect, two different magnetization switching processes are presented. For both of them analytical predictions are present in literature, which will be briefly reported. Next, the issue of finding quasi-periodic solutions of LLG equation under circularly polarized field is addressed. This situation commonly arises when typical ferromagnetic resonance experiments are considered. Finally the self-oscillating behavior of LLG equation with spin-transfer torque term is investigated and analytical results regarding critical values of the control parameters are derived. This topic has been recently under the focus of considerable research for its applications to magnetic recording devices and microwave electronics.

2.1 The uniform mode approximation

In many technological applications, where the size of the magnetic media has reached the nanometric scale, it is reasonable to assume that the exchange in-

teraction is prevalent with respect to the others and, therefore, that the particle tends to be uniformly magnetized. In other words, the uniform mode is energy-favored with respect to disuniformities as soon as the characteristic dimension of the body is comparable or even smaller than the exchange length. In this framework, it does make sense to neglect non-uniform modes and consider the particle as uniformly magnetized. This has considerable simplifications as far as the mathematical model is concerned, but nevertheless the uniform mode analysis can give, in certain applications, very interesting analytical indications and, in some cases, the predictions are also very accurate with respect to non-uniform micromagnetic simulations, as we will see in the following chapter. Last but not least, the uniform mode analysis has been used for long time in the design of magnetic recording devices. In our analysis we will use quite extensively the tools provided by dynamical systems theory [43], since in the case of single domain particle we deal with low dimensional systems (2D and 3D).

2.2 The static model. Stoner-Wohlfarth theory

We start our discussion from the static model proposed by Stoner and Wohlfarth [77] in 1948. Basically it can be obtained from the study of the Brown's equations in the case of appropriate single domain particle. Below we summarize the basic hypotheses of this model:

1. Single domain particle
2. Spheroidal geometry
3. Uniaxial anisotropy along the rotational-symmetry axis.

First, assuming uniform magnetization within the body, the exchange energy (1.38) gives zero contribution to the free energy. Next, the ellipsoidal geometry permits a significant simplification in the computation of magnetostatic field, since it can be shown that it can be expressed by a straightforward tensorial relationship with magnetization [12]:

$$\mathbf{H}_{\mathrm{m}} = -\mathcal{N} \cdot \mathbf{M} \quad , \tag{2.1}$$

where $\mathcal{N}$ is the so-called *demagnetizing tensor* which is always positive semidefinite. By expressing $\mathcal{N}$ with respect to its principal axes x, y, z, which coincide with the principal axes of the ellipsoid, one can rewrite Eq. (2.1) in the following way:

$$\begin{pmatrix} H_x \\ H_y \\ H_z \end{pmatrix} = - \begin{pmatrix} N_x & 0 & 0 \\ 0 & N_y & 0 \\ 0 & 0 & N_z \end{pmatrix} \cdot \begin{pmatrix} M_x \\ M_y \\ M_z \end{pmatrix} \quad , \tag{2.2}$$

where N_x, N_y, N_z are the demagnetizing factors such that $N_x + N_y + N_z = 1$. Then, the assumption of uniaxial anisotropy implies that the corresponding energy term is quadratic. For instance, if the easy axis is the $z-$axis, then $\mathbf{e}_{\text{an}} = \mathbf{e}_z$ and the anisotropy energy (1.43) becomes:

$$F_{\text{an}}(\mathbf{m}) = K_1(1 - m_z^2)\, V_0 \quad , \tag{2.3}$$

where V_0 is the volume of the spheroidal particle. Finally, the hypothesis of rotational symmetry implies that

$$N_x = N_y = N_\perp \quad . \tag{2.4}$$

Under these assumptions, the expression of the free energy is the following:

$$G(\mathbf{m}, \mathbf{H}_{\text{a}}) = K_1(1 - m_z^2)\, V_0 + \frac{1}{2}\mu_0 M_s^2 \mathbf{m} \cdot \mathcal{N} \cdot \mathbf{m}\, V_0 - \mu_0 M_s \mathbf{m} \cdot \mathbf{H}_{\text{a}}\, V_0 \quad . \tag{2.5}$$

From now on, we will carry out the derivation with dimensionless quantities. Thus, by dividing both members by $\mu_0 M_s^2 V_0$ and remembering that $1 - m_z^2 = m_x^2 + m_y^2$, one obtains:

$$g(\mathbf{m}, \mathbf{h}_{\text{a}}) = \frac{K_1}{\mu_0 M_s^2}(1 - m_z^2) + \frac{1}{2}N_\perp(1 - m_z^2) + \frac{1}{2}N_z m_z^2 - \mathbf{m} \cdot \mathbf{h}_{\text{a}} \quad , \tag{2.6}$$

where the expression of magnetostatic energy has been explicitly developed. By collecting terms in m_z^2 one ends up with:

$$g(\mathbf{m}, \mathbf{h}_{\text{a}}) = \frac{K_1}{\mu_0 M_s^2} + \frac{1}{2}N_\perp + \left(\frac{1}{2}N_z - \frac{K_1}{\mu_0 M_s^2} - \frac{1}{2}N_\perp\right) m_z^2 - \mathbf{m} \cdot \mathbf{h}_{\text{a}} \quad . \tag{2.7}$$

By neglecting constant terms (which disappear in a minimization procedure) and by factorizing the expression in parenthesis we end up with:

$$g(\mathbf{m}, \mathbf{h}_{\text{a}}) = -\frac{1}{2}\left(N_\perp + \frac{2K_1}{\mu_0 M_s^2} - N_z\right) m_z^2 - \mathbf{m} \cdot \mathbf{h}_{\text{a}} \quad . \tag{2.8}$$

With the position:

$$k_{\text{eff}} = N_\perp + \frac{2K_1}{\mu_0 M_s^2} - N_z \quad , \tag{2.9}$$

the latter equation assumes the simple form:

$$g(\mathbf{m}, \mathbf{h}_{\text{a}}) = -\frac{1}{2}k_{\text{eff}} m_z^2 - \mathbf{m} \cdot \mathbf{h}_{\text{a}} \quad . \tag{2.10}$$

It is important to notice that, in the case of rotationally-symmetric ellipsoidal particle, magnetostatic interaction energy is a quadratic form in m_z as uniaxial anisotropy energy. For this reason it is often said in literature that the quantity k_{eff} takes into account *shape and crystalline anisotropy*, although they have very

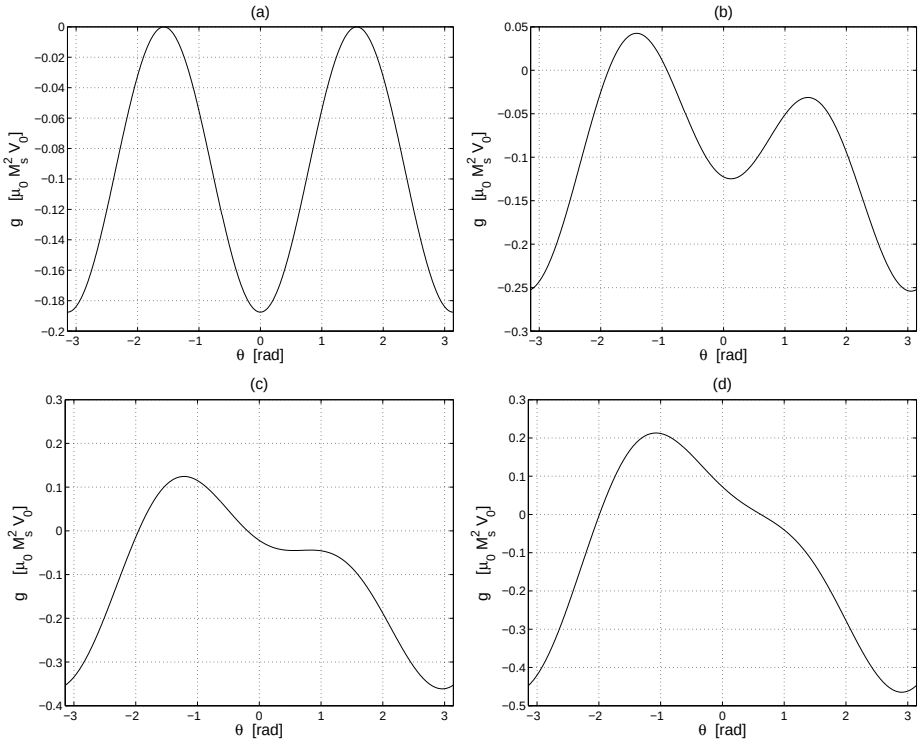

Figure 2.1: Free energy as a function of angle θ, $k_{\rm eff} > 0$. (a) for $h_a = 0$ two minima $\theta = 0, \pi$ and two maxima $\theta = \pm\pi/2$ exist. (b) for small h_a with given $\theta_h \neq 0$ there still exist two minima and two maxima. (c) a critical value $h_{\rm SW}(\theta_h)$ of h_a exist such that a saddle point appears in place of one minimum and one maximum. (d) for $h_a > h_{\rm SW}(\theta_h)$ only one minimum and one maximum remain.

different physical meanings[1]. We observe that, for symmetry reasons, at the equilibrium the magnetization lies in the plane defined by the easy axis $\mathbf{e}_z$ and the applied field $\mathbf{h}_{\rm a}$. At this point, it is useful to introduce the spherical angles θ, θ_h between $\mathbf{m}$, $\mathbf{h}_{\rm a}$ and $\mathbf{e}_z$, respectively. In this respect, one has:

$$m_z = \cos\theta \quad , \quad \mathbf{m}\cdot\mathbf{h}_{\rm a} = h_a\cos(\theta_h - \theta) \quad . \tag{2.11}$$

By using these expressions in Eq. (2.10) one obtains:

$$\begin{aligned} g(\theta,\theta_h) &= -\frac{1}{2}k_{\rm eff}\cos^2\theta - h_a\cos(\theta_h-\theta) = \\ &= -\frac{1}{2}k_{\rm eff}\cos^2\theta - h_a\cos\theta_h\cos\theta - h_a\sin\theta_h\sin\theta = \\ &= -\frac{1}{2}k_{\rm eff}\cos^2\theta - h_{az}\cos\theta - h_{a\perp}\sin\theta \quad , \end{aligned} \tag{2.12}$$

where h_{az} and $h_{a\perp}$ are respectively the parallel and perpendicular component of the applied field with respect to $z-$axis. Let us now suppose that no field is

[1]The term shape anisotropy recalls the fact that magnetostatic field depends on the geometry of the body, whereas the crystalline anisotropy depends on the lattice structure of the material.

applied and that the particle is initially magnetized along the positive $z-$axis ($\theta = 0$). In this situation, the particle minimizes its energy and therefore this is an equilibrium position, as well as the reversed orientation $\theta = \pi$ (see Fig. 2.1a). The energy is instead maximum for $\theta = \pm\pi/2$. Now, if we apply a small external field, opposite to the initial magnetization ($\theta_h = 0$), the free energy (2.10) will still have two minima and two maxima. By further increasing h_a we arrive at a critical configuration for which one minimum and one maximum disappear. We call h_{SW} the applied field value corresponding to this critical situation. If we increase $h_a > h_{\mathrm{SW}}$ only one minimum and one maximum of the free energy will exist. This means that for fields $h_a < h_{\mathrm{SW}}$ the particle will remain in the initial configuration along z, whereas as soon as $h_a > h_{\mathrm{SW}}$ the magnetization will switch to the only remaining energy minimum, corresponding to the reversed orientation.

It is important to underline that, in the general case (see Fig. 2.1), the critical field h_{SW} will be a function of θ_h. Thus, the idea of Stoner-Wohlfarth model, is to represent, in the control plane (h_a, θ_h in polar coordinates, or equivalently $h_{az}, h_{a\perp}$ in cartesian coordinates), the separating curve between the region where two minima exist and the region where only one minimum remains. This bifurcation line justifies the switching behavior. It can be found analytically by means of the following relationship:

$$\frac{\partial g}{\partial \theta} = 0 \quad , \quad \frac{\partial^2 g}{\partial \theta^2} = 0 \quad , \tag{2.13}$$

which determines the saddle points of the free energy in the $h_{az}, h_{a\perp}$ plane. By imposing the above conditions, one ends up with the following equations:

$$\begin{cases} \dfrac{h_{a\perp}}{\sin\theta} - \dfrac{h_{az}}{\cos\theta} = k_{\mathrm{eff}} \\ \dfrac{h_{a\perp}}{\sin^3\theta} + \dfrac{h_{az}}{\cos^3\theta} = 0 \end{cases} \tag{2.14}$$

By solving these equations one ends up with the parametric expression of the bifurcation line, which is referred to as the *Stoner-Wohlfarth astroid*:

$$\begin{cases} h_{az} = -k_{\mathrm{eff}} \cos^3\theta \\ h_{a\perp} = k_{\mathrm{eff}} \sin^3\theta \end{cases} \tag{2.15}$$

The curve defined by the latter equations is represented in Fig. 2.2. The polar representation can be also found:

$$h_a = k_{\mathrm{eff}} (\sin^{2/3}\theta_h + \cos^{2/3}\theta_h)^{-3/2} \quad . \tag{2.16}$$

In the particular case of $\theta_h = 0$, one can easily verify that

$$h_{\mathrm{SW}} = k_{\mathrm{eff}} = N_\perp + \frac{2K_1}{\mu_0 M_s^2} - N_z \quad . \tag{2.17}$$

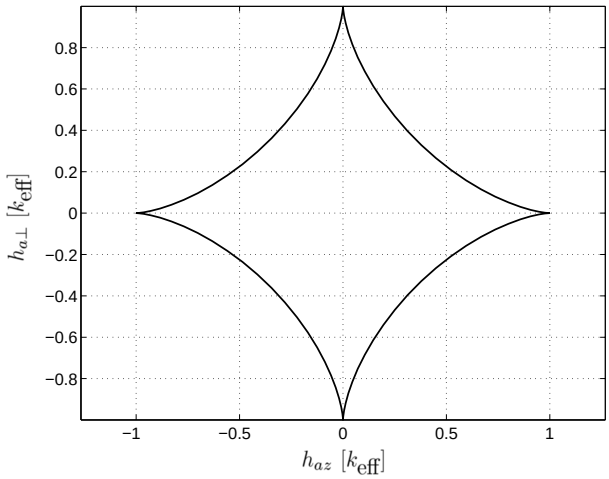

Figure 2.2: The Stoner-Wohlfarth astroid in the $h_{az}, h_{a\perp}$ plane.

Thus, when the external field has components such that the point $(h_{az}, h_{a\perp})$ lies outside the astroid, only one minimum of the free energy is present and magnetization will end up there. For example, in the case of initial magnetization $\mathbf{m} = \mathbf{e}_z$, the application of an external field along $\mathbf{e}_z$ with amplitude h_a greater than the critical value computed from Eq. (2.17), the switching of the particle occurs. In fact, the initial configuration is no longer stable and the only minimum of the free energy (stable equilibrium) remains $\mathbf{m} = -\mathbf{e}_z$.

Conversely, as soon as the field is such that the point $(h_{az}, h_{a\perp})$ lies inside the astroid, the situation is more complicated since there exist still two minima of the free energy, namely two stable equilibria. Which one will be reached by magnetization depends on the dynamics of magnetization motion, which is not described by the Stoner-Wohlfarth model. In this situation, one can say that the switching from one minimum to the other is not precluded, but is not guaranteed. Recently, the possibility to obtain magnetization switching with field amplitudes below the Stoner-Wohlfarth limit has been investigated. We will discuss this possibility in the following sections and in chapter 3.

2.3 UNIFORM MODE MAGNETIZATION DYNAMICS

The Stoner-Wohlfarth model has been extensively used to explain the occurrence of hysteresis loops in the $M - H$ relationship for magnetic recording media (see Fig. 2.3). Nevertheless, as far as magnetic storage devices are required to be faster and faster, and on the other hand the dimensions of magnetic media decrease more and more, the inclusion of dynamical effects in the switching analysis becomes unavoidable. For this reason, we start our analysis from uniform mode dynamics,

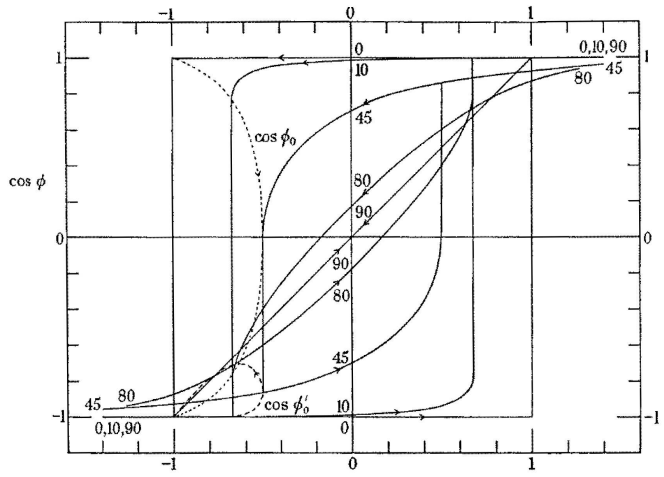

Figure 2.3: Stoner-Wohlfarth model. Picture of hysteresis loops from the original paper [77] for different applied field directions. The external field in abscissa is measured in units of k_{eff}. Magnetization in ordinate is measured in units of M_s.

which is governed by the Landau-Lifshitz-Gilbert equation (1.95) rewritten in case of spatial magnetization uniformity:

$$\frac{d\mathbf{m}}{dt} = -\mathbf{m} \times \mathbf{h}_{\text{eff}} + \alpha \mathbf{m} \times \frac{d\mathbf{m}}{dt} \quad , \tag{2.18}$$

where the effective field and the free energy have now the simple expressions:

$$\mathbf{h}_{\text{eff}}(\mathbf{m}, t) = -\frac{\partial g}{\partial \mathbf{m}} = -D_x m_x \mathbf{e}_x - D_y m_y \mathbf{e}_y - D_z m_z \mathbf{e}_z + \mathbf{h}_{\text{a}}(t) \quad , \tag{2.19}$$

$$g(\mathbf{m}, \mathbf{h}_{\text{a}}) = \frac{1}{2} D_x m_x^2 + \frac{1}{2} D_y m_y^2 + \frac{1}{2} D_z m_z^2 - \mathbf{h}_{\text{a}} \cdot \mathbf{m} \quad . \tag{2.20}$$

The coefficients D_x, D_y, D_z take into account shape and crystalline anisotropy. Assuming that the uniaxial anisotropy is along the x axis, the relationship of the D coefficients with material parameters and demagnetizing factors is the following:

$$D_x = N_x - \frac{2K_1}{\mu_0 M_s^2} \quad , \quad D_y = N_y \quad , \quad D_z = N_z \quad . \tag{2.21}$$

In this framework the LLG equation defines a dynamical system evolving on the unit-sphere $|\mathbf{m}| = 1$, according to property (1.97). If we assume that the external field $\mathbf{h}_{\text{a}}$ is constant, LLG equation (2.18) describes an autonomous dynamical system whose phase space is 2D, and therefore, it cannot exhibit chaotic behavior [22, 23]. Moreover, by recalling the Lyapunov structure (1.102) of LLG equation for constant field, which states that energy is a decreasing function of time ($\alpha > 0$), one can immediately conclude that the only steady solutions are fixed points. The number of these fixed points is at least two and in any case is even, due to Poincaré index theorem [43]. Thus, any bifurcation of fixed points

involves two equilibria at the same time. The fixed points of the dynamics can be computed from the following equations:

$$\begin{cases} \mathbf{m} \times \mathbf{h}_{\text{eff}}(\mathbf{m}) = \mathbf{0} \quad \Leftrightarrow \quad \mathbf{h}_{\text{eff}}(\mathbf{m}) = \lambda \mathbf{m} \quad , \\ |\mathbf{m}| = 1 \quad , \end{cases} \tag{2.22}$$

in the four scalar unknowns $\mathbf{m} = (m_x, m_y, m_z)$ and λ. Conversely, if the applied field is time-varying the onset of chaos and self-oscillating behavior cannot be excluded in principle [24], but there exist particular cases in which the non-autonomous system can be reduced to an autonomous one by means of appropriate change of the reference frame. An example of this occurrence will be examined in section 2.5 when the dynamics of rotationally-symmetric particles subject to circularly polarized field will be analyzed.

In the following sections, extensively use of the *phase portraits* [43] of dynamical system (2.18) will be made. In many cases it is convenient to project the unit-sphere on the plane to visualize the structure of the LLG vector field. This can be done by means of the stereographic projection which maps the coordinates m_x, m_y, m_z onto w_1, w_2 according to the following transformation:

$$w_1 = \frac{m_x}{1 + m_z} \quad , \quad w_2 = \frac{m_y}{1 + m_z} \quad . \tag{2.23}$$

This stereographic projection has a geometric interpretation, sketched in Fig. 2.4 for the case of $\alpha = 0$. The points along $x-$axis $\mathbf{m} = (\pm 1, 0, 0)$ are mapped to $(w_1, w_2) = (\pm 1, 0)$, while the points along $y-$axis $\mathbf{m} = (0, \pm 1, 0)$ are mapped to $(w_1, w_2) = (0, \pm 1)$. The north pole $\mathbf{m} = (0, 0, 1)$ is mapped to $(w_1, w_2) = (0, 0)$, whereas the south pole $\mathbf{m} = (0, 0, -1)$ is mapped towards infinity onto the plane. Moreover, image through Eq. (2.23) of closed curves on the unit-sphere remain closed, and also angles are preserved. In the derivation of phase portraits of the dynamical system (2.18) we will need to perform numerical integration of LLG equation. We will adopt the numerical semi-implicit scheme proposed in Ref. [25], which in spite of low computational effort, preserves the magnetization magnitude conservation property (1.97). Geometric integration of Landau-Lifshitz-Gilbert equation will be discussed deeply in chapter 4.

2.4 MAGNETIZATION SWITCHING PROCESS

In this section we will present the analysis, in the framework of dynamical systems theory, of some relevant technological applications connected with magnetic recording devices. In particular, we will focus our attention on magnetization reversal processes, commonly referred to as *magnetization switching processes*.

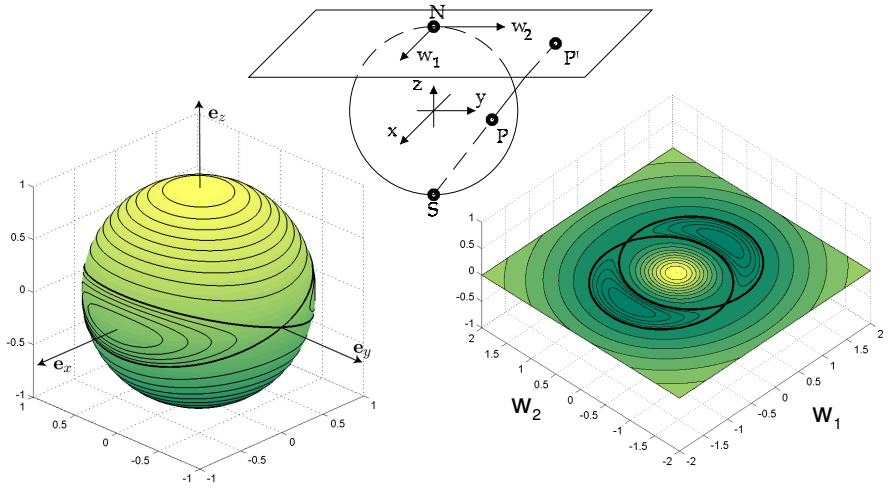

Figure 2.4: Stereographic projection of the unit-sphere on the plane for the case of $\alpha = 0$.

Basically, if we assume that initially the magnetization is aligned in the positive easy axis direction (for example corresponding to the bit value 0), the switching problem consists in manipulating the control variables in order to drive definitely magnetization into the opposite orientation (bit 1). At present time, there are more than one way to achieve switching. The conventional way obtains the switching by using magnetic field produced by external currents, and this technique is mostly used in hard disks realizations. Recently, the possibility of using spin-polarized currents, injected directly into the ferromagnetic medium, has been investigated both experimentally and theoretically. This way to control switching has considerable applications in MRAMs technology, since in this way it is possible to circumvent the difficulty of generating magnetic fields that switch only the target cell. The spin-polarized current driven switching will be analyzed in section 2.6.

2.4.1 Critical parameters for magnetization switching

Before starting to analyze specific kinds of switching processes, it is convenient to indicate what we mean with critical parameters. In this respect, let us refer to the case of switching with external magnetic fields. Generally, at time instant $t = 0$, a field pulse is applied to realize switching. Referring for sake of simplicity to a rectangular pulse (see Fig. 2.5), we can say that our critical parameters are:

- Applied field direction.

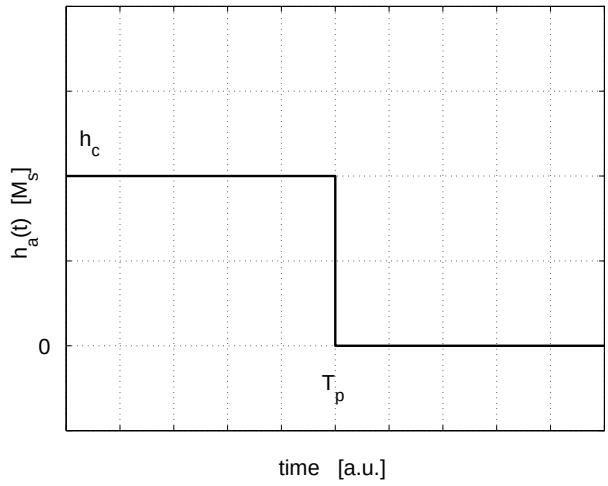

Figure 2.5: Design parameters for external field pulse amplitude.

- Minimum field pulse amplitude h_c to obtain successful switching.
- Minimum field pulse duration T_p to obtain successful switching.
- Switching time, namely the time instant T_s at which magnetization is approximately in the reversed orientation.

Generally, given an applied field direction, the critical pulse amplitude h_c can be found as a function of material parameters K_1, M_s and shape parameters N_x, N_y, N_z (or equivalently coefficients D_x, D_y, D_z). Then, the time T_p, as well as the time instant T_s, will be a function of the field amplitude h_c.

Next we report some recent results present in literature regarding two different ways to achieve magnetization switching: the so-called "damping switching" and "precessional switching". We refer to the derivations worked out in Refs. [26, 27] for the former and in Refs. [28, 35] for the latter. These results are very important since in chapter 3 we will demonstrate that some of them can be used to predict the values of control parameters in micromagnetic (non-uniform) simulations of switching processes for thin-films having spatial dimensions of technological interest.

2.4.2 DAMPING SWITCHING

The traditional mode to realize the switching is the one sketched in Fig. 2.6 and it is here referred to as "damping switching" following a terminology introduced by Mallinson [26]. The switching is realized by applying the external field in the direction opposite to the initial magnetization state. If the field is strong enough (the threshold field can be computed by the Stoner-Wohlfarth theory) the initial

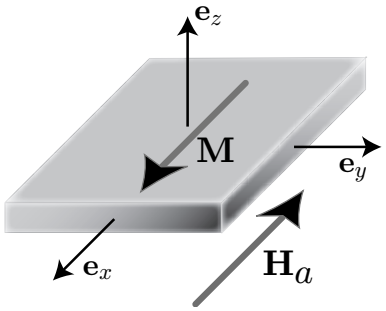

Figure 2.6: Typical mode of operation in damping switching: the field is applied against the initial magnetization.

magnetization state becomes unstable and magnetization dynamics tends to relax toward the new minimum of energy in the direction of the applied field. In the following the analytical treatment of damping switching will be presented. This is possible indeed only in the special case in which the magnetic body is rotationally symmetric around a certain axis and the external field is applied exactly along the symmetry axis. If the symmetry axis is $\mathbf{e}_z$, the effective field is given by the formula

$$\mathbf{h}_{\text{eff}} = -D_{\perp}(m_x\mathbf{e}_x + m_y\mathbf{e}_y) - D_z m_z\mathbf{e}_z + \mathrm{h}_{az}\mathbf{e}_z \tag{2.24}$$

Here, coefficients $D_{\perp} = N_{\perp}$ and $D_z = N_z - (2K_1)/(\mu_0 M_s^2)$ account for demagnetizing fields and crystalline anisotropy, while h_{az} is the applied field, which is assumed to be constant during the pulse duration. R. Kikuchi [30] considered a similar problem for the case of isotropic ferromagnetic sphere when the effective field is defined by the formula:

$$\mathbf{h}_{\text{eff}} = -D\mathbf{m} + \mathrm{h}_{az}\mathbf{e}_z \tag{2.25}$$

The difference in the mathematical forms of the effective fields (2.24) and (2.25) results in the profound difference in the physical phenomena of magnetization switching. In the case of effective field (2.25), there exists an infinite set of equilibrium states for $\mathrm{h}_{az} = 0$ and no critical field is required to switch from one equilibrium state to another. In the case of effective field (2.24), there are only two equilibrium states for $\mathrm{h}_{az} = 0$ with $m_z = 1$ and $m_z = -1$, respectively, and the switching from one equilibrium state to another is only possible if the applied field h_{az} exceeds some critical field h_c.

J. Mallinson [26] studied the problem with the effective field given by the formula (2.24). His analysis is based on the solution of LLG equation in spherical coordinates. Conversely, the following approach exploits the rotational symmetry of the problem.

It is apparent that the mathematical form of LLG equation with the effective field equation given by Eq. (2.24) is invariant with respect to rotations of coordinate axes x and y around z axis. As a results of this rotational symmetry, it is expected that dm_z/dt depends only on the z-component of $\mathbf{m}$. Indeed, by using simple algebra, it is easy to find that:

$$(\mathbf{m}\times\mathbf{h}_{\text{eff}})\cdot\mathbf{e}_z = 0\,, \qquad [\mathbf{m}\times(\mathbf{m}\times\mathbf{h}_{\text{eff}})]\cdot\mathbf{e}_z = (\mathrm{h}_{az}-\mathrm{h}_c m_z)(1-m_z^2)\,, \quad (2.26)$$

where

$$\mathrm{h}_c = D_\perp - D_z = h_{\text{SW}} \quad , \tag{2.27}$$

is the classical Stoner-Wohlfarth field (see Eq. (2.17)). Thus from LLG equation and from Eqs. (2.26), we derive the following equation

$$\frac{dm_z}{dt} = \frac{\alpha}{1+\alpha^2}(\mathrm{h}_c m_z - \mathrm{h}_{az})(1-m_z^2) \tag{2.28}$$

It is clear from Eq. (2.28) that the magnetization switching from the state $m_z = 1$ to the state $m_z = -1$ (or vice versa) is driven exclusively by damping: in the conservative case $\alpha = 0$ the z-component of magnetization remains constant. In this sense, this switching can be regarded as "damping" switching. It seems from Eq. (2.28) that no switching is possible if magnetization is in equilibrium state $m_z = 1$. However, due to thermal effects, magnetization $\mathbf{m}$ slightly fluctuates around the above equilibrium state. As a result, the value of m_z at the instant when the applied field is turned on may be slightly different from 1 and the switching process can take place.

This argument justifies the solution of Eq. (2.28) with the initial condition:

$$m_z(t=0) = \mathrm{m}_{z0} \tag{2.29}$$

where m_{z0} is close to 1. It is apparent from Eq. (2.28) that if $\mathrm{h}_{az} > \mathrm{h}_c$ then $dm_z/dt < 0$ and the switching to the equilibrium state $m_z = 1$ will proceed for any m_{z0}. On the other hand, if $\mathrm{h}_{az} < \mathrm{h}_c$, then for m_{z0} sufficiently close to 1 it can be found from Eq. (2.28) that $dm_z/dt > 0$ and no switching is possible. This clearly reveals that h_c has the meaning of critical field. In the sequel, it is assumed that $\mathrm{h}_{az} > \mathrm{h}_c$.

By separating variables in Eq. (2.28), we obtain:

$$\int_{\mathrm{m}_{z0}}^{m_z} \frac{dm_x}{(1-m_z^2)(\mathrm{h}_c m_z - \mathrm{h}_{az})} = \frac{\alpha}{1+\alpha^2}\,t\,. \tag{2.30}$$

Performing integration, one obtains:

$$\frac{1}{2(\mathrm{h}_{az}-\mathrm{h}_c)}\ln\frac{1-m_z}{1-\mathrm{m}_{z0}} - \frac{1}{2(\mathrm{h}_{az}+\mathrm{h}_c)}\ln\frac{1+m_z}{1+\mathrm{m}_{z0}} + \\ + \frac{\mathrm{h}_c}{\mathrm{h}_c^2-\mathrm{h}_{az}^2}\ln\frac{\mathrm{h}_{az}-\mathrm{h}_c m_z}{\mathrm{h}_{az}-\mathrm{h}_c \mathrm{m}_{z0}} = \frac{\alpha}{1+\alpha^2}\,t \tag{2.31}$$

By using the last equation, the minimal pulse time needed for switching can be found. Indeed, if the duration of magnetic field pulse is such that a negative value of m_z is reached, then the magnetization will be in the basin of attraction of the equilibrium state $m_z = -1$, and the switching will be achieved. This can be clearly seen by setting $m_z = 0$ into Eq. (2.28), which implies $dm_z/dt < 0$ for $\mathrm{h}_{az} > h_c$. Thus, the minimal time can be found from Eq. (2.31) and the condition $m_z = 0$. By taking into account formula (2.31) and the fact that time and magnetic field in this formula are normalized by $\gamma \mathrm{M_s}$ and $\mathrm{M_s}$, respectively, we derive the following expression for the minimal pulse time T_p mentioned in section 2.4.1:

$$T_p = \frac{1+\alpha^2}{\alpha\gamma}\left[\frac{\ln(1-\cos\theta_0)}{2(\mathrm{H}_c-\mathrm{H}_{az})} + \frac{\ln(1+\cos\theta_0)}{2(\mathrm{H}_c+\mathrm{H}_{az})} + \frac{\mathrm{H}_c}{\mathrm{H}_c^2-\mathrm{H}_{az}^2}\ln\frac{\mathrm{H}_{az}}{\mathrm{H}_{az}-\mathrm{H}_c\cos\theta_0}\right] . \tag{2.32}$$

Here $\mathrm{H}_c = (D_\perp - D_z)\mathrm{M_s}$ and $\mathrm{m}_{z0} = \cos\theta_0$, where θ_0 is the angle formed by the initial magnetization with z-axis.

It is interesting to point out that for the typical case of small angles θ_0, the minimal pulse time T_p is very close to the actual switching time T_s (see section 2.4.1) at which m_z reaches a value almost equal to -1. This is because, for sufficiently small m_z (large angles θ), m_z decreases much faster (see Eq. (2.28)) than when m_z is close to its equilibrium values. This assertion is supported by numerical calculations, performed by using the analytical expression for m_z extracted from formula (2.31) and shown in Fig. 2.7.

It is apparent from this figure that the initial (near equilibrium) dynamics of m_z is very slow and takes most of the time, while the magnetization dynamics away from equilibrium is very fast. Thus, the switching time is close to the minimal pulse field time, calculated above:

$$T_s \simeq T_p \quad . \tag{2.33}$$

It is also apparent from formula (2.32) that for the typical case of very small initial angles θ_0, the first term in the right hand side of formula (2.32) is dominant. Thus, by neglecting two other terms and using simple trigonometry, one can derive the following expression for the minimal pulse time (switching time):

$$\frac{1}{T_p} = \frac{1}{\ln(\sqrt{2}/\theta_0)}\frac{\alpha\gamma}{(1+\alpha^2)}(\mathrm{H}_{az}-\mathrm{H}_c) . \tag{2.34}$$

It turns out from Eq. (2.34) that, for short pulse duration T_p, the value of applied field needed for switching increases inversely proportional to T_p, i.e. $\mathrm{H}_{az} \sim 1/T_p$. In this sense, one may say that the dynamic (short-time) coercivity appreciably exceeds the static coercivity H_c. The last formula is also similar to the one that

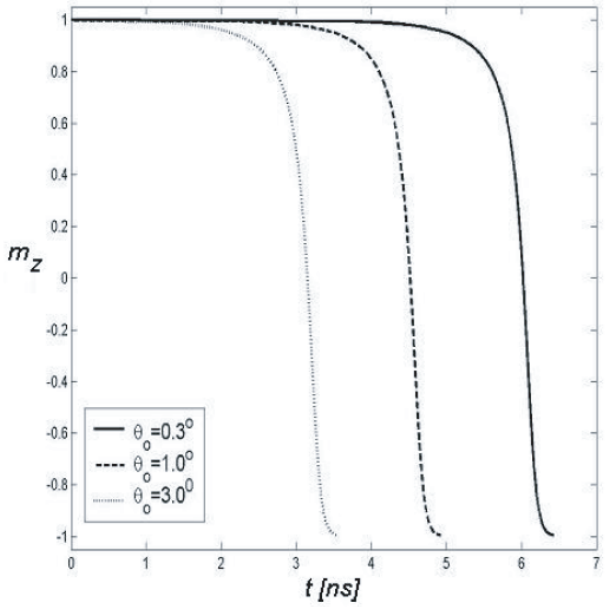

Figure 2.7: Evolution of m_z with time for different initial angles $\theta_0 = 0.3^o, 1^o, 3^o$. $\mathrm{H}_{az}/H_c = 1.2$.

has been observed in numerous experiments [31], [32], [33]. It is usually written in the form:

$$\frac{1}{T_p} = \frac{1}{S}(\mathrm{H}_{az} - \mathrm{H}_c)\,. \tag{2.35}$$

The switching time (see formulas (2.32), (2.34)) depends on the value of initial angle θ_0. An expected value of this angle can be evaluated by using Maxwellian equilibrium distribution for θ_0:

$$\rho(\theta_0) = c\sin\theta_0 \exp\left[\frac{-g(\mathbf{m})}{kT}\right] = c\sin\theta_0 \exp\left[-\frac{\mu_0(D_\perp - D_z)\mathrm{M_s^2}V_0\cos\theta_0}{k_BT}\right], \tag{2.36}$$

where k_B is the Boltzmann constant, c an appropriate constant to normalize the integral of the distribution, μ_0 the vacuum magnetic permeability, and V_0 is the volume of the magnetic body. If we assume that the magnetic body is a Permalloy film with dimension (0.5 μm, 0.5 μm, 10 nm), the typical expected value of θ_0 is 0.5^o. The expected value of θ_0 is increased as the volume dimensions are decreased.

2.4.3 PRECESSIONAL SWITCHING

Precessional switching is a new strategy to realize magnetization reversal which has been recently the focus of considerable research [34],[37]. In the usual switching process, the external field is applied in the direction opposite to the initial

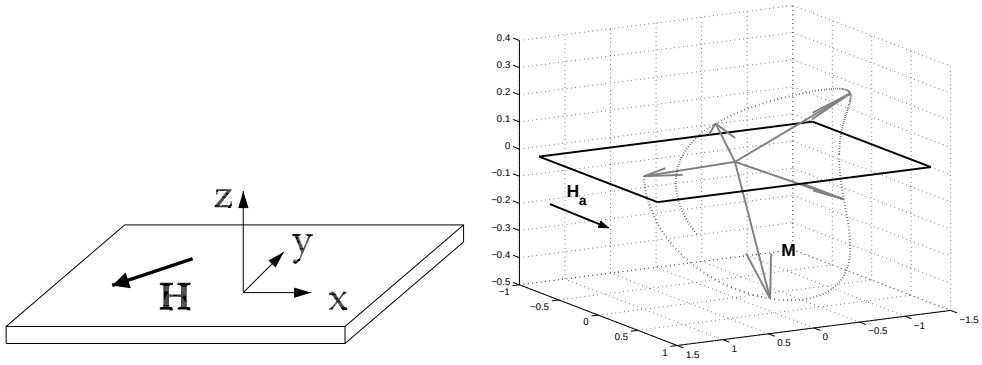

Figure 2.8: (left) Magnetic thin film subject to in-plane applied field. (right) Example of precessional motion of magnetization for in-plane applied field.

magnetization and the reversal is achieved after several precessional oscillations due to dissipative effects [26]. In precessional switching, the field is applied at a certain angle (usually orthogonal) with respect to initial magnetization in order to use the associated torque to control magnetization precessional motion. In fact, this torque pushes the magnetization out-of-plane, creating a strong demagnetizing field in the direction perpendicular to the film plane. Then the magnetization start to precess around the demagnetizing field (see Fig. 2.8). The reversal is obtained after half precessional oscillation and it is realized by switching the external field off precisely when the magnetization is close to its reversed orientation. This kind of switching is usually much faster and it requires lower applied fields with respect to the traditional switching. However, the switching is realized only if the field pulse duration is accurately chosen. In the following, the analytical formula that provide this information is derived. We assume that the magnetic body has a thin-film like shape with $\mathbf{e}_z$ normal to the film plane (see Fig. 2.8).

Since the film is assumed to be very thin, the demagnetizing factors in the film plane N_x, N_y and perpendicular to the film N_z are practically equal to zero and -1, respectively. This leads to the following expression for the effective field:

$$\mathbf{h}_{\text{eff}}(\mathbf{m}) = (Dm_x - h_{ax})\mathbf{e}_x + h_{ay}\mathbf{e}_y - m_z\mathbf{e}_z\,, \tag{2.37}$$

where $D = 2K_1/(\mu_0 M_s^2)$ accounts for the in-plane x-axis anisotropy, and h_{ax}, h_{ay} are normalized components[2] of the applied magnetic field that is assumed to be constant during the pulse duration.

The magnetic free energy corresponding to the effective field (2.37) has the

[2]The external field is supposed to be $\mathbf{h}_{\text{a}} = -h_{ax}\mathbf{e}_x + h_{ay}\mathbf{e}_y$, with $h_{ax} > 0$.

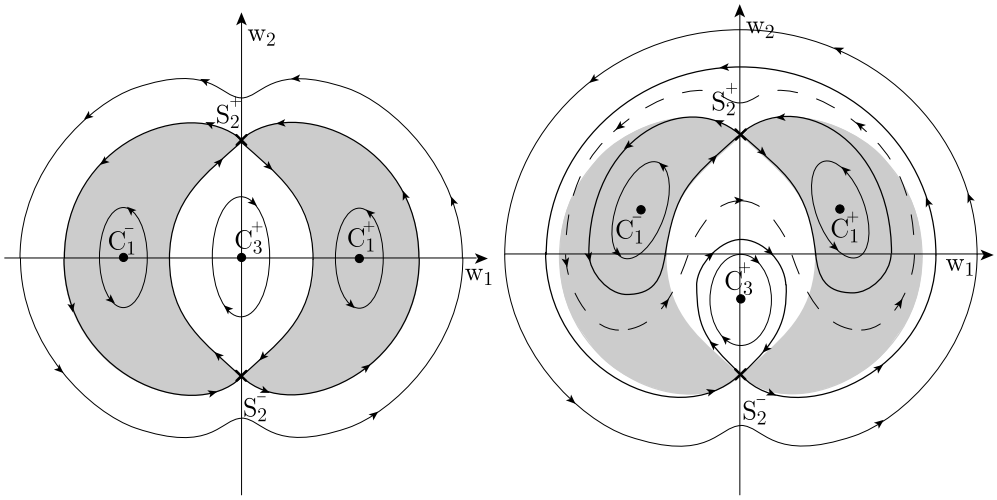

Figure 2.9: Sketch of the conservative phase portraits in the stereographic plane. (left) zero applied field. (right) the external field is applied along the y axis.

form

$$g(\mathbf{m}) = -\frac{1}{2}Dm_x^2 + \frac{1}{2}m_z^2 + h_{ax}m_x - h_{ay}m_y\,. \tag{2.38}$$

The precessional switching process consists of two stages: in the first stage the magnetization precesses under the influence of the applied external field until its orientation is almost reversed, in the second stage the external field is switched off and the magnetization undergoes relaxation oscillations toward the nearby equilibrium point. In the first part of the process, the magnetization dynamics is typically so fast that dissipative effects can be neglected. On the other hand, dissipation has to be taken into account during the relaxation process. For this reason, we shall first analyze the precessional switching dynamics in the conservative case $\alpha = 0$. The conservative phase portraits of the LLG equation, which can be obtained by plotting the contour lines of the energy function (2.38), can be conveniently represented in the plane by using the stereographic projection defined by Eqs. (2.23). The result is schematically depicted in Fig. 2.9.

In the case of zero applied field (Fig. 2.9 on the left), the phase portrait is characterized by 6 equilibrium points: the 4 centers C_1^+, C_1^-, C_3^+, $C_3^- = +\infty$, and the two saddles S_2^+, S_2^- doubly connected by heteroclinic trajectories. All trajectories, except the heteroclinic ones, circle around the centers. The two centers in the shaded regions are low energy states ($\mathbf{m}$ along the easy axis) while the centers C_3^+, $C_3^- = +\infty$ are high energy states. Notice that when no field is applied there is no way to reverse magnetization from one shaded region to the other.

In the case of field applied along the y axis, (see Fig. 2.9 on the right), the

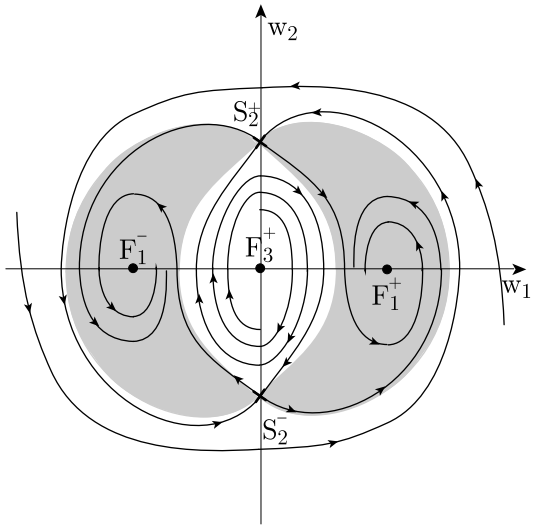

Figure 2.10: Sketch of the phase portrait on the stereographic plane in the case of zero applied field and $\alpha > 0$.

heteroclinic trajectories break into two homoclinic structures, one for each saddle. In this situation, along with trajectories that circle around centers, a new type of trajectories appears: the ones that encircle the saddle homoclinic structure (e.g. the dashed curve in Fig. 2.9, right). This type of trajectory allows the magnetization to move from one shaded region to another and, thus, to realize the switching. However, for a given initial condition, it is necessary a certain field amplitude (critical field for switching) for realizing the situation that the trajectory starting from that initial condition will enter the target shaded region. This aspect will be discussed later.

Once that magnetization has entered the target shaded region, the field can be switched off and the magnetization remains trapped around the target equilibrium. After certain time, the relaxation process will bring magnetization to the equilibrium. This stage of the switching process has to be analyzed in the dissipative case $\alpha > 0$. In this case, the phase portrait of LLG equation on the stereographic plane is sketched in Fig. 2.10. It can be observed that, with the introduction of damping, the Landau-Lifshitz-Gilbert equation (2.18) has now two stable equilibrium points $F_1^{\pm}$ with $\mathbf{m} = \pm\mathbf{e}_x$, two saddle points $S_2^{\pm}$ with $\mathbf{m} = \pm\mathbf{e}_y$, and two unstable equilibrium points $F_3^{\pm}$ with $\mathbf{m} = \pm\mathbf{e}_z$. In Fig. 2.10, shaded regions are the regions where the magnetic free energy is below the energy of the saddle points, while in white regions the energy is above the energy of the saddle points. Since the dissipation results in the decrease of the magnetic free energy, it can be concluded that the time evolution of magnetization within any shaded region inevitably leads to the focus inside that region. If the magnetiza-

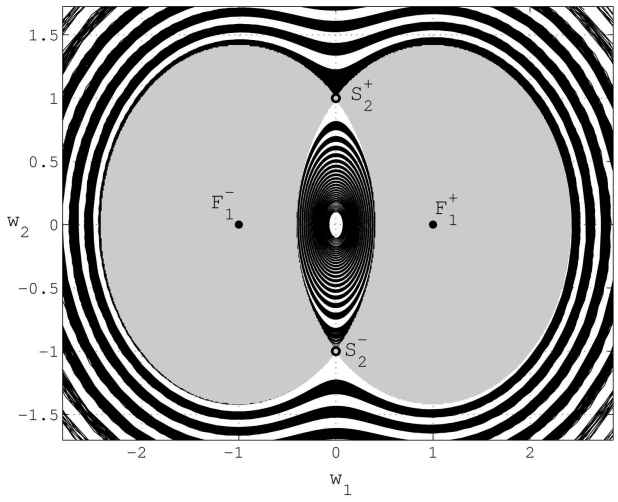

Figure 2.11: Numerically computed entangled structure of the basins of attraction for LLG equation with no applied field. The black region is the high energy portion of the basin of attraction of F_1^- while the white region is the high energy portion of the basin of attraction of F_1^+.

tion motion starts in white regions, then depending on the initial conditions it may relax to one of the two stable foci in the shaded regions. This is because in the high energy (white) regions magnetization trajectories leading to different foci are closely entangled resulting in entangled basins of attractions [35] (see Fig. 2.11).

By using the phase portraits shown in Figs. 2.9-2.10, the essence of the precessional switching can be summarized as follows. The applied magnetic field creates the torque that tilts magnetization up (or down) with respect to the film plane. This results in a strong vertical demagnetizing field that forces magnetization to precess in the film plane. When this precession brings magnetization from one shaded region to another, the applied field is switched off. Then, due to the damping, magnetization relaxes to the new equilibrium that coincides with the focus of the latter shaded region. It is clear that the precessional switching is accomplished if the applied field is above some critical field necessary to bring the magnetization from one shaded region to another and if the applied field is switched off at appropriate times. Thus, the knowledge of critical magnetic fields and appropriate duration of applied magnetization field pulses is crucial for proper controlling of precessional switching. Before proceeding to the discussion of critical fields and timing of switching-off, it is worthwhile to note that if magnetic field is switched off when the magnetization is in the high energy (white) regions, the result of subsequent (damping driven) relaxation of magnetization

is practically uncertain. This is due to a very convoluted and close entanglement in the high energy regions of magnetization trajectories leading to different equilibria (see Fig. 2.11). The smaller the damping, the more pronounced this entanglement in the high energy regions. This entanglement may lead to seemingly stochastic nature of precessional switching if the applied magnetic field is switched off when magnetization is in the high energy regions. This seemingly stochastic nature of precessional switching has been experimentally observed (see Figure 1 in Ref. [37]).

Next, the issue of finding critical fields for precessional switching is addressed. Since the magnetization precession is typically (i.e. for short-time field pulses and small damping) so fast that dissipative effects can be neglected, magnetization motion in the first stage of the switching can be studied by using the conservative LLG equation

$$\frac{d\mathbf{m}}{dt} = -\mathbf{m} \times \mathbf{h}_{\text{eff}}(\mathbf{m})\,. \tag{2.39}$$

We recall that this equation has two integrals of motions (see section 1.3.5):

$$m_x^2 + m_y^2 + m_z^2 = 1\,, \tag{2.40}$$

$$-\frac{1}{2}Dm_x^2 + \frac{1}{2}m_z^2 + h_{ax}m_x - h_{ay}m_y = -\frac{1}{2}D + h_{ax}\,. \tag{2.41}$$

The second integral of motion is the conservation of the free energy (1.103) in the case where the initial magnetization is at $\mathbf{m} = \mathbf{e}_x$. From Eqs. (2.40) and (2.41) one can see that on (m_x, m_y)-plane, the precessional magnetization motion occurs along the elliptic curve:

$$(1+D)m_x^2 + m_y^2 - 2h_{ax}m_x + 2h_{ay}m_y = (1+D) - 2h_{ax}\,. \tag{2.42}$$

confined within the unit circle:

$$m_x^2 + m_y^2 \leq 1\,. \tag{2.43}$$

The possible elliptic magnetization trajectories on (m_x, m_y)-plane are shown in Fig. 2.12. Here, the shaded regions correspond to the low energy (shaded) regions of the stereographic plane (see Fig. 2.9), while two high energy (white) regions of stereographic plane are projected into the same high energy region on (m_x, m_y)-plane confined by the following ellipse:

$$(1+D)m_x^2 + m_y^2 = 1\,. \tag{2.44}$$

The components of the applied field h_{ax} and h_{ay}, determine the type of elliptic trajectories. In fact, some elliptic trajectories consist of a single piece of elliptic

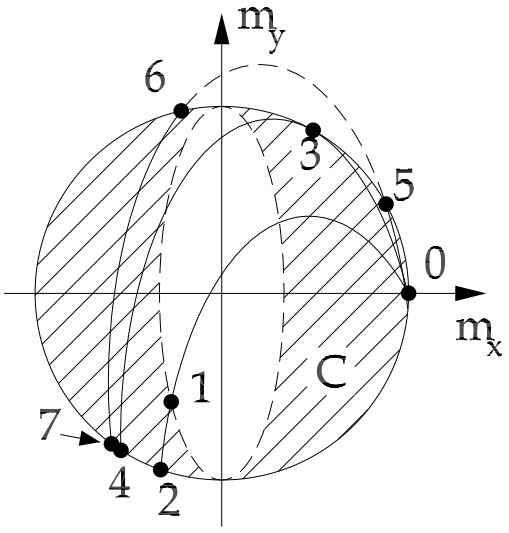

Figure 2.12: "Single-piece" and "Disjoint" trajectories on (m_x, m_y)-plane.

curves (for example, trajectory 0-1-2), while other elliptic trajectories can be made of two disjoint pieces of elliptic curves (for instance, trajectories 0-5 and 6-7).

As far as magnetization motion is concerned, one can see that every piece of elliptic trajectories on (m_x, m_y)-plane corresponds to periodic motion on the unit spherical surface. In fact, magnetization oscillates back-and-forth along the curves located on the surfaces of positive ($m_z > 0$) and negative ($m_z < 0$) hemispheres. In addition, since these curves are symmetric with respect to (m_x, m_y)-plane, the back and forth pieces of actual magnetization trajectories are orthogonally projected into the same pieces of elliptic trajectories on (m_x, m_y)-plane. Thus, it turns out that the precessional switching may only occur along the "single-piece" elliptic trajectories that intersect the unit circle (2.43) at negative values of m_x. The "disjoint" elliptic trajectories are separated from "single-piece" elliptic trajectories by the elliptic trajectory 0-3-4 that is tangential to the unit circle. It can be shown [28] that the condition of tangency of the elliptic trajectory to the unit circle leads to the following relation:

$$D m_x m_y - h_{ax} m_y - h_{ay} m_x = 0\,. \tag{2.45}$$

At the point 3 of tangency (see Fig. 2.12), equations (2.42), (2.43) and (2.45) are satisfied. These three equations define the curve h_{ay} vs h_{ax} that separates the values of h_{ax} and h_{ay} that correspond to single-piece and disjoint elliptic trajectories, respectively. A parametric representation of this h_{ay} vs h_{ax} curve can be found by introducing the polar angle θ such that

$$m_x = \cos\theta\,, \quad m_y = \sin\theta \quad . \tag{2.46}$$

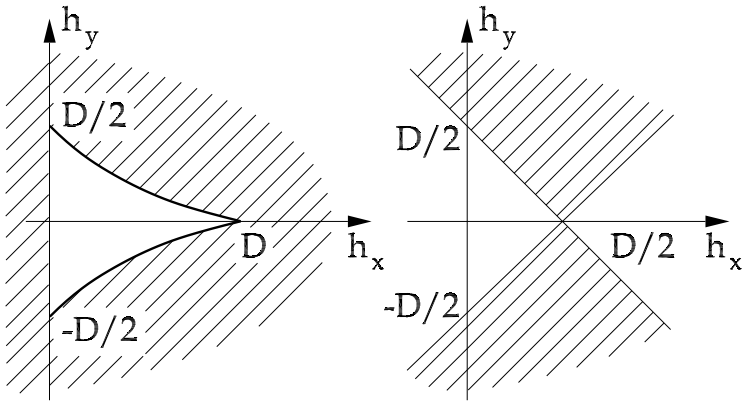

(a) (b)

Figure 2.13: (a) Separating curve on (h_{ax}, h_{ay})-plane; (b) region corresponding to single-piece elliptic trajectory intersecting the unit-circle at negative m_x.

In fact, by substituting Eq. (2.46) into Eqs. (2.42) and (2.45) and solving with respect to h_{ax} and h_{ay}, the following parametric representation can be found:

$$h_{ax} = D\cos\theta\cos^2\frac{\theta}{2}\,, \quad h_{ay} = D\sin\theta\sin^2\frac{\theta}{2}\,, \tag{2.47}$$

The separating curve, defined parametrically by Eqs. (2.47), is valid only for positive values[3] of h_{ax}, which correspond to values of the parameter $|\theta| \leq \pi/2$. For negative values of h_{ax}, it can be shown that all the elliptic trajectories starting from point 0 (Fig. 2.12) intersect the unit circle only once.

Thus, the points (h_{ax}, h_{ay}) in the shaded region of Fig. 2.13(a) correspond to "single-piece" elliptic trajectories, while the points (h_{ax}, h_{ay}) in the white region correspond to "disjoint" elliptic trajectories.

In Ref. [28] the conditions on h_{ax} and h_{ay} that guarantee that "single-piece" elliptic trajectories intersect the unit circle (2.43) at negative values are also derived. The appropriate values of h_{ax} and h_{ay} correspond to the shaded regions formed by the intersecting lines (see Fig. 2.13(b)).

$$h_{ay} = \pm\,(h_{ax} - D/2) \tag{2.48}$$

The values of h_{ax} and h_{ay}, that guarantee "single-piece" elliptic trajectories intersecting the unit circle at negative values of m_x, correspond to the points of (h_{ax}, h_{ay})-plane that belong to the intersection of the shaded regions shown in Figures 2.13(a) and 2.13(b). This intersection is the shaded region shown in Fig. 2.14. The boundary of this region corresponds to the critical fields for precessional switching. It is useful to notice that, in the case of field applied

[3]We recall that the applied field is expressed here as $\mathbf{h}_\mathrm{a} = -h_{ax}\mathbf{e}_x + h_{ay}\mathbf{e}_y$.

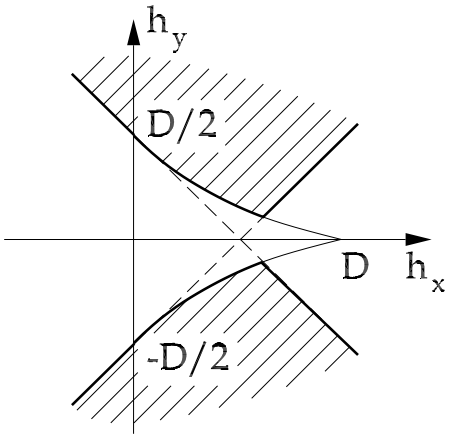

Figure 2.14: Switching region in (h_{ax}, h_{ay})-plane.

orthogonally to the x axis, that is $\mathbf{h}_\mathrm{a} = h_{ay}\mathbf{e}_y$, the critical field for precessional switching is

$$h_c = \frac{D}{2} \quad , \tag{2.49}$$

which is half the critical value provided by Stoner-Wohlfarth theory in the case $N_\perp = 0$ (see[4] Eq. (2.17)). In this respect, this is an example of magnetization switching with external field below the Stoner-Wohlfarth limit. As we mentioned in section 2.2, the switching is not guaranteed with the only application of the external field, but one has to take care of magnetization motion to realize successful reversal by switching the field off at the right time. Interestingly enough, precessional switching dynamics is less energy-consuming than traditional one.

It has been previously mentioned that in the case of precessional switching the timing of switching-off the applied magnetic field is crucial in the sense that there exists a certain time-window during which this switching-off must occur. One can be convinced from Fig. 2.12 that this time-window is the time interval of the back-and-forth motion between the points 1 and 2 on a single piece trajectory, as for instance the trajectory 0-1-2. To find this time-window [28], one can write the Eq. (2.42) of this elliptic trajectory in parametric form

$$m_x = \mathrm{a}_x + \frac{p}{k}\sin u\,, \quad m_y = \mathrm{a}_y + p\cos u \tag{2.50}$$

where $u \in [0, 2\pi]$ is the parameter, $k^2 = 1 + D$, $\mathrm{a}_x = h_{ax}/(1 + D)$, $\mathrm{a}_y = -h_{ay}$, $p^2 = h_{ay}^2 + (1+D)[1 - h_{ax}/(1+D)]^2$. From the conservative LLG equation (2.39), one obtains:

$$\frac{dm_x}{dt} = (m_y + h_{ay})m_z\,. \tag{2.51}$$

[4]Notice that here the role of easy axis z is played by the x axis.

By substituting Eq. (2.50) into (2.51), one has

$$\frac{du}{\sqrt{1-(\mathrm{a}_x+(p/k)\sin u)^2-(\mathrm{a}_y+p\cos u)^2}}=kdt\,. \tag{2.52}$$

By using the last formula, the time-window $t_1 < t < t_2$ for switching the applied field off can be derived:

$$t_1=\int_{u_0}^{u_1}\frac{du}{k\sqrt{1-(\mathrm{a}_x+(p/k)\sin u)^2-(\mathrm{a}_y+p\cos u)^2}}\,, \tag{2.53}$$

$$t_2-t_1=2\int_{u_1}^{u_2}\frac{du}{k\sqrt{1-(\mathrm{a}_x+(p/k)\sin u)^2-(\mathrm{a}_y+p\cos u)^2}}\,, \tag{2.54}$$

and u_0, u_1 and u_2 correspond to points 0,1 and 2 in Fig. 2.12, respectively. The values of the parameters u_0, u_1, u_2 can be determined by finding the intersections of the unit circle (2.43) with the elliptic trajectory (2.42) and by using the parametric representation (2.50) of the ellipse. Moreover, one can derive the time instant at which magnetization is in the closest position with respect to the reversed orientation. This position is determined by the intersection of the single-piece ellipse with the unit disk occurring at negative m_x. We denote this instant as

$$T_s=\int_{u_0}^{u_2}\frac{du}{k\sqrt{1-(\mathrm{a}_x+(p/k)\sin u)^2-(\mathrm{a}_y+p\cos u)^2}}=\frac{t_2+t_1}{2}\quad . \tag{2.55}$$

Thus, to summarize, in the conservative case, t_1 is the time instant at which the magnetization enters the potential well around the reversed state and t_2 is the time instant at which magnetization goes out from that potential well. With the notations introduced in section 2.4.1 we have:

$$T_p=t_1\quad . \tag{2.56}$$

In presence of a small damping, the separation between the high energy regions and the low energy regions is very close to that in the conservative case. Therefore, one reasonably expects that switching the applied field off when $t_1 < t < t_2$ lets the magnetization relax towards the reversed state. This analysis works very well in the case of uniformly magnetized particles. In Chapter 3 we will remove this simplifying assumption and we will demonstrate with micromagnetic simulations that precessional switching process, for thin-films having dimensions and material parameters of technological interest, is a quasi-uniform process, whereas damping switching is not. Moreover, we will show that the evaluation of the switching time window t_1, t_2 with Eqs. (2.53)-(2.54) gives very accurate results also in non-uniform cases.

2.5 LLG DYNAMICS UNDER CIRCULARLY POLARIZED FIELD

The Landau-Lifshitz-Gilbert (LLG) equation has also played a central role in the interpretation of ferromagnetic resonance (FMR) phenomena [38]. Typical experiments involve small particles and thin-disks with rotational symmetry with respect to an axis (say $z-$axis). A DC external field is applied along the $z-$axis and a circularly polarized radio-frequency field is then applied in the $x-y$ plane. In this condition it has been shown that the absorbed power exhibits a maximum for a suitable resonance frequency. Analytical derivation of the resonance frequency for uniformly magnetized ellipsoidal particles was found by Kittel in 1948 [39] under the hypothesis of harmonic magnetization motion in m_x, m_y plane, which occurs for small angles of $\mathbf{m}$ with respect to the $z-$axis. In generic conditions the LLG equation has to be solved numerically. In fact, exact analytical solution can be derived in few cases and are generally obtained by linearizing the equation around some given state. In a new approach recently proposed [40], exact analytical solutions were derived for the full nonlinear LLG equation with damping in the case when the magnetic body is an ellipsoidal particle with rotational symmetry around a certain axis and the external field is circularly polarized. In this situation, one can prove that exact solutions of LLG equation always exist. These solutions are characterized by uniform magnetization rotating at the angular velocity ω with certain lag angle with the respect to the rotating applied field. The rotational invariance of this system and the fact that LLG equation conserves magnetization amplitude, permit one to reduce the problem to the study of an autonomous dynamical system on the unit sphere. This reduction is achieved by introducing an appropriate rotating frame of reference. The resulting autonomous dynamical system may exhibit various phase portraits characterized by equilibrium points and limit cycles [40]. The limit cycles in the rotating frame correspond to uniform quasiperiodic magnetization motions in the laboratory frame, deriving from the combination of the rotation of the frame and the periodicity of the limit cycle. The study of these quasiperiodic solutions is then reduced to the study of limit cycles of a vector field on the sphere. Despite the simplicity of the system, this study is extremely difficult and no general technique is available. In this respect, our purpose is to present a technique to predict the existence, the number, the form and the stability of these limit cycles (and therefore of the quasiperiodic magnetization modes) in the special case, often encountered in the applications, of small value of the damping constant in the LLG equation. The analysis is carried out by using an appropriate perturbation technique which is generally referred to as Poincaré-Melnikov

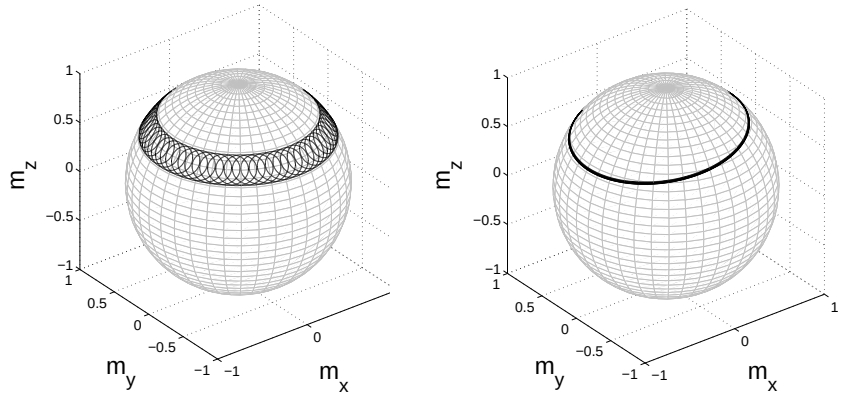

Figure 2.15: Trajectories of magnetization on the unit sphere in the laboratory (left) and the rotating frames (right).

function technique (see Appendix B and Ref. [43]).

2.5.1 Equation of motion

We consider an uniformly magnetized thin film or spheroidal particle subject to a time-varying external magnetic field. The magnetization dynamics is governed by the LLG equation which is written in the usual dimensionless form (see section 2.3),

$$\frac{d\mathbf{m}}{dt} - \alpha\mathbf{m} \times \frac{d\mathbf{m}}{dt} = -\mathbf{m} \times \mathbf{h}_{\text{eff}}(t, \mathbf{m}) \quad . \tag{2.57}$$

The effective field is given by

$$\mathbf{h}_{\text{eff}}(t, \mathbf{m}) = -D_{\perp}\mathbf{m}_{\perp} - D_z m_z \mathbf{e}_z + \mathrm{h}_{az}\mathbf{e}_z + \mathbf{h}_{a\perp}(t) \tag{2.58}$$

where $\mathbf{e}_z$ is the unit vector along the symmetry axis z, the subscript "$\perp$" denotes components normal to the symmetry axis, $D_{\perp}$, D_z describe (shape and crystalline) anisotropy of the body. The applied field has the dc component h_{az} along the z-axis and the time-harmonic component $\mathbf{h}_{a\perp}(t)$ uniformly rotating with angular frequency ω in the plane normal to the symmetry axis:

$$\mathbf{h}_{a\perp}(t) = \mathrm{h}_{a\perp}\left[\cos(\omega t)\mathbf{e}_x + \sin(\omega t)\mathbf{e}_y\right] \quad , \tag{2.59}$$

where $\mathbf{e}_x$, $\mathbf{e}_y$ are the unit vectors along the axis x and y respectively. The dynamical system defined by Eq. (2.57) is non autonomous ($\mathbf{h}_{\text{eff}}$ explicitly depends on time) and it is characterized by magnetization dynamics with $|\mathbf{m}| = 1$. In other words, Eq. (2.57) defines a non autonomous vector field on the unit sphere. The analysis of this system is greatly simplified when Eq. (2.57) is studied in the reference frame rotating at angular velocity ω around the symmetry axis $\mathbf{e}_z$. By

choosing an appropriate origin of the time, we can obtain that in the rotating frame $\mathbf{h}_{a\perp} = \mathrm{h}_{a\perp}\mathbf{e}_x$ and

$$\mathbf{h}_{\text{eff}}(\mathbf{m}) = -D_\perp \mathbf{m}_\perp - D_z m_z \mathbf{e}_z + \mathrm{h}_{az}\mathbf{e}_z + \mathrm{h}_{a\perp}\mathbf{e}_x\,. \tag{2.60}$$

In addition, in passing to the new frame, the derivative of $\mathbf{m}(t)$ transforms according to the rule

$$\left.\frac{d\mathbf{m}}{dt}\right|_{\text{lab}} \mapsto \left.\frac{d\mathbf{m}}{dt}\right|_{\text{rot}} + \omega\mathbf{e}_z \times \mathbf{m} \quad , \tag{2.61}$$

and thus Eq. (2.57), written in the rotating reference frame, takes the following autonomous form:

$$\frac{d\mathbf{m}}{dt} - \alpha\mathbf{m} \times \frac{d\mathbf{m}}{dt} = -\mathbf{m} \times (\mathbf{h}_{\text{eff}}(\mathbf{m}) - \omega\mathbf{e}_z + \alpha\omega\mathbf{m} \times \mathbf{e}_z)\,. \tag{2.62}$$

Equation (2.62) describes an autonomous dynamical system evolving on the surface of the unit sphere $|\mathbf{m}| = 1$. The fixed points of the dynamics can be computed from the following equations similar to Eqs. (2.22):

$$\begin{cases} \mathbf{h}_{\text{eff}}(\mathbf{m}) - \omega\mathbf{e}_z + \alpha\omega\mathbf{m} \times \mathbf{e}_z = \lambda\mathbf{m} \quad , \\ |\mathbf{m}| = 1 \quad . \end{cases} \tag{2.63}$$

It is interesting to notice that equilibria in the rotating frame correspond to periodic solutions in the laboratory frame while limit cycles in the rotating frame correspond to quasiperiodic magnetization solutions in the laboratory frame (see Fig. 2.15). The quasiperiodicity derives from the combination of the rotation of the frame with angular frequency ω and the periodicity of the limit cycle in the rotating frame with angular frequency self-generated by the dynamical system (and in general not commensurable with ω). Notice also that chaos is not permitted in this dynamical system, despite the presence of a driving sinusoidal field, due to the rotational symmetry and the consequent reduction to a dynamical system on a 2D manifold.

2.5.2 QUASIPERIODIC SOLUTIONS OF LLG DYNAMICS UNDER CIRCULARLY POLARIZED FIELD

Let us focus our analysis on the quasiperiodic solutions (limit cycles in the rotating frame). In order to establish the existence, the number and the locations of the limit cycles we can exploit the fact that α is generally a small parameter $\lesssim 0.1$. Thus, we can start our analysis by considering the case $\alpha = 0$ which can be easily treated because the dynamical system (2.62) admits the following integral of motion (similar to energy conservation (1.103)):

$$g(\mathbf{m}) = \frac{1}{2}D_z m_z^2 + \frac{1}{2}D_\perp \mathrm{m}_\perp^2 - \mathrm{h}_{a\perp}m_x - (\mathrm{h}_{az} - \omega)m_z. \tag{2.64}$$

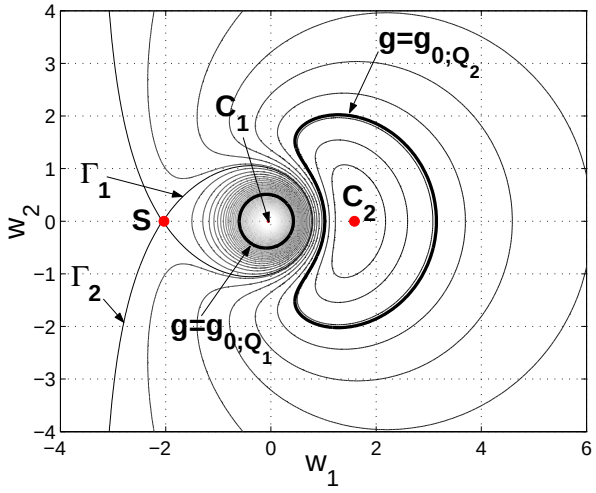

Figure 2.16: Phase portrait of conservative system on the stereographic plane $w_1 = m_x/(1+m_z)$, $w_2 = m_y/(1+m_z)$. Value of the parameters: $\alpha = 0$, $D_z = 1$, $D_\perp = 0$, $\mathrm{h}_{az} = 0.6$, $\mathrm{h}_{a\perp} = 0.15$, $\omega = 1.1$.

It is interesting to notice that the function $g(\mathbf{m})$ satisfies the following equation along the trajectory of the dynamical system

$$\frac{dg}{dt} = \alpha \left[\omega(\mathbf{m} \times \mathbf{e}_z) \cdot \frac{d\mathbf{m}}{dt} - \left| \frac{d\mathbf{m}}{dt} \right|^2 \right] = -\alpha\, \mathcal{P}(\mathbf{m})\,, \tag{2.65}$$

where $\mathcal{P}(\mathbf{m})$ is the "absorbed power" function which is defined by the opposite of the above expression in square bracket. This function will be instrumental in the following to give an energy interpretation of limit cycles.

The phase portrait for $\alpha = 0$ is given by the contour lines of the function $g(\mathbf{m})$. To give a planar representation of the phase portraits, we use the stereographic variables w_1, w_2 introduced in section 2.3. In Fig. 2.16, the phase portrait is represented on the (w_1, w_2)-plane for the case of a thin film. This phase portrait is characterized by three centers C_1, C_2 and C_3 (outside Fig. 2.16) and a saddle S with two homoclinic orbits Γ_1 and Γ_2. When the small damping is introduced, almost all closed trajectories around centers are slightly modified and collectively form spiral-shaped trajectories toward attractors. There are only special trajectories which remain practically unchanged under the introduction of the small damping. Two of these trajectories are indicated by Q_1 and Q_2 in Fig. 2.16. These trajectories can be found by using a perturbation technique which is generally called Poincarè-Melnikov function method [43]. This perturbative approach is reported, for a generic 2D dynamical system, in Appendix B. In order to apply this technique it is convenient to transform Eq. (2.62) in the

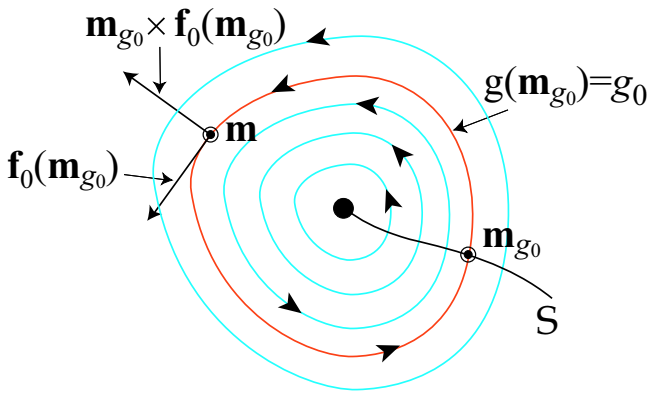

Figure 2.17: Sketch of a portion of the phase portrait of LLG equation around a center equilibrium.

following perturbative form (α is a small parameter).

$$\frac{d\mathbf{m}}{dt} = \mathbf{f}_0(\mathbf{m}) + \alpha \mathbf{f}_1(\mathbf{m}, \alpha) \tag{2.66}$$

where

$$\mathbf{f}_0(\mathbf{m}) = -\mathbf{m} \times (\mathbf{h}_{\text{eff}} - \omega \mathbf{e}_z) = \mathbf{m} \times \nabla_{\mathbf{m}} g(\mathbf{m}) \tag{2.67}$$

$$\mathbf{f}_1(\mathbf{m}, \alpha) = \frac{\alpha}{1+\alpha^2} \mathbf{m} \times \mathbf{h}_{\text{eff}} - \frac{1}{1+\alpha^2} \mathbf{m} \times (\mathbf{m} \times \mathbf{h}_{\text{eff}}) \tag{2.68}$$

For $\alpha = 0$ the dynamical system is integrable and trajectories are given by $g(\mathbf{m}) = g_0$ with g_0 varying in the appropriate range. In addition, the vector field $\mathbf{f}_0(\mathbf{m})$ is hamiltonian and, as it can be derived from Eq. (2.67), it is divergeless on the unit sphere $\Sigma : \nabla_\Sigma \cdot \mathbf{f}_0(\mathbf{m}) = 0$. The technique is based on the extraction of a Poincarè map [43] (associated to an arbitrarly chosen line S transveral to the vector field, as sketched in Fig. 2.17) of the perturbed system by using an expansion in terms of the perturbation parameter α, around $\alpha = 0$. The zero order term of this expansion is the identity since for $\alpha = 0$ all trajectories (except separitrices) goes back to the initial point (see Fig. 2.16). The first order term of the expansion with respect to α is proportional to the Melnikov function which, in the case of divergenceless unperturbed vector field, is given by the following integral along the trajectories of the unperturbed system (see Eq. (B.39) in Appendix B)

$$M(g_0) = \int_0^{T_{g_0}} \mathbf{f}_0(\mathbf{m}_{g_0}(t)) \wedge \mathbf{f}_1(\mathbf{m}_{g_0}(t), 0) dt \tag{2.69}$$

where $\mathbf{m}_{g_0}(t)$ is the trajectory of the unperturbed system with $g(\mathbf{m}_{g_0}(t)) = g_0$, T_{g_0} is its period and

$$\mathbf{f}_0(\mathbf{m}) \wedge \mathbf{f}_1(\mathbf{m}, 0) = \mathbf{m} \cdot (\mathbf{f}_0(\mathbf{m}) \times \mathbf{f}_1(\mathbf{m}, 0)) \quad . \tag{2.70}$$

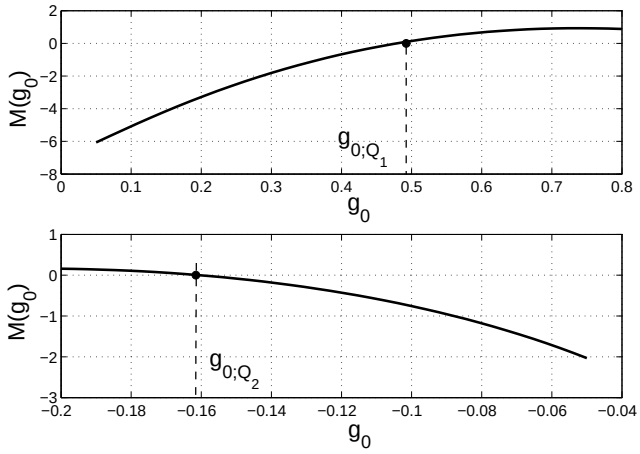

Figure 2.18: Two branches of the Melnikov function vs the value of g_0: $g_{0;Q_1}$ and $g_{0;Q_2}$ correspond to conservative trajectories $g = g_{0;Q_1}$ and $g = g_{0;Q_2}$ in Fig. 2.16, which become limit cycles Q_1 and Q_2 in the perturbed system.

By using the expressions of $\mathbf{f}_0(\mathbf{m})$ and $\mathbf{f}_1(\mathbf{m}, 0)$ and appropriate algebraic manipulations one can derive that:

$$M(g_0) = -\int_0^{T_{g_0}} \left[\omega(\mathbf{m}_{g_0} \times \mathbf{e}_z) \cdot \frac{d\mathbf{m}_{g_0}}{dt} - \left| \frac{d\mathbf{m}_{g_0}}{dt} \right|^2 \right] dt \,. \tag{2.71}$$

The last equation can be also transformed in the following line-integral form which permits one to compute $M(g_0)$ without deriving the time dependence of $\mathbf{m}_{g_0}(t)$:

$$M(g_0) = -\oint_{g=g_0} \mathbf{m} \times \mathbf{h}_{\text{eff}} \cdot d\mathbf{m} \,. \tag{2.72}$$

Periodic orbits of the dissipative system are given by the zeros of the Melnikov function. In Fig. 2.18, the Melnikov function computed from Eq. (2.69) is plotted versus the value of g_0 and the zeros of $M(g_0)$, which correspond to the trajectories $g = g_{0;Q_1}$ and $g = g_{0;Q_2}$ in Fig. 2.16, are emphasized. In Fig. 2.19, by sketching the phase portrait for the dissipative case ($\alpha = 0.05$), we have then verified that the limit cycles (Q_1, Q_2) predicted by the theory are preserved under the introduction of the damping. Let us notice that the introduction of damping transformed centers in foci F_1(unstable), F_2(stable) and F_3(unstable) and disconneted the homoclinic trajectories (L_1 and L_2 are the separatrices). It is interesting to notice that the Melnikov function given by Eq. (2.71) can be rewritten as

$$M(g_0) = \int_0^{T_{g_0}} \mathcal{P}(\mathbf{m}_{g_0}(t))\, dt \quad . \tag{2.73}$$

In this respect, it is possible to give a physical interpretation of limit cycles: the limit cycle arise from those unperturbed trajectories on which there is an average

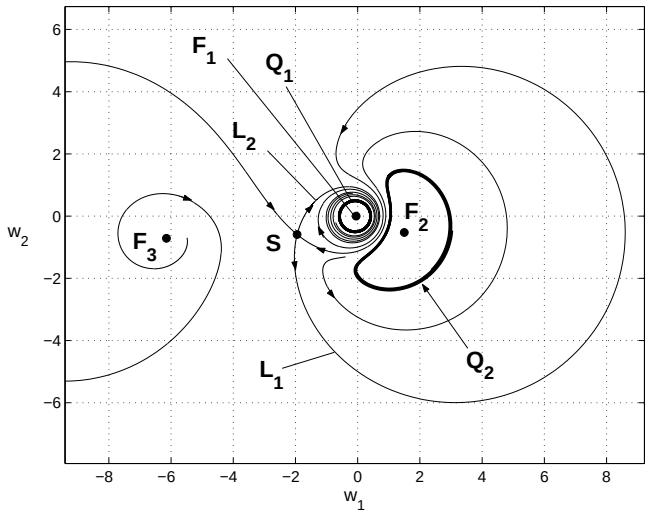

Figure 2.19: Phase portrait of dissipative system. The parameters are the same as in Fig. 2.16 except for $\alpha = 0.05$.

balance between "dissipation" ($\mathcal{P}(\mathbf{m}) \geq 0$) and "absorption" ($\mathcal{P}(\mathbf{m}) \leq 0$) of energy.

By using the technique we have just illustrated, it is possible to predict the existence and the number of the limit cycles in a certain interval of values of α around $\alpha = 0$. The stability of the limit cycles can be obtained by studying the sign of the derivative of the Melnikov function at its zeros [43]: a limit cycle is stable for positive derivative (in our case Q_1 is stable, see Figs. 2.18-2.19), unstable for negative derivative (in our case Q_2 is unstable, see Figs. 2.18-2.19). Finally the shape of the limit cycles can be estimated by taking, as first order approximation, the unperturbed trajectories corresponding to the values of the energy function $g(\mathbf{m})$ where the Melnikov function vanishes.

2.6 Spin-transfer Effect and Current-induced Magnetization Switching

It has been recently shown, both theoretically and experimentally, that a spin-polarized current when passing through a small magnetic conductor can affect its magnetization state. The interaction between spin polarized current and magnetization in small ferromagnetic bodies can produce steady state precessional magnetization dynamics, that is self-oscillating behavior, or even the switching of magnetization direction [44]-[46]. Both types of dynamical behavior have potential applications in magnetic storage technology and spintronics. In this respect, it was predicted, and later confirmed, that spin-polarized current can lead to current-controlled hysteretic switching in magnetic nanostructures. This kind of

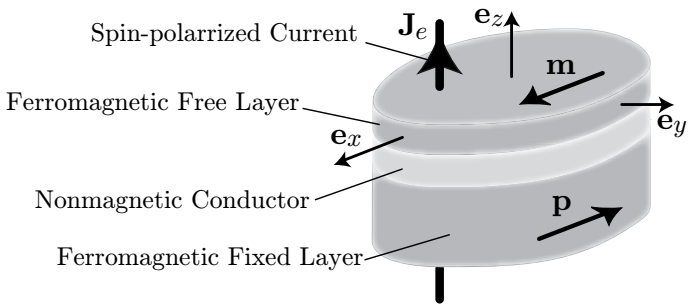

Figure 2.20: Sketch of Trilayers Co-Cu-Co structure.

behavior may become very important for applications such as current-controlled switching of magnetic random access memory elements and stabilization of magnetic hard-disk read heads. Steady precessional oscillations of magnetization due to spin polarized currents have also interesting potential applications for the realization of current-controlled microwave oscillators integrable with semiconductor electronics. This kind of oscillators could be used to realize a very new design of clocks for synchronization of electronic devices.

Here spin-polarized current induced dynamics is studied in the case of a uniformly magnetized ferromagnetic thin film [47]. Magnetization dynamics is described by the Landau-Lifshitz-Gilbert equation and the effect of spin-polarized currents is taken into account through the additional torque term derived by Slonczewski in Ref. [44]. This model can be applied to describe the magnetization dynamics in the free layer of trilayers structures constituted by two ferromagnetic layers separated by nonmagnetic metal layer (typically the system is a Co-Cu-Co trilayers as sketched in Fig. 2.20). One of the magnetic layer is "fixed", namely has a given and constant value of magnetization (indicated with **p** in Fig. 2.20) while the second magnetic layer is a thin film where the magnetization is "free" to change and where dynamics takes place. This kind of structure is traversed by an electric current whose direction is normal to the plane of the layer (generally this configuration in called "current perpendicular to plane (CPP) geometry"). The fixed layer is instrumental to provide a controlled polarization (on the average parallel to the fixed magnetization direction) of the electron spins which travel across the trilayers, from the fixed to the free layer. It important to underline that the effect of spin induced torque is predominant on the effect of the magnetic field generated by the current itself for structures which have small enough transversal dimensions. By using reasonably estimate it has been predicted and then verified experimentally that the effect of the current generated magnetic field can be considered negligible for transversal dimension as small as 100 nm.

2.6.1 LANDAU-LIFSHITZ-GILBERT EQUATION WITH SLONCZEWSKI SPIN-TRANSFER TORQUE TERM

In order to introduce a model equation for magnetization dynamics in presence of spin polarized currents, let us first consider the model derived by Slonczewski in Ref. [44]. In his paper, a five layers structure is considered. In this structure, the first, the third and the fifth layers are constituted by paramagnetic conductors and the second and the fourth layers are ferromagnetic conductors (it is a three layers structure as the one mentioned in the introduction with paramagnetic conductors as spacer and contacts). The multilayers system is traversed by electric current normal to the layers plane. The electron spins, polarized by the fixed ferromagnetic layer (the second layer) are injected by passing through the paramagnetic spacer into the free ferromagnetic layer (the forth layer) where the interaction between spin polarized current and magnetization takes place. The magnetic state of the ferromagnetic layers is described by two vectors $\mathbf{S}_1$ and $\mathbf{S}_2$ representing macroscopic (total) spin orientation per unit area of the fixed and the free ferromagnetic layers, respectively. The connection of this two vectors with the total spin momenta $\mathbf{L}_1$ and $\mathbf{L}_2$ (which have the dimension of angular momenta) is given by the equations $\mathbf{L}_1 = \hbar \mathbf{S}_1 A$, $\mathbf{L}_2 = \hbar \mathbf{S}_2 A$, where A is the cross-sectional area of the multilayers structure. By using a semiclassical approach to treat spin transfer between the two ferromagnetic layers, Slonczewski derived the following generalized LLG equation (see Eq.(15) in [44]):

$$\frac{d\mathbf{S}_2}{dt} = \mathbf{s}_2 \times \left(\gamma H_u \mathbf{c} \cdot \mathbf{S}_2 \mathbf{c} - \alpha \frac{d\mathbf{S}_2}{dt} + \frac{I_e g}{e} \mathbf{s}_1 \times \mathbf{s}_2 \right) \tag{2.74}$$

where $\mathbf{s}_1$, $\mathbf{s}_2$ are the unit-vectors along $\mathbf{S}_1$, $\mathbf{S}_2$, γ is the absolute value of the gyromagnetic ratio, H_u is the anisotropy field constant, $\mathbf{c}$ is the unit vector along the anisotropy axis (in-plane anisotropy), α the Gilbert damping constant, I_e the current density (electric current per unit surface), e is the absolute value of the electron charge, g a scalar function given by the following expression

$$g(\mathbf{s}_1 \cdot \mathbf{s}_2) = \left[-4 + (1+P)^3 \frac{(3 + \mathbf{s}_1 \cdot \mathbf{s}_2)}{4P^{3/2}} \right]^{-1} \tag{2.75}$$

and P is the spin polarizing factor of the incident current which gives the percent amount of electrons that are polarized in the $\mathbf{p}$ direction (see Ref. [44] for details). The current I_e in Eq. (2.74) is assumed to be positive when the charges move from the fixed to the free layer. Let us notice that in Eq. (2.74) the ferromagnetic body is assumed to be uniaxial with anisotropy axis along $\mathbf{c}$. In the sequel, we will remove this simplifying assumption by taking into account the effect of the strong demagnetizing field normal to the plane of the layer in order to consider

the thin-film geometrical nature of the free layer. Our next purpose is to derive from Eq. (2.74) an equation for magnetization dynamics. We will carry out this derivation by using slightly different notation and translating all the quantities in practical MKSA units.

First of all, let us introduce a system of cartesian unit vectors $\mathbf{e}_x$, $\mathbf{e}_y$ $\mathbf{e}_z$, where $\mathbf{e}_z$ is normal to the film plane and pointing in the direction of the fixed layer, and $\mathbf{e}_x$ is along the in-plane easy axis (in the Slonczewski notation $\mathbf{e}_x = \mathbf{c}$). The current density will be denoted by J_e (instead of I_e as in Eq. (2.74)), the anisotropy field as $H_{\rm an}$ and the function $g(\mathbf{s}_1 \cdot \mathbf{s}_2)$ in Eq. (2.75) will be denoted with b to avoid confusion with the free energy and the Landé factor g_e that will be used in the following. In this reference frame the current density vector is $\mathbf{J} = J_e\mathbf{e}_z$, which means that when $J_e > 0$ the electrons travel in the direction opposite to $\mathbf{e}_z$, namely from the fixed to the free layer.

By using these modified notations and by including the effects of the demagnetizing field $\mathbf{H}_m$ and the applied field $\mathbf{H}_a$, Eq. (2.74) becomes

$$\frac{d\mathbf{S}_2}{dt} = \mathbf{s}_2 \times \left(\gamma H_{\rm an}(\mathbf{e}_x \cdot \mathbf{S}_2)\mathbf{e}_x - \gamma(\mathbf{H}_m + \mathbf{H}_a)\mathrm{S}_2 - \alpha\frac{d\mathbf{S}_2}{dt} + \frac{J_e b}{e}\mathbf{s}_1 \times \mathbf{s}_2 \right), \quad (2.76)$$

where $\mathrm{S}_2 = |\mathbf{S}_2|$. The sum of the demagnetizing field $\mathbf{H}_m$ and the applied field $\mathbf{H}_a$ will be indicated in he following by $\mathbf{H}$ to shorten the notation, i.e.

$$\mathbf{H} = \mathbf{H}_m + \mathbf{H}_a\,. \quad (2.77)$$

In order to check the correctness of the signs of precessional terms in Eq. (2.76), let us transform this equation in a slightly different form, by factoring out from the parenthesis the constant S_2. For the sake of simplicity, we will carry out this derivation in the case $\alpha = 0$ and $J_e = 0$. We have then the following equation

$$\frac{d\mathbf{S}_2}{dt} = \mathbf{S}_2 \times \left(\gamma H_{\rm an}(\mathbf{e}_x \cdot \mathbf{s}_2)\mathbf{e}_x - \gamma(\mathbf{H}_m + \mathbf{H}_a)\right). \quad (2.78)$$

We observe now that what is generally defined as effective anisotropy field is given by

$$\mathbf{H}_{\rm an} = -H_{\rm an}(\mathbf{e}_x \cdot \mathbf{s}_2)\mathbf{e}_x\,. \quad (2.79)$$

The minus sign in this equation is due to the fact that the direction of $\mathbf{s}_2$ is opposite to the direction of magnetization. This issue will be discussed below. By substituting Eq. (2.79) into Eq. (2.78) we obtain

$$\frac{d\mathbf{S}_2}{dt} = -\gamma\mathbf{S}_2 \times (\mathbf{H}_{\rm an} + \mathbf{H}_m + \mathbf{H}_a) = -\gamma\mathbf{S}_2 \times \mathbf{H}_{\rm eff}, \quad (2.80)$$

where

$$\mathbf{H}_{\rm eff} = \mathbf{H}_{\rm an} + \mathbf{H}_m + \mathbf{H}_a = -H_{\rm an}(\mathbf{e}_x \cdot \mathbf{s}_2)\mathbf{e}_x + \mathbf{H}_m + \mathbf{H}_a\,. \quad (2.81)$$

Equation (2.80) is the correct precession equation for the spin vector dynamics.

Next, we want to derive the dynamical equation for the magnetization vector $\mathbf{M}$ associated with the free layer. In this respect, we have first to consider the relation between $\mathbf{S}_2$ and $\mathbf{M}$. The total magnetic moment $\vec{\mu}$ associated with the free layer is given by

$$\vec{\mu} = -\gamma \mathbf{L}_2 = -\gamma \hbar \mathbf{S}_2 A = -\gamma \hbar \mathbf{S}_2 A \,, \tag{2.82}$$

where A has been introduced above and coincides with the area of the surface of the film. The magnetization $\mathbf{M}$ is obtained by dividing the total magnetic moment by the volume of the film V:

$$\mathbf{M} = \frac{\vec{\mu}}{V} = \frac{\vec{\mu}}{Ad} \tag{2.83}$$

where d is the free layer thickness, thus we obtain the following relations

$$\mathbf{M} = \frac{-\gamma \hbar \mathbf{S}_2 A}{Ad} = \frac{-\gamma \hbar \mathbf{S}_2}{d} = \frac{-g_e \mu_{\mathrm{B}}}{d} \mathbf{S}_2 \tag{2.84}$$

where g_e is the Landè factor for electrons, μ_{B} is the Bhor magneton, and the relation $\gamma = g_e \mu_{\mathrm{B}}/\hbar$ has been used. Let us notice that, as a consequence of Eq. (2.84), we have

$$\mathbf{s}_2 = -\mathbf{m} = -\frac{\mathbf{M}}{\mathrm{M}_s} \tag{2.85}$$

where $\mathrm{M}_s = |\mathbf{M}|$ is the saturation magnetization and $\mathbf{m}$ is the unit vector along $\mathbf{M}$. By multiplying both sides of Eq. (2.76) by the factor $-g_e \mu_{\mathrm{B}}/d$ and taking into account Eq. (2.85), one ends up with the following equation

$$\frac{d\mathbf{M}}{dt} = -\mathbf{m} \times \left(\gamma H_{\mathrm{an}} (\mathbf{e}_x \cdot \mathbf{M}) \mathbf{e}_x + \gamma \mathbf{H} \mathrm{M}_s - \alpha \frac{d\mathbf{M}}{dt} + \frac{g_e \mu_{\mathrm{B}} J_e b}{ed} \mathbf{s}_1 \times \mathbf{m} \right) , \tag{2.86}$$

which can be further normalized by dividing both sides by M_s, leading to

$$\frac{d\mathbf{m}}{dt} - \alpha \mathbf{m} \times \frac{d\mathbf{m}}{dt} = -\mathbf{m} \times \left(\gamma H_{\mathrm{an}} (\mathbf{e}_x \cdot \mathbf{m}) \mathbf{e}_x + \gamma \mathbf{H} + \frac{g_e \mu_{\mathrm{B}} J_e b}{ed \mathrm{M}_s} \mathbf{s}_1 \times \mathbf{m} \right) . \tag{2.87}$$

In order to derive a time normalized form of the equation, we factor out from the parenthesis the term γM_s which has the dimension of a frequency, and thus we have

$$\frac{d\mathbf{m}}{dt} - \alpha \mathbf{m} \times \frac{d\mathbf{m}}{dt} = -\gamma M_s \, \mathbf{m} \times \left(\kappa_{\mathrm{an}} (\mathbf{e}_x \cdot \mathbf{m}) \mathbf{e}_x + \mathbf{h} + \frac{1}{\gamma M_s} \frac{g_e \mu_{\mathrm{B}}}{ed \mathrm{M}_s} J_e b \, \mathbf{s}_1 \times \mathbf{m} \right) , \tag{2.88}$$

where

$$\kappa_{\mathrm{an}} = \frac{H_{\mathrm{an}}}{\mathrm{M}_s}, \qquad \mathbf{h} = \frac{\mathbf{H}_m + \mathbf{H}_a}{\mathrm{M}_s} = \mathbf{h}_{\mathrm{m}} + \mathbf{h}_{\mathrm{a}} \,, \tag{2.89}$$

where $\mathbf{h}_{\mathrm{a}} = \mathbf{H}_{\mathrm{a}}/M_s$, $\mathbf{h}_{\mathrm{m}} = \mathbf{H}_{\mathrm{m}}/M_s$. Finally, let us denote the direction of magnetization in the fixed layer by $\mathbf{p}$. According to the previous reasoning, this

direction is opposite to $\mathbf{s}_1$, i.e. $\mathbf{s}_1 = -\mathbf{p}$. We also define the following constant which has the physical dimension of a current density:

$$J_p = \gamma M_s \frac{e\mathrm{M}_s d}{g_e \mu_\mathrm{B}} \,. \tag{2.90}$$

By using the notations defined above, we arrive to the following form of Eq. (2.88):

$$\frac{d\mathbf{m}}{dt} - \alpha \mathbf{m} \times \frac{d\mathbf{m}}{dt} = -\gamma M_s \mathbf{m} \times \left(\kappa_\mathrm{an} (\mathbf{e}_x \cdot \mathbf{m}) \mathbf{e}_x + \mathbf{h} + \frac{J_e}{J_p} b\, \mathbf{m} \times \mathbf{p} \right) , \tag{2.91}$$

where the scalar (and dimensionless) function b, in the new notations, is

$$b = b(\mathbf{m}) = \left[-4 + (1+P)^3 \frac{(3 + \mathbf{m} \cdot \mathbf{p})}{4P^{3/2}} \right]^{-1} . \tag{2.92}$$

By measuring the time t in units of $(\gamma M_s)^{-1}$, and introducing the following definitions,

$$\mathbf{h}_\mathrm{eff} = \kappa_\mathrm{an} (\mathbf{e}_x \cdot \mathbf{m}) \mathbf{e}_x + \mathbf{h}_\mathrm{m} + \mathbf{h}_\mathrm{a} \,, \qquad \beta = \beta(\mathbf{m}) = \frac{J_e}{J_p} b(\mathbf{m}) \,, \tag{2.93}$$

equation (2.91) can be written in the compact form

$$\frac{d\mathbf{m}}{dt} - \alpha \mathbf{m} \times \frac{d\mathbf{m}}{dt} = -\mathbf{m} \times (\mathbf{h}_\mathrm{eff} + \beta\, \mathbf{m} \times \mathbf{p}) \,. \tag{2.94}$$

In the following, we will find convenient to recast LLG equation in the following compact form:

$$\frac{d\mathbf{m}}{dt} - \alpha \mathbf{m} \times \frac{d\mathbf{m}}{dt} = -\mathbf{m} \times \mathcal{H}_\mathrm{eff} \,, \tag{2.95}$$

where

$$\mathcal{H}_\mathrm{eff}(\mathbf{m}) = \mathbf{h}_\mathrm{eff}(\mathbf{m}) + \beta\, \mathbf{m} \times \mathbf{p} \,. \tag{2.96}$$

Equation (2.95) is formally identical to LLG when there are no current-driven torque term. With the definition of the generalized effective field $\mathcal{H}_\mathrm{eff}$ we included the current-driven torque inside the effective field. The micromagnetic equilibria including spin torque effect are now related to the following equations similar to Eqs. (2.22):

$$\begin{cases} \mathbf{m} \times \mathcal{H}_\mathrm{eff}(\mathbf{m}) = \mathbf{0} \quad \Leftrightarrow \quad \mathcal{H}_\mathrm{eff}(\mathbf{m}) = \lambda \mathbf{m} \quad , \\ |\mathbf{m}| = 1 \quad . \end{cases} \tag{2.97}$$

The basic difference between the ordinary effective field $\mathbf{h}_\mathrm{eff}(\mathbf{m})$ and the generalized effective field $\mathcal{H}_\mathrm{eff}(\mathbf{m})$ is that the first one can be derived by the gradient of a free energy, while the second one cannot.

2.6.2 Discussion about units and typical values of parameters

In order to have an idea about the order of magnitude of the different terms of Eq. (2.94), in the following we report values of relevant constants appearing in the equations. The values of these constants will be specified in the SI (MKSA) units.

Fundamental constants and value of characteristic current density J_p

One of the fundamental constant of the LLG equation is the electron gyromagnetic ratio which, in SI units, is generally given as the ratio between electron charge e and mass m_e:

$$\gamma_e = \frac{e}{m_e} = \frac{1.602 \cdot 10^{-19}\mathrm{C}}{9.109 \cdot 10^{-31}\mathrm{kg}} = 1.7587 \cdot 10^{11}\ \mathrm{s}^{-1}\mathrm{T}^{-1} \tag{2.98}$$

where it has been used the fact that (1 C)/(1 kg) = 1/(1 T × 1 s). The gyromagnetic ratio γ appearing in Eq. (2.91) (and previous equations) is measured in such units that γM_s should have the dimension of a frequency. We will use the MKSA system and measure magnetization in A/m. To have the corresponding measure in Tesla we have to multiply magnetization by $\mu_0 = 4\pi \cdot 10^{-7}$ F/m, i.e. the magnetic permeability of vacuum. Therefore the value of γ to be used in Eq. (2.91) is

$$\gamma = \gamma_e \cdot \mu_0 = 2.21 \cdot 10^5\ \mathrm{s}^{-1}(\mathrm{A/m})^{-1}\,. \tag{2.99}$$

As far as the value of M_s, if we assume that the free layer is constituted by cobalt, we have

$$M_s = 1.42 \cdot 10^6\ \mathrm{A/m}\ \ \text{(Cobalt)} \quad \longrightarrow \quad \gamma M_s = 3.14 \cdot 10^{11}\ \mathrm{s}^{-1}\,. \tag{2.100}$$

This means that the unit time in the normalized equation (2.91) correspond to

$$\tau = \frac{1}{\gamma M_s} = 3.2\ \mathrm{ps}\ = 3.2\ 10^{-12}\ \mathrm{s}\,. \tag{2.101}$$

Another fundamental constant involved in the characteristic current density (2.90) is the Bhor magneton μ_B which, in SI units, has the following value

$$\mu_B = 927.4 \cdot 10^{-26}\ \mathrm{A\ m}^2\ = 9.274 \cdot 10^{-24}\ (\mathrm{A/m}) \cdot \mathrm{m}^3\,, \tag{2.102}$$

namely, it has the physical dimension of a magnetic moment. In addition to μ_B, it is necessary to specify the Landè factor g_e which is a pure number very close to 2. Finally, the characteristic current J_p is proportional to the thickness d of the free layer. A sensible choice of this parameter should be in the range of the nanometers. Let us choose $d = 3$ nm. Now, we can compute J_p :

$$J_p = \gamma M_s \frac{e\mathrm{M}_s d}{g_e \mu_\mathrm{B}}\ \approx 1.15 \cdot 10^{13} A\, m^{-2} = 1.15 \cdot 10^9 \mathrm{A\ cm}^{-2}\,. \tag{2.103}$$

This value of current is reference to establish if a current is small or big as far as current induced spin torque is concerned. In this respect, it is useful to mention that in most reported experiment in Co-Cu-Co pillars the largest injected current densities are in the order of 10^7A m^{-2}. Thus the factor β in Eq. (2.94) is at most in the order of 10^{-2}.

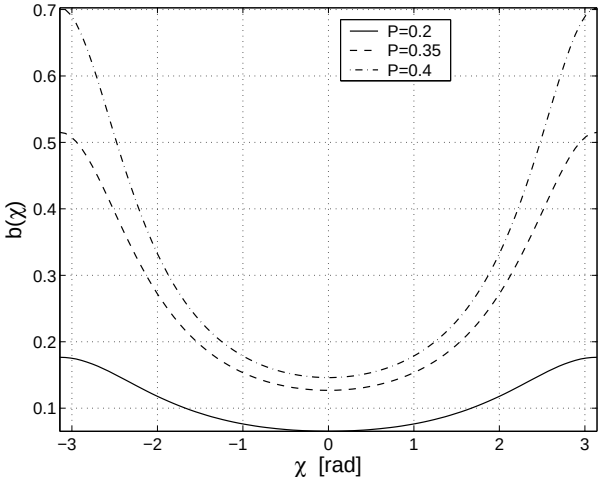

Figure 2.21: Plot of $b(\chi)$ versus χ for different values of P.

Discussion about the function $b(\boldsymbol{m})$

Actually, the value of beta is generally even smaller due to the contribution of the function $b(\mathbf{m})$. Then, let us now analyze this function and its order of magnitude. We denote with $b(\chi)$ the following function

$$b = b(\chi) = \left[-4 + (1+P)^3 \frac{(3+\cos(\chi))}{4P^{3/2}}\right]^{-1} . \tag{2.104}$$

where χ is the angle between $\mathbf{m}$ and $\mathbf{p}$. It is evident that $b(\chi)$ is periodic function of χ and it assumes its minimum at $\chi = 0$ and its maximum at $\chi = \pm\pi$. If we take as value of P the one indicated for Cobalt in the paper of Slonczewski, we have $P = 0.35$. Plots of the function $b(\chi)$ versus χ are reported for three different value of P in Fig. 2.21 . In the case $P = 0.35$ the function b assume a minimum value $b(0) \approx 0.13$ (parallel configuration of fixed and free layers) and a maximum value $b(\pi) \approx 0.52$ (antiparallel configuration of fixed and free layers). With this further information we can estimate the value of β which according to the treatment above is in the order of $10^{-3} \div 10^{-2}$.

The second parameter in the normalized equation (2.94) is α which is generally considered also in the range $10^{-3} \div 10^{-2}$.

2.6.3 Analytical investigation of self-oscillating behavior and current-induced switching

In the following we will present an analytical approach to study magnetization self-oscillations and reversal in the free layer of a trilayers structure traversed by a spin-polarized electric current perpendicular to the layers plane (see Fig. 2.20).

According to the derivation performed in section 2.6.1, the model equation which describe the dynamics of the free layer is:

$$\frac{d\mathbf{m}}{dt} - \alpha\mathbf{m} \times \frac{d\mathbf{m}}{dt} = -\mathbf{m} \times (\mathbf{h}_{\text{eff}} + \beta\mathbf{m} \times \mathbf{p}) \ . \tag{2.105}$$

which is written in dimensionless form with usual normalizations introduced in section 1.3.4; $\mathbf{p}$ is the direction of spin polarization and $\beta = \beta(\mathbf{m})$ is the dimensionless function describing the intensity of the spin-transfer torque. We model the free layer as a flat ellipsoidal particle in order that the effective field is given by the usual expression

$$\mathbf{h}_{\text{eff}} = \mathbf{h}_a - D_x m_x \mathbf{e}_x - D_y m_x \mathbf{e}_y - D_z m_z \mathbf{e}_z \quad , \tag{2.106}$$

where $\mathbf{h}_a$ is the applied field, $\mathbf{e}_x$, $\mathbf{e}_y$, $\mathbf{e}_z$, are cartesian unit vectors and $D_x \leq D_y \leq D_z$ take into account both shape and crystalline anisotropy. As far as the anisotropy field is concerned, most publications on Co-Cu-Co trilayers report value of H_{an} in the range of $10 \div 100$ mT which correspond to value of the normalized anisotropy constant κ_{an} around $10^{-2} \div 10^{-1}$.

In the analysis below we will assume that β is constant, which is a condition reasonably verified for $P \leq 0.1$. A more general analysis including the dependence of β on $\mathbf{m}$ has been performed in Ref. [49].

To start our discussion, let us consider the energy balance equation associated to Eq. (2.105):

$$\frac{dg(\mathbf{m})}{dt} = -\mathcal{P}(\mathbf{m}) = -\alpha \left| \frac{d\mathbf{m}}{dt} \right|^2 + \beta \, (\mathbf{m} \times \mathbf{p}) \cdot \frac{d\mathbf{m}}{dt} \, , \tag{2.107}$$

where

$$g(\mathbf{m}) = \frac{D_x}{2} m_x^2 + \frac{D_y}{2} m_y^2 + \frac{D_z}{2} m_z^2 - \mathbf{h}_{\text{a}} \cdot \mathbf{m} \tag{2.108}$$

is the free energy of the magnetic body and $\mathcal{P}(\mathbf{m})$ is the "absorbed power" function. Equation (2.107) has very interesting implications: in appropriate conditions the spin-transfer torque term may provide energy to the system and counterbalance dissipation associated to the Gilbert term. If this is the case, the dynamical system (2.105) may exhibit limit cycles i.e. periodic self-oscillation.

Perturbative technique

In order to establish the existence, the number, the stability and the locations of these limit cycles we can exploit the fact that both α and β are small quantities (in the order of $10^{-2} \div 10^{-3}$). Thus, we can study the dynamics under the influence of spin-injection as perturbation of the case $\alpha = 0$, $\beta = 0$. To this end, we

introduce the perturbation parameter ϵ such that $\alpha = \alpha_0\epsilon$, $\beta = \beta_0\epsilon$, and write Eq.(2.105) in the following perturbative form

$$\frac{d\mathbf{m}}{dt} = \mathbf{f}_0(\mathbf{m}) + \epsilon\mathbf{f}_1(\mathbf{m}) + \mathcal{O}\left(\epsilon^2\right) , \tag{2.109}$$

where

$$\mathbf{f}_0(\mathbf{m}) = -\mathbf{m} \times \mathbf{h}_{\text{eff}} \tag{2.110}$$

$$\mathbf{f}_1(\mathbf{m}) = -\beta_0\mathbf{m} \times (\mathbf{m} \times \mathbf{p}) - \alpha_0\mathbf{m} \times (\mathbf{m} \times \mathbf{h}_{\text{eff}}) \quad . \tag{2.111}$$

The unperturbed dynamics described by the undamped LLG

$$\frac{d\mathbf{m}}{dt} = -\mathbf{m} \times \mathbf{h}_{\text{eff}} \quad , \tag{2.112}$$

can be treated analytically [50], for any constant applied field, by using the fact that conservative dynamics admits two integrals of motions (section 1.3.5):

$$m_x^2 + m_y^2 + m_z^2 = 1 \tag{2.113}$$

$$g(\mathbf{m}) = g_0 \quad , \tag{2.114}$$

where g_0 is a constant depending on initial conditions. Similarly to the analysis performed in section 2.5, we will denote the trajectory of the unperturbed LLG equation, corresponding to the value g_0, with the notation $\mathbf{m}_{g_0}(t)$ and the corresponding period with T_{g_0}. These trajectories are all closed and periodic (except separatrices which begin and finish at saddles equilibria). When the perturbation term $\epsilon\mathbf{f}_1(\mathbf{m})$ is introduced, almost all closed trajectories are slightly modified and collectively form spiral-shaped trajectories toward attractors. There are only special trajectories which remain (at first order in ϵ) practically unchanged and become limit cycles of the perturbed system, provided that ϵ is small enough. In addition, each limit cycle is ϵ-close to the conservative trajectory from which it has been generated. The value of energy of the unperturbed special trajectories which generate limit cycles can be found from the zeros of the Melnikov function (see Appendix and Ref. [43]):

$$M(g_0) = \int_0^{T_{g_0}} \mathbf{m}_{g_0}(t) \cdot [\mathbf{f}_0(\mathbf{m}_{g_0}(t)) \times \mathbf{f}_1(\mathbf{m}_{g_0}(t))]\, dt\,. \tag{2.115}$$

In our case, by using straightforward algebra, one can prove that the function $M(g_0)$ can be expressed as:

$$\epsilon M(g_0) = \int_0^{T_{g_0}} \mathcal{P}(\mathbf{m}_{g_0}(t))dt = \alpha M^{\alpha}(g_0) + \beta M^{\beta}(g_0), \tag{2.116}$$

where $\alpha M^{\alpha}(g_0)$ and $\beta M^{\beta}(g_0)$ respectively correspond to the integral over one period of the first and second terms at the right hand side of Eq. (2.107). The expression (2.116) of the $M(g_0)$ provides also a physical justification of the method:

the existence of limit cycles requires an average balance between loss and gain of energy. We observe that this result is analogous to the one discussed in section 2.5.

Current-driven switching experiment. Analytical and numerical results

In the sequel, we apply the perturbation technique outlined above to a special case relevant to the spintronics applications: self-oscillations and reversal of magnetization driven by the current in absence of applied field ($\mathbf{h}_a = 0$). In the discussion we will assume that the injected spin polarization $\mathbf{p}$ is aligned with the easy axis of the magnetic free layer ($\mathbf{p} = \mathbf{e}_x$). More general cases, with nonzero applied field and arbitrary orientation of $\mathbf{p}$, can be treated by following a very similar line of reasoning [49].

We suppose that the system is initially in the potential well around the equilibrium state $\mathbf{m} = \mathbf{e}_x$. This region is characterized by magnetization states with energies values

$$\frac{D_x}{2} \leq g_0 \leq \frac{D_y}{2} \quad . \tag{2.117}$$

In the latter equation $g_0 = D_x/2$ is the energy of $\mathbf{m} = \mathbf{e}_x$, while $g_0 = D_y/2$ corresponds to the saddles points $\mathbf{m} = \pm\mathbf{e}_y$. The analytical solution of the unperturbed dynamics in this region is given by [50]

$$m_x(t) = k_g \, \mathrm{dn}(\Omega_L t, k_L) \quad , \tag{2.118}$$

$$m_y(t) = (k'_g/k') \, \mathrm{sn}(\Omega_L t, k_L) \quad , \tag{2.119}$$

$$m_z(t) = -k'_g \, \mathrm{cn}(\Omega_L t, k_L) \quad , \tag{2.120}$$

where $\mathrm{sn}(u, k_L)$, $\mathrm{dn}(u, k_L)$, $\mathrm{cn}(u, k_L)$ are the Jacobi elliptic functions[5] of modulus k_L. The following relationship hold for the quantities appearing in Eqs. (2.118)-(2.120):

$$k_g^2 = (D_z - 2g_0)/(D_z - D_x) \quad , \tag{2.121}$$

$$k^2 = (D_z - D_y)/(D_z - D_x) \quad , \tag{2.122}$$

$$k_g'^2 = 1 - k_g^2 \quad , \tag{2.123}$$

$$k'^2 = 1 - k^2 \quad , \tag{2.124}$$

$$k_L = (k k'_g)/(k_g k') \quad , \tag{2.125}$$

$$\Omega_L = k_g k' (D_z - D_x) \quad . \tag{2.126}$$

The period of the solution is given by the following formula:

$$T_{g_0} = 4K(k_L)/\Omega_L \quad , \tag{2.127}$$

[5] See Appendix B.

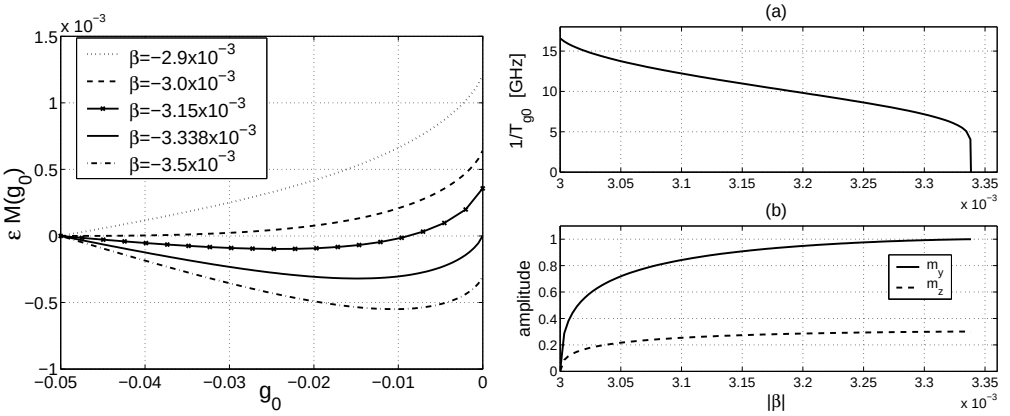

Figure 2.22: (left) Melnikov function for different values of β ($\alpha = 5 \cdot 10^{-3}$, $D_x = -0.1$, $D_y = 0$, $D_z = 1$). $\beta_{c1} = -3 \cdot 10^{-3}$, $\beta_{c2} = -3.338 \cdot 10^{-3}$. (right) Frequency $(1/T_{g_0})$ and amplitude of self-oscillations of the limit cycles vs the value of $|\beta|$ in the interval $[\beta_{c1}, \beta_{c2}]$ ($\alpha = 5 \cdot 10^{-3}$, $D_x = -0.1$, $D_y = 0$, $D_z = 1$).

where $K(k_L)$ is the complete elliptic integral of the first kind. By using the above expressions in Eq. (2.116), the following analytical formulas can be derived

$$\begin{aligned} M^{\alpha}(g_0) &= 4\Omega_L \left[\mathrm{K}(k_L) \left(\frac{k_g'^2}{k'^2} - 1 \right) + \mathrm{E}(k_L) \right] . \\ M^{\beta}(g_0) &= 2\pi \frac{1}{k'} \frac{(2g_0 - D_x)}{(D_z - D_x)} \end{aligned} \tag{2.128}$$

where $\mathrm{E}(k_L)$ is the complete elliptic integral of the second kind. Notice that $M^{\alpha}(g_0)$ and $M^{\beta}(g_0)$ are positive functions, zero only for $g_0 = D_x/2$ (equilibrium at $\mathbf{m} = \mathbf{e}_x$). Plots of the $M(g_0)$ versus g_0 for different values of β are reported in Fig. 2.22. The interpretation of Melnikov function in terms of energy balance, expressed by Eq. (2.107) and Eq. (2.116), can help one to qualitatively understand the dynamics and the stability of limit cycles. In fact, zeros of the Melnikov function determine trajectories on which there is average balance between power dissipation and absorption. Conversely, a positive (negative) value of the Melnikov function indicates, according to Eq. (2.107), that the system has to move towards periodic trajectories with lower (upper) energy[6].

It is clear from Fig. 2.22 that $M(g_0)$ has another zero for β negative and such that $|\beta| > |\beta_{c1}|$ where β_{c1} is the value such that the derivative of $M(g_0)$ in $D_x/2$ is equal to zero. This corresponds to the condition of tangency of the Melnikov function diagram at $g_0 = D_x/2$:

$$\frac{dM}{dg_0}(D_x/2) = 0 \quad . \tag{2.129}$$

[6]We notice that a fixed point is a degenerate periodic trajectory.

By using Eq. (2.128) and simple algebra one can derive that

$$\beta_{c1} = -\frac{\alpha}{2}[(D_z - D_x) + (D_y - D_x)]\,. \tag{2.130}$$

This value of β_{c1} correspond to an Hopf bifurcation [43] of the equilibrium $\mathbf{m} = \mathbf{e}_x$: the equilibrium becomes unstable and a stable limit cycle around the equilibrium is created (see Fig. 2.23). If we further increase the value $|\beta|$ the zero of $M(g_0)$ will move toward larger value of energy. Since the limit cycle is $\epsilon-$close to the conservative trajectory corresponding the zero of $M(g_0)$, we can derive its properties from the property of the corresponding conservative trajectory. In Fig. 2.22 the amplitude and the frequency of the limit cycle as function of $|\beta|$ are reported. Notice that due to the thin film geometry the amplitude of the oscillation of $m_z(t)$ remains rather small. When $|\beta|$ is increased further we arrive to the value β_{c2} such that $M(D_y/2) = 0$, which is given by

$$\beta_{c2} = -\alpha\frac{M^{\alpha}(D_y/2)}{M^{\beta}(D_y/2)} \quad . \tag{2.131}$$

At this value of β the system undergoes an homoclinic connection bifurcation [43] in which the limit cycle first degenerates in a homoclinic connection and then is destroyed (see Fig. 2.24). The system then relaxes toward the equilibrium $\mathbf{m} = -\mathbf{e}_x$. In order to the test the accuracy of the perturbation technique we have carried out numerical simulations of Eq. (2.105) for different values of β. The results are presented in Fig. 2.25. Notice that the two bifurcations, Hopf and Homoclinic connection, occur at critical values that are very close to the ones predicted by the theory.

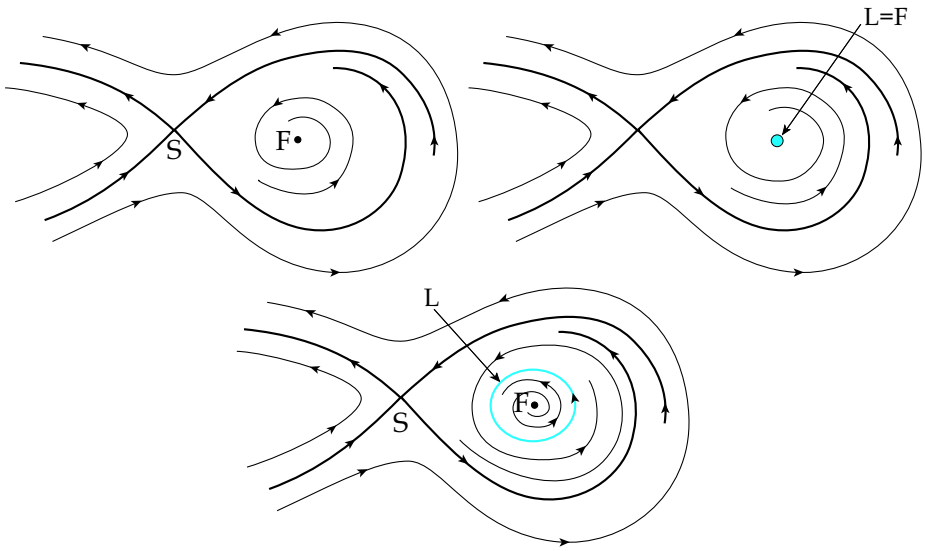

Figure 2.23: Mechanism of the Hopf bifurcation. (up left) The focus F is a stable equilibrium. (up right) For $\beta = \beta_{c1}$ the limit cycle L coincides with the equilibrium F. (bottom) For $|\beta| > |\beta_{c1}|$ the focus F becomes unstable and a stable limit cycle L is created. This mechanism justifies the onset of self-oscillations driven by the spin-transfer torque term.

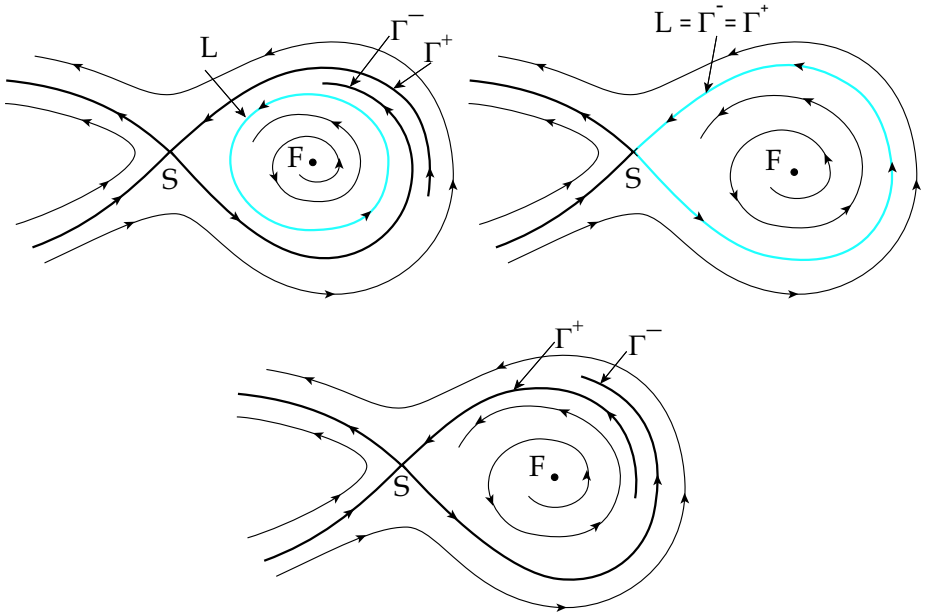

Figure 2.24: Mechanism of the homoclinic bifurcation. (up left) For $|\beta_{c1}| < |\beta| < |\beta_{c2}|$ there is a stable limit cycle L around the unstable equilibrium F. (up right) For $\beta = \beta_{c2}$ the limit cycle L disappears and a homoclinic connection $\Gamma^+ \equiv \Gamma^- \equiv L$ is created. (bottom) For $|\beta| > |\beta_{c2}|$ the homoclinic connection disappears but the mutual position of the separatrices Γ^+ and Γ^- is exchanged. The region around the unstable equilibrium F is now in the basin of attraction of the reversed state. This mechanism permits the switching of the free layer.

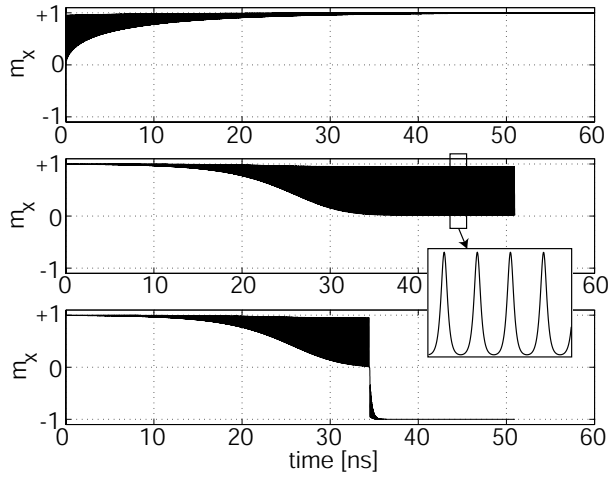

Figure 2.25: Numerical simulation of Eq. (2.105) with $\alpha = 5 \cdot 10^{-3}$, $D_x = -0.1$, $D_y = 0$, $D_z = 1$. Top: $\beta = -2.9 \cdot 10^{-3}$. Middle: $\beta = -3.336 \cdot 10^{-3}$. Bottom: $\beta = -3.339 \cdot 10^{-3}$.

Chapter 3

Non-uniform Magnetization Dynamics in thin-films reversal processes

When one wants to remove the simplifying hypothesis that the body is uniformly magnetized, some issues arise which considerably complicate the solution of Landau-Lifshitz-Gilbert (LLG) equation. First of all, LLG equation becomes an integro-partial differential equation in the unknown vector field $\mathbf{m}(\mathbf{r}, t)$. Moreover, the LLG equation is nonlinear and this implies that, in general, it is not possible to find exact analytical solutions. Therefore, the most general method to solve LLG equation lies on appropriate numerical techniques. In this respect, usually a semi-discretization approach is adopted. First, a spatial discretization of the equation is performed, by using finite differences or finite elements methods [52]. As a result, a discretized version of the micromagnetic free energy and a corresponding system of ordinary differential equations are derived. Finally, this system of ordinary differential equations is numerically solved with appropriate time-stepping schemes.

In this framework, many problems arise. One is the fact that micromagnetics, although is applicable in principle to magnetic bodies within a broad spatial scale (form few nm to many μm), cannot be practically used for dimensions exceeding 1 μm. In fact, for sub-micron particles, numerical simulations reasonably agree with experimental results, whereas for increasing dimensions of the bodies the agreement with experimental observations is only qualitative. Amikam Aharoni pointed out few years ago [51] that the reasons of such a 'failure' can be found in bad understanding of theoretical results, like nucleation theory [5], as well as bad approximations and rough discretization in energy computations. More specifically, regarding the latter point, he emphasized that the correctness of the results strongly depends from an accurate computation of magnetostatic field. In fact, once that magnetization becomes space-dependent and for arbitrary body shape, the analytical expression (2.19) does not hold anymore. For these reasons, few years ago, some researchers at NIST proposed a set of micromagnetic stan-

dard problems [79], with simple rectangular geometries and material properties, to test micromagnetic numerical codes. In this respect, the standard problem no. 1, involving a $2 \times 1 \times 0.02$ μm permalloy thin-film, represents the most appropriate example of the above issues. In fact, the results provided by different groups showed qualitative agreement between the computed hysteresis loops, but the quantitative evaluations of coercive fields were different even for two orders of magnitude! After that, much more attention has been paid to the correct formulation of numerical models. It has been recognized that the bottleneck of micromagnetic simulations is always the fast and accurate evaluation of the magnetostatic demagnetizing field. In the following sections we will present mostly used methods for demagnetizing field computation. Afterwards, we will perform a comparison between damping and precessional switching processes for rectangular thin-film geometry and we will show that damping switching is intrinsically a non-uniform process, involving domain nucleation and wall motion, whereas precessional switching can be reasonably considered a quasi-uniform process also for body dimensions of hundreds of nanometers. Finally, in the framework of quasi-uniform magnetization dynamics, we will analyze the fast switching, below Stoner-Wohlfarth field, of tilted media for magnetic recording.

3.1 MAGNETOSTATIC FIELD COMPUTATION

We recall that magnetostatic field is defined by the Maxwell equations (1.45)-(1.46):

$$\begin{cases} \nabla \cdot \mathbf{H}_{\mathrm{m}} = -\nabla \cdot \mathbf{M} & \text{in } \Omega \\ \nabla \cdot \mathbf{H}_{\mathrm{m}} = 0 & \text{in } \Omega^c \\ \nabla \times \mathbf{H}_{\mathrm{m}} = \mathbf{0} \end{cases} , \tag{3.1}$$

with the following conditions at the body discontinuity surface $\partial\Omega$

$$\begin{cases} \mathbf{n} \cdot [\mathbf{H}_{\mathrm{m}}]_{\partial\Omega} = \mathbf{n} \cdot \mathbf{M} \\ \mathbf{n} \times [\mathbf{H}_{\mathrm{m}}]_{\partial\Omega} = \mathbf{0} \end{cases} . \tag{3.2}$$

From the simple inspection of the above equations, two important considerations can be drawn:

1. There is a functional relationship between magnetization $\mathbf{M}$ and magnetostatic field $\mathbf{H}_{\mathrm{m}}$, that is, the value of $\mathbf{H}_{\mathrm{m}}$ at a spatial location $\mathbf{r}$ depends on the value of magnetization vector field at every location $\mathbf{r}'$ within Ω. This is a consequence of the nonlocal (long range) character of magnetostatic maxwellian interactions. Each elementary dipole in the body contributes

to produce the magnetostatic field at an assigned location within the body. Quoting Aharoni, "...In a numerical computation of N unit cells, the long range means the magnetostatic energy term includes an interaction of every cell with all the other cells, thus involving N^2 terms, whereas only N terms are required for computing the other energy terms. Therefore, computing the magnetostatic energy takes almost all the computer time in a typical micromagnetic computation. It is also the energy term with the heaviest demand on the computer memory, which means that it determines the limit of the size of the body that a computer can handle...".

2. The differential problem (3.1)-(3.2) is an open boundary problem, that is, even if one is interested in the computation of magnetostatic field $\mathbf{H}_{\mathrm{m}}$ at locations $\mathbf{r} \in \Omega$, one has to solve Eqs. (3.1)-(3.2) in the whole space. This means that, in the framework of numerical modeling, one should preform in principle the discretization of the whole space, which is, of course, not feasible. For this reason, numerical methods consistent with the continuum model have to be used in numerical simulations.

In this respect, the methods based on truncation of the interaction range of magnetostatic fields [61], mean-field approximation for distant particles [62], hierarchical dipole interaction evaluation schemes [63] cause loss of accuracy and indeed don't save very much computational time. In general, all the methods for the computation of the demagnetizing field have a cost scaling function that is something in between the minimum $\mathcal{O}(N)$ and the maximum $\mathcal{O}(N^2)$.

In the sequel, we will analyze two different methods which are commonly used for magnetostatic field computations respectively in case of finite-differences and finite elements spatial discretization [52].

3.1.1 FFT Discrete convolution method

This method is mostly used as soon as a spatial discretization based on Finite Differences (FD) [52] can be defined over a structured mesh. This occurs for example, if one considers a magnetic body with rectangular geometry and subdivides it into a collection of square rectangular prisms with edges d_x, d_y, d_z parallel to the coordinate axes. To start our discussion we recall the fact that the solution of magnetostatic problem (3.1)-(3.2) can be obtained in terms of the scalar potential φ such that $\mathbf{H}_{\mathrm{m}} = -\nabla\varphi$, solution of the following boundary value

problem:

$$\begin{cases} \nabla^2\varphi = \nabla\cdot\mathbf{M} & \text{in } \Omega \\ \nabla^2\varphi = 0 & \text{in } \Omega^c \\ [\varphi]_{\partial\Omega} = 0 \\ \left[\dfrac{\partial\varphi}{\partial\mathbf{n}}\right]_{\partial\Omega} = -\mathbf{n}\cdot\mathbf{M} \end{cases} . \tag{3.3}$$

The boundary value problem (3.3) admits the following solution [13]:

$$\varphi(\mathbf{r}) = -\frac{1}{4\pi}\int_\Omega \frac{\nabla'\cdot\mathbf{M}(\mathbf{r}')}{|\mathbf{r}-\mathbf{r}'|}\,dV_{\mathbf{r}'} + \frac{1}{4\pi}\int_{\partial\Omega}\frac{\mathbf{M}(\mathbf{r}')\cdot\mathbf{n}}{|\mathbf{r}-\mathbf{r}'|}\,dS_{\mathbf{r}'} \quad . \tag{3.4}$$

By using the divergence theorem, the surface integral can be rewritten as volume integral. Equation (3.4) can be put in the compact form:

$$\varphi(\mathbf{r}) = \frac{1}{4\pi}\int_\Omega \left[-\frac{\nabla'\cdot\mathbf{M}(\mathbf{r}')}{|\mathbf{r}-\mathbf{r}'|} + \nabla'\cdot\left(\frac{\mathbf{M}(\mathbf{r}')}{|\mathbf{r}-\mathbf{r}'|}\right)\right] dV_{\mathbf{r}'} \quad . \tag{3.5}$$

By using the fact that $\nabla\cdot(f\mathbf{v}) = f\nabla\cdot\mathbf{v} + \mathbf{v}\cdot\nabla f$, one ends up with:

$$\varphi(\mathbf{r}) = \frac{1}{4\pi}\int_\Omega \nabla'\left(\frac{1}{|\mathbf{r}-\mathbf{r}'|}\right)\cdot\mathbf{M}(\mathbf{r}')\,dV_{\mathbf{r}'} \quad . \tag{3.6}$$

Thus, the magnetostatic field $\mathbf{H}_\mathrm{m}$ is given by

$$\begin{aligned}\mathbf{H}_\mathrm{m}(\mathbf{r}) = -\nabla\varphi &= -\frac{1}{4\pi}\nabla\int_\Omega \nabla'\left(\frac{1}{|\mathbf{r}-\mathbf{r}'|}\right)\cdot\mathbf{M}(\mathbf{r}')\,dV_{\mathbf{r}'} = \\ &= -\int_\Omega \mathcal{N}(\mathbf{r}-\mathbf{r}')\cdot\mathbf{M}(\mathbf{r}')\,dV_{\mathbf{r}'} \quad ,\end{aligned} \tag{3.7}$$

where $\mathcal{N}(\mathbf{r}-\mathbf{r}')$ is the demagnetizing tensor. The product $-\mathcal{N}(\mathbf{r}-\mathbf{r}')\cdot\mathbf{M}(\mathbf{r}')\,dV_{\mathbf{r}'}$ gives the magnetostatic field produced at location $\mathbf{r}$ by an elementary magnetic moment situated at location $\mathbf{r}'$. The expression (3.7) remains formally unchanged if one assumes suitable discretization over N elementary cells. For instance, if we subdivide the magnetic body into $N = n_x n_y n_z$ rectangular square prisms with edges parallel to the coordinate axes, with n_x, n_y, n_z cells along the x, y, z axis respectively, each cell can be uniquely determined by means of three indexes i, j, k. As far as magnetization within the cells is concerned, there are two approaches proposed in literature. The first is often referred to as *constant volume charges*[1] method, that is, $\nabla\cdot\mathbf{M}$ is supposed to be constant within each cell. The second approach supposes the magnetization $\mathbf{M}$ uniform within each cell. A comparison between these two approach has been performed in Ref. [53] with respect to the solution of the standard problem no. 2 (see $\mu-$mag website [79] for details).

[1] Recalling the Coulomb approach to magnetic materials, which is in term of equivalent volume charges $\rho_m = -\nabla\cdot\mathbf{M}$ and surface charges $\sigma_m = \mathbf{M}\cdot\mathbf{n}$. See Ref. [13] for details.

Thus, apart from this particular choice, one can rewrite Eq. (3.7) as a discrete convolution:

$$\mathbf{H}_{\mathrm{m};i,j,k} = -\sum_{i,j,k\neq i',j',k'} N_{i-i',j-j',k-k'} \cdot \mathbf{M}_{i',j',k'}\, d_x d_y d_z \quad , \tag{3.8}$$

where $N_{p,q,r}$ is the demagnetizing tensor associated to the prism cell (p,q,r):

$$N_{p,q,r} = \begin{pmatrix} N_{xx} & N_{xy} & N_{xz} \\ N_{yx} & N_{yy} & N_{yz} \\ N_{zx} & N_{zy} & N_{zz} \end{pmatrix} \quad . \tag{3.9}$$

The discrete convolution (3.8) can be computed by means of the Discrete Fourier Transform (DFT), which can be implemented very efficiently with the well-known algorithm referred to as Fast Fourier Transform [60]. In fact, the time-domain convolution can be changed into a scalar product in frequency space using the Fourier transform. To properly take care of the finite size effect of the system and, therefore, to avoid circular convolution, the standard zero-padding techniques [64] can be used. In fact, the inverse Fourier transform will yield the correct field in real space, if the number of cells in each dimension after zero-padding is not less than twice the number of physical cells. The latter requirement ensures that the inferred periodic boundary condition of this enlarged region with padded zeros will not affect the physical data in real space after the inverse FFT is performed. In fact, to perform the FFT which does require overall periodicity, and yet not to allow the cells in the simulated region to be affected by the fields in the extended periods, the void buffer area between a physical cell and the first image cell in the adjacent period must exceed the interaction force range given by the number of the cells N [65].

Assuming that the dimensions of the zero-padded discretization grid are $2n_x, 2n_y, 2n_z$, along the directions x, y, z respectively, and referring for instance to the x component of $\mathbf{H}_{\mathrm{m}}$, the discrete convolution (3.8) can be written as:

$$\underline{\mathrm{H}}_{x;i,j,k} = -\sum_{i,j,k\neq i',j',k'} \sum_{\eta}^{\{x,y,z\}} \underline{\mathrm{N}}_{x\eta;i-i',j-j',k-k'} \underline{\mathrm{M}}_{\eta;i',j',k'}\, d_x d_y d_z \quad , \tag{3.10}$$

where $\underline{\mathrm{H}}_x, \underline{\mathrm{M}}_\eta, \underline{\mathrm{N}}_{x\eta}$ $(\eta \in \{x,y,z\})$ are $2n_x \times 2n_y \times 2n_z$ matrices. The Discrete Fourier Transform (DFT) $\hat{\underline{\mathrm{H}}}_x$ of $\underline{\mathrm{H}}_x$ can be expressed as:

$$\hat{\underline{\mathrm{H}}}_x(\omega_x,\omega_y,\omega_z) = \sum_{i=1}^{2n_x-1} \sum_{j=1}^{2n_y-1} \sum_{k=1}^{2n_z-1} \underline{\mathrm{H}}_{x;i,j,k} \exp\left[2\pi\iota\left(\frac{\omega_x i}{2n_x} + \frac{\omega_y j}{2n_y} + \frac{\omega_z k}{2n_z}\right)\right] \quad , \tag{3.11}$$

where ι is the imaginary unit $\iota = \sqrt{-1}$ and $\omega_x, \omega_y, \omega_z$ are the frequency domain variables. Analogous expressions can be written for $\hat{\underline{\mathrm{M}}}_x$ and $\hat{\underline{\mathrm{N}}}_{x\eta}$. Therefore, the

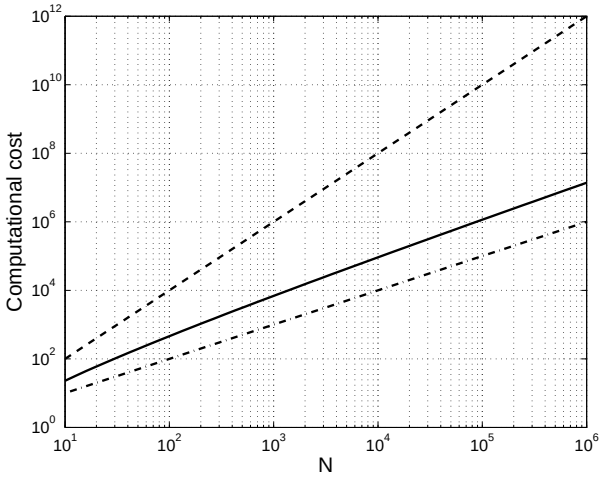

Figure 3.1: Computational cost scaling plot. Dashed line represents $\mathcal{O}(N^2)$ scaling. Dash-dotted line represents $\mathcal{O}(N)$ scaling. Solid line represents $\mathcal{O}(N \log N)$ scaling.

discrete convolution theorem states that Eq. (3.10) can be written in frequency domain as sum of matrix element-by-element product:

$$\hat{\underline{\mathrm{H}}}_x(\omega_x, \omega_y, \omega_z) = \sum_{\eta}^{\{x,y,z\}} \hat{\underline{\mathrm{N}}}_{x\eta}(\omega_x, \omega_y, \omega_z)\hat{\underline{\mathrm{M}}}_{\eta}(\omega_x, \omega_y, \omega_z) \quad . \tag{3.12}$$

The x component $\underline{\mathrm{H}}_x$ can be obtained by computing the inverse FFT of the expression (3.12). Therefore, the cost of the evaluation of the demagnetizing field can be summarized as follows:

- In the preprocessing stage of the simulation, the FFTs of the 9 demagnetizing matrices $\underline{\mathrm{N}}_{x\eta}, \underline{\mathrm{N}}_{y\eta}, \underline{\mathrm{N}}_{z\eta}$ ($\eta \in \{x, y, z\}$) has to be evaluated and stored in memory.

- For each computation of the demagnetizing field, six FFTs has to be computed: three related to magnetization matrices, namely $\hat{\underline{\mathrm{M}}}_x, \hat{\underline{\mathrm{M}}}_y, \hat{\underline{\mathrm{M}}}_z$ and three inverse FFTs of the components $\hat{\underline{\mathrm{H}}}_x, \hat{\underline{\mathrm{H}}}_y, \hat{\underline{\mathrm{H}}}_z$ in frequency domain.

The cost of a single FFT evaluation scales according to the $\mathcal{O}(N \log N)$ behavior. Thus, by using the FFT method the computational cost for the calculation of the magnetostatic field can be considerably reduced with respect to the $\mathcal{O}(N^2)$ scaling connected with the direct evaluation of the integral (3.7) (see Fig. 3.1).

3.1.2 Hybrid Finite elements-Boundary elements method

In this section we briefly describe a numerical method for the evaluation of the demagnetizing field which is commonly used when spatial discretization based on

Finite Elements (FE) Method is performed [52]. The main advantage of FE discretization lies in the possibility of simulating processes occurring in bodies with in principle arbitrary geometry. This is crucial for the design of technological devices, whose geometry is often very far from being approximated with a 'staircase'. Nevertheless, as mentioned in section 3.1, plain FE method would require that the whole space was discretized. For this reason, many researchers have dealt with the derivation of FE modifications to take into account the open-boundary nature of the problem.

In fact, in order to impose the regularity condition at infinity, Chen suggests that the FE mesh has to be extended over a large region outside the magnetic particles (at least five times the extension of the particle [54]). Various other techniques have been proposed to reduce the size of the external mesh or to avoid a discretization of the exterior space. The use of asymptotic boundary conditions [55] reduces the size of the external mesh as compared to truncation. At the external boundary, Robbin conditions, which are derived from a series expansion of the solution of the Laplace equation for outside the magnet and give the decay rate of the potential at a certain distance from the sample, are applied [56]. A similar technique that considerably reduces the size of the external mesh is the use of space transformations to evaluate the integral over the exterior space. Among the various transformations proposed to treat the open boundary problem, the parallelepipedic shell transformation [57], which maps the external space into shells enclosing the parallelepipedic interior domain, has proved to be most suitable in micromagnetic calculations. The method can be easily incorporated into standard FE programs transforming the derivatives of the nodal shape functions. This method was applied in static three-dimensional micromagnetic simulations of the magnetic properties of nanocrystalline permanent magnets (see Refs. [58] and [59]).

An alternative approach was proposed by Fredkin and Koehler [70] in 1990. The main idea, due to the linearity of Poisson problem, is to split the scalar potential φ into φ_1 and φ_2 such that:

$$\varphi = \varphi_1 + \varphi_2 \quad . \tag{3.13}$$

The boundary value problem for the potential φ_1 can be formulated as an internal Neumann problem in the following way:

$$\begin{cases} \nabla^2 \varphi_1 = \nabla \cdot \mathbf{M} & \text{in } \Omega \\ \varphi_1 = 0 & \text{in } \Omega^c \\ \left. \dfrac{\partial \varphi_1}{\partial \mathbf{n}} \right|_{\partial\Omega} = \mathbf{n} \cdot \mathbf{M} \end{cases} . \tag{3.14}$$

By comparing the problem (3.14) with the original problem (3.3), we can derive the boundary value problem for φ_2:

$$\begin{cases} \nabla^2\varphi_2 = 0 & \text{in } \Omega \cup \Omega^c = \Omega_\infty \\ [\varphi_2]_{\partial\Omega} = \varphi_1\big|_{\partial\Omega^-} \\ \left[\dfrac{\partial\varphi_2}{\partial\mathbf{n}}\right]_{\partial\Omega} = 0 \\ \varphi_2 \quad \text{regular at infinity } \partial\Omega_\infty \end{cases} , \tag{3.15}$$

where $\partial\Omega^-$ indicates the internal layer of the boundary $\partial\Omega$. The solution φ_2 of the latter boundary value problem is the well-known double layer potential [13]:

$$\varphi_2(\mathbf{r}) = \frac{1}{4\pi}\int_{\partial\Omega} \varphi_1(\mathbf{r}')\nabla'\left(\frac{1}{|\mathbf{r}-\mathbf{r}'|}\right)\cdot\mathbf{n}\,dS \quad . \tag{3.16}$$

Until now, it is not yet evident the advantage of the method, since the evaluation of the potential $\varphi_2(\mathbf{r})$ at each location $\mathbf{r} \in \Omega$ is very expensive from computational point of view. Indeed the situation seems more complicated with respect to the direct evaluation of the original integral (3.7), since now $N \times N_b$ operations (N_b is the number of boundary nodes) plus the solution of boundary value problem (3.14) are required in order to obtain φ.

The nice idea is to use Eq. (3.16) to evaluate the potential φ_2 *only* on the boundary $\partial\Omega^-$. In fact, it is known from potential theory [66] that if $\partial\Omega$ is sufficiently smooth at location $\mathbf{r}_0$, then

$$\lim_{\substack{\mathbf{r}\to\mathbf{r}_0^- \\ \mathbf{r}_0\in\partial\Omega}} \varphi_2(\mathbf{r}) = -\frac{\varphi_1(\mathbf{r}_0)}{2} + \frac{1}{4\pi}\int_{\partial\Omega} \varphi_1(\mathbf{r}')\nabla'\left(\frac{1}{|\mathbf{r}_0-\mathbf{r}'|}\right)\cdot\mathbf{n}\,dS \quad . \tag{3.17}$$

It can be shown [67] that the discretized version of the latter equation is:

$$\underline{\varphi}_2 = B\underline{\varphi}_1 \quad , \tag{3.18}$$

where B is a suitable $N_b \times N_b$ boundary matrix and $\underline{\varphi}_1, \underline{\varphi}_2$ are the vector containing the boundary nodal values of the scalar potentials φ_1, φ_2. From the knowledge of φ_2 on the boundary $\partial\Omega$, which now costs N_b^2 operations, then the boundary value problem (3.15), now with Dirichlet boundary conditions on $\partial\Omega$, can be solved with the usual FE technique [52].

Let us summarize the costs of this hybrid technique. We assume that the mesh (typically consisted of tetrahedrons) has N nodes. In most situations, one can think that the boundary nodes N_b are in the order $\mathcal{O}(N^{2/3})$. In particular, this happens when characteristic dimensions of the body, along the coordinates axes, are of the same order of magnitude. We will discuss remarkable exceptions after. Therefore,

- at the preprocessing stage, the boundary matrix B $[N_b \times N_b]$ has to be computed and stored. The storage requirement is $\mathcal{O}(N_b^2)$.
- In a single evaluation of the demagnetizing field:
  1. the internal Neumann problem (3.14) has to be solved with the usual FE technique to find φ_1. This implies that it costs the inversion of an $N \times N$ linear system.
  2. The value of φ_2 on the boundary has to be computed by means of Eq. (3.18), which costs N_b^2 operations.
  3. The internal Dirichlet problem, given by Eq. (3.15) with boundary conditions obtained at step 2, has to be solved with FE technique, which costs another $N \times N$ linear system inversion, but with same stiffness matrix used at step 1.
  4. Finally, the demagnetizing field $\mathbf{H}_{\mathrm{m}} = -\nabla(\varphi_1 + \varphi_2)$ has to be evaluated.

We observe that this method has the advantage to manage arbitrarily complicated geometries, whereas the FFT convolution method is optimal with a structured mesh. Nevertheless, if one deals with somehow "flat" magnetic bodies, like for instance thin-films, the assumption $N_b \sim \mathcal{O}(N^{2/3})$ fails, since it happens instead $N \simeq N_b$, unless than one performs additional (and maybe useless) refinement along the "small" dimension. Thus, one can conclude that the hybrid FE-BE method is not optimal for thin-film geometries.

In the sequel, this method will be used in full micromagnetic simulations of damping and precessional switching processes to investigate how far they can be treated within the framework of the uniform mode approximation analyzed in chapter 2. The FFT convolution method described in section 3.1.1 will be used in chapter 4 where the solution of micromagnetic standard problem no. 4 [79] will be addressed.

3.2 Comparison between Damping and Precessional switching in magnetic thin-films

We have seen in section 2.4.2 that traditionally, magnetization reversal in thin films is realized by applying a sufficiently large magnetic field almost antiparallel to the initial magnetization state and that the resulting reversal dynamics is driven by dissipative processes. This kind of switching is referred to as *damping switching* in literature [26, 27]. Nevertheless, as seen in section 2.4.3, the pos-

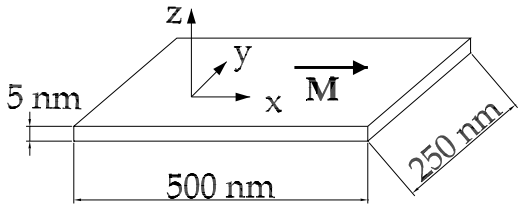

Figure 3.2: Sketch of the thin-film geometry.

sibility of using precessional motion of magnetization to realize the switching of thin films and particles has been recently investigated [34, 37, 68]. In this kind of switching, referred to as precessional switching [28], the in-plane external field is approximately orthogonal to the initial magnetization state and produces a torque that drives precessional motion of magnetization; this results in a faster and less energy-consuming magnetization dynamics. Magnetization reversal is realized by switching the external field off precisely when precession has brought the magnetization state close to its reversed orientation. Therefore, the applied field pulse duration has to be carefully chosen, while in damping switching there is no such need. Although it is generally desired that thin films and nanoelements in magnetic storage devices are in almost uniform magnetization states, both conventional switching and precessional switching are nonuniform dynamic processes. Here, we investigate the switching process of a permalloy magnetic rectangular thin-film: the thickness is $c = 5$ nm, the major and mean edge length are respectively $a = 500$ nm and $b = 250$ nm (see Fig. 3.2). The thin-film medium has a uniaxial magneto-crystalline anisotropy whose easy axis is along the x-axis (long axis), the uniaxial anisotropy constant is $K_1 = 2 \times 10^3$ J/m^3, the exchange stiffness constant is $A = 1.3 \times 10^{-11}$ J/m, the saturation magnetization $M_s \approx 795$ kA/m (such that $\mu_0 M_s = 1$ T) and the damping constant is $\alpha = 0.02$; the exchange length of the material, defined by Eq. 1.92, is

$$l_{\text{ex}} = \sqrt{\frac{2A}{\mu_0 M_s^2}} = 5.7160 \text{ nm} \quad . \tag{3.19}$$

We assume that magnetization dynamics of the thin-film is described by the Landau-Lifshitz-Gilbert equation (1.83), namely:

$$\frac{\partial \mathbf{M}}{\partial t} = -\gamma \mathbf{M} \times \mathbf{H}_{\text{eff}} + \frac{\alpha}{M_s} \mathbf{M} \times \frac{\partial \mathbf{M}}{\partial t} \quad , \tag{3.20}$$

where $\mathbf{H}_{\text{eff}}$ is the effective field defined by Eq. (1.68)

$$\mathbf{H}_{\text{eff}}(\mathbf{M}(\cdot)) \quad = \quad \mathbf{H}_{\text{m}} + \mathbf{H}_{\text{exc}} + \mathbf{H}_{\text{an}} + \mathbf{H}_a \quad , \tag{3.21}$$

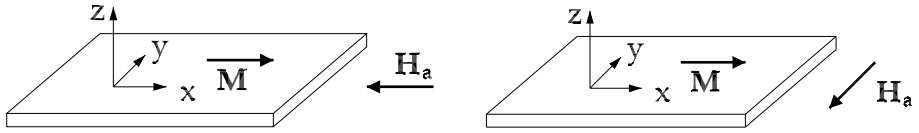

(*a*) (*b*)

Figure 3.3: (a) Conventional (damping) switching process. (b) Precessional switching process.

which includes the applied field $\mathbf{H}_a$, the exchange field $\mathbf{H}_{\text{exc}}$, the anisotropy field $\mathbf{H}_{\text{an}}$ and the magnetostatic (demagnetizing) field $\mathbf{H}_m$, as seen in section 1.2.2.

In micromagnetic simulations, the numerical time integration of Eq. (3.20) is performed by using a backward differentiation formula [69]; the spatial discretization is done using the finite element method [52] with a mesh consisted of tetrahedrons; the mesh is finer near the corners of the thin-film (mesh edge length= 5 nm $< l_{\text{exc}}$) where a stronger accuracy is required for the computation of magnetostatic field. The hybrid finite element boundary element method [70], discussed in section 3.1.2, is used to solve the magnetostatic problem.

All the numerical simulations that we will present in this section have been performed with the parallel code *MAGPAR* [73] developed by W. Scholz at Vienna University of Technology [80].

First, we perform micromagnetic simulations of conventional (damping) and precessional switching process for the thin-film. Initially, the thin-film is saturated along the y direction and then relaxed, by switching the external field off, to the remanent C-state (see Fig. 3.4, on the right), which is one of the equilibrium configurations really observed in experiments on magnetic thin-films[2]. At time $t = 0$ the external field is applied, respectively antiparallel and orthogonal to the easy axis, as sketched in figure 3.3. We compare two aspects of the switching processes: the switching speed and the uniformity of the magnetization during the reversal process.

3.2.1 Reversal speed in the switching process

We consider, as a measure of the switching speed, the time instant t_0 at which the average x component $< m_x >$ ($< \cdot >$ means spatial average) is zero after the application of the external field (the external field strength is the same in both the simulations):

$$t_0 = \min\{t > 0 :< m_x >= 0\} \quad . \tag{3.22}$$

[2]The S-state was obtained by first saturating the thin-film along the $[1, 1, 1]$ direction and then by switching the external field off.

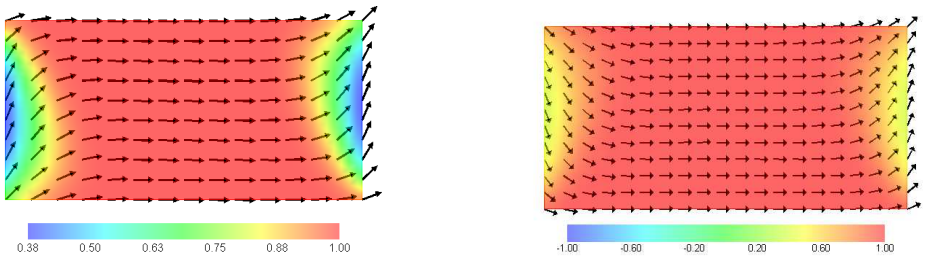

Figure 3.4: Numerical results. Remanent states of magnetic thin-film. (left) S-state. (right) C-state.

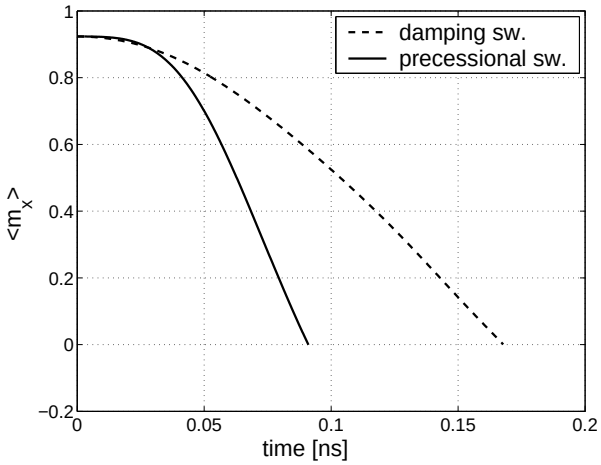

Figure 3.5: Numerical results. Comparison between damping (dashed line) and precessional (solid line) switching: time for average m_x component to reach zero from the starting configuration for $H_a = 19.51$ kA/m.

In figure 3.5 one can observe the behavior of the average m_x component until it reaches zero, showing that the precessional switching dynamics is much faster ($t_0 = 0.09$ ns) than damping switching's ($t_0 = 0.17$ ns). This is due to the different nature of the mechanism driving magnetization motion in the two processes: in conventional switching there is only one equilibrium configuration after the application of the external field, namely the reversed state, so the switching process is a kind of relaxation process towards the equilibrium and therefore the damping process is crucial. Conversely, in precessional switching the main role is played by the magnetic torque acting on the magnetization, which causes a fast precessional motion around the effective field driving the magnetization back and forth between the initial and the reversed state. Therefore, in most cases this process is so fast that dissipative effects can be neglected.

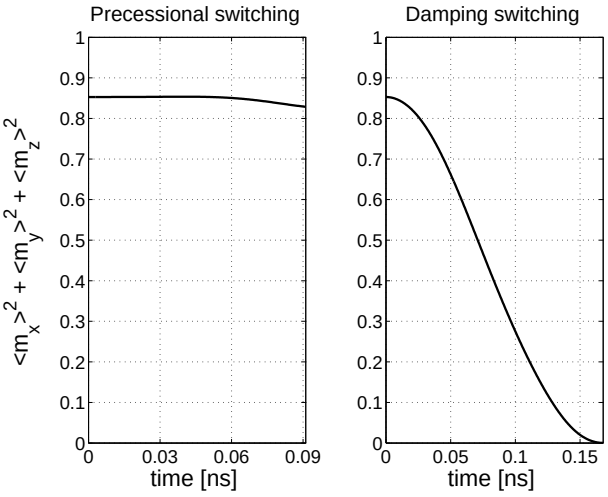

Figure 3.6: Numerical results. Plot of the uniformity indicator u vs time in the interval $(0, t_0)$ for damping (right) and precessional switching (left). The external field is $H_a = 19.51$ kA/m.

3.2.2 Spatial Magnetization uniformity

As far as the uniformity of magnetization is concerned, we consider a very simple indicator $u(t)$, given by the sum of the square values of the average magnetization components

$$u(t) =< m_x(t) >^2 + < m_y(t) >^2 + < m_z(t) >^2 \quad , \tag{3.23}$$

where the symbol $< \cdot >$ means spatial average. The indicator $u(t)$ is useful to check the spatial uniformity of magnetization as function of time, that is, during the reversal process. The results are reported in Fig. 3.6. One can easily observe that precessional switching is a quasi-uniform process, because the sum of the square values of the average magnetization components remain almost constant during time and close to unity, whereas for damping switching it decreases rapidly towards zero, showing the occurring of domain nucleation and domain wall motion. In fact, the spatial behavior of magnetization vector field, at given time instants, is depicted in Fig. 3.7 for the case of damping switching. One can clearly observe that the nucleated domains at the ends of the thin-film enlarge during time, giving rise to the so-called *head-to-head configuration* involving the motion of two domain walls. At the end of the process the two walls collapse and determine again a quasi-uniform configuration with average orientation in the opposite direction to the initial one. In this way the switching is realized.

The spatial behavior of magnetization is reported in Fig. 3.8 for the case of precessional switching. One can clearly observe that rather than domain wall

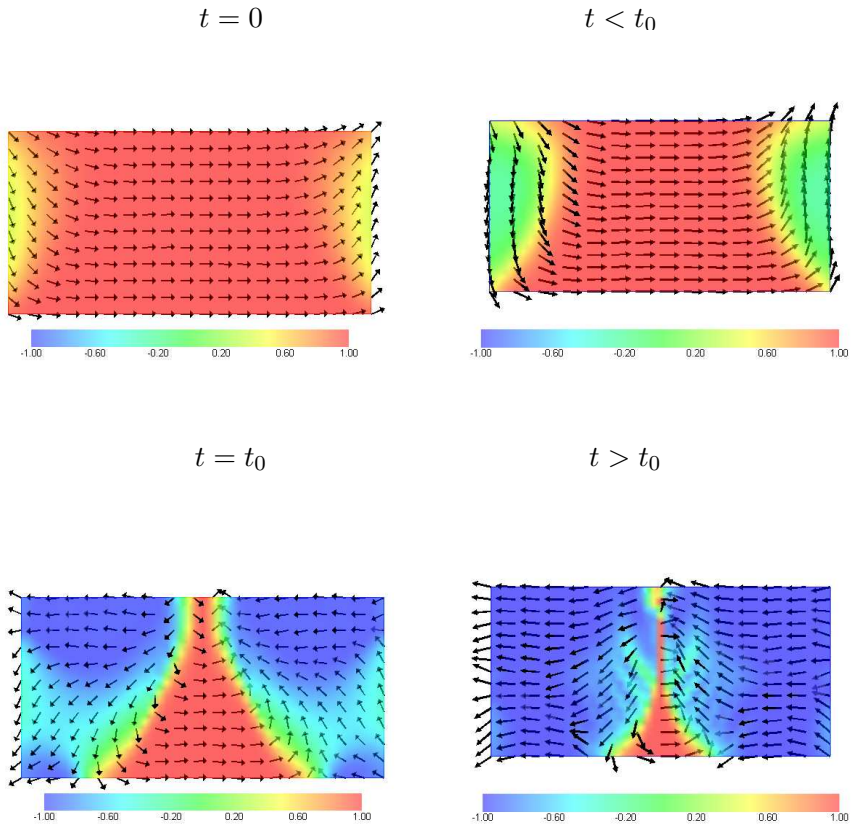

Figure 3.7: Numerical results. Screenshots of magnetization vector field during reversal for damping switching. The external field is $H_a = 19.51$ kA/m.

motion, coherent rotation can be observed, that is, the magnetization rotates almost at the unison, driven by the magnetic torque produced by the applied field. This kind of motion recalls the term "quasi-ballistic" used in Ref. [68] to describe precessional switching.

Thus we can conclude that for precessional switching, in our case of thin-film medium, one can reasonably apply the uniform mode theory to predict the duration of the external field pulse, which is necessary to achieve successful switching, as described in section 2.4.3.

3.2.3 UNIFORM MODE APPROXIMATION

To this end, we model the thin-film as a flat ellipsoid, characterized by the demagnetizing factors N_x, N_y, N_z. such that $N_x \ll N_z, N_y \ll N_z$. The demagnetizing factors can be computed as function of the aspect ratios c/a and b/a by means

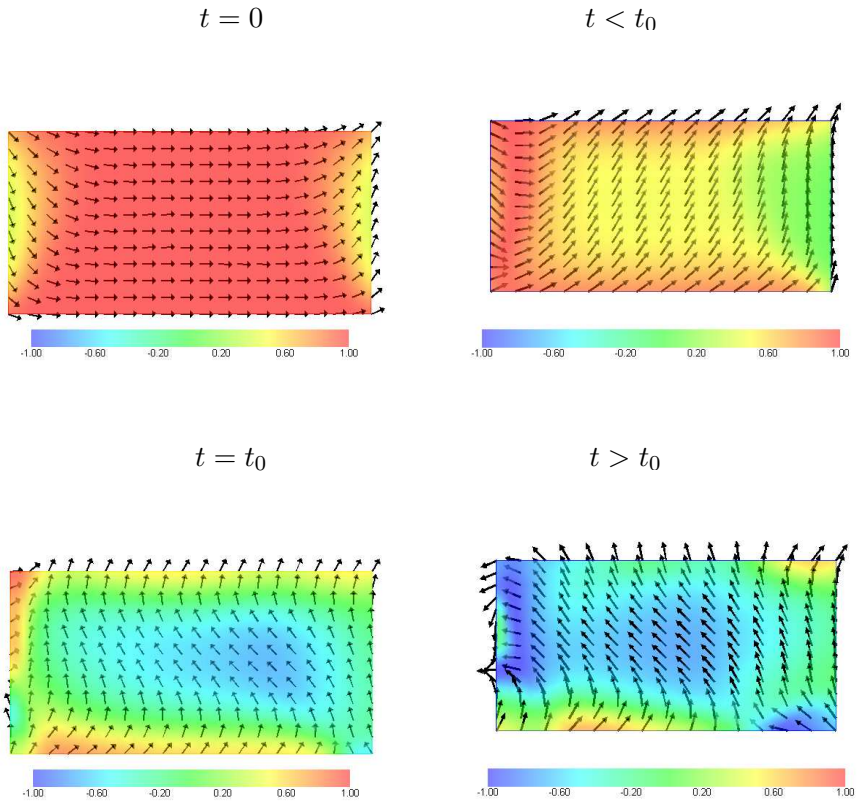

Figure 3.8: Numerical results. Screenshots of magnetization vector field during reversal for precessional switching. The external field is $H_a = 19.51$ kA/m.

of the following expressions [71]:

$$N_x = \frac{\cos\phi\cos\theta}{\sin^3\theta\sin^2\psi}\left[F(k,\theta) - E(k,\theta)\right] \quad , \tag{3.24}$$

$$N_y = \frac{\cos\phi\cos\theta}{\sin^3\theta\sin^2\psi\cos^2\psi}\left[E(k,\theta) - \cos^2\psi\, F(k,\theta) - \frac{\sin^2\psi\sin\theta\cos\theta}{\cos\phi}\right] , \tag{3.25}$$

$$N_z = \frac{\cos\phi\cos\theta}{\sin^2\theta\cos^2\psi}\left[\frac{\sin\theta\cos\phi}{\cos\theta} - E(k,\theta)\right] \quad , \tag{3.26}$$

where $\cos\theta = c/a$, $\cos\phi = b/a$, and the angle ψ is defined by

$$\sin\psi = \left[\frac{1-(b/a)^2}{1-(c/a)^2}\right]^{1/2} = \frac{\sin\phi}{\sin\theta} = k \quad ; \tag{3.27}$$

$F(k,\theta)$ and $E(k,\theta)$ are the incomplete elliptic integrals [72] of the first and second kind respectively. All the angles θ, ϕ, ψ are intended to belong to the interval $[0, \pi/2]$.

In our case, the application of the above formulas gives:

$$N_x = 0.0062 \quad , \quad N_y = 0.0175 \quad , \quad N_z = 0.9763 \quad , \tag{3.28}$$

which, give the following values for the D_x, D_y, D_z coefficients (shape and magnetocrystalline anisotropy):

$$D_x = N_x - \frac{2K_1}{\mu_0 M_s^2} = 1.2 \times 10^{-3},\ D_y = N_y,\ D_z = N_z \quad . \tag{3.29}$$

We assume that the external field $\mathbf{h}_\mathrm{a}$ is applied along the y axis:

$$\mathbf{h}_\mathrm{a} = h_a \mathbf{e}_y \quad . \tag{3.30}$$

We compute the critical time instants t_1, t_2, T_s expressed by Eqs. (2.53)-(2.55), slightly generalized [50] for the case $D_x, D_y, D_z \neq 0$:

$$t_1 = \int_{u_0}^{u_1} \frac{du}{k(D_z - D_x)\sqrt{1 - p^2\cos^2 u - [a_y - (p/k)\sin u]^2}} \quad , \tag{3.31}$$

$$t_2 = t_1 + 2\int_{u_1}^{u_2} \frac{du}{k(D_z - D_x)\sqrt{1 - p^2\cos^2 u - [a_y - (p/k)\sin u]^2}} \quad , \tag{3.32}$$

$$T_s = \int_{u_0}^{u_2} \frac{du}{k(D_z - D_x)\sqrt{1 - p^2\cos^2 u - [a_y - (p/k)\sin u]^2}} \quad . \tag{3.33}$$

where the parameters are given by:

$$k^2 = (D_z - D_y)/(D_z - D_x) \quad , \tag{3.34}$$

$$a_y = -h_a/(D_z - D_y) \quad , \tag{3.35}$$

$$p^2 = k^2 a_y^2 + \frac{D_z - 2g_0}{D_z - D_x} \quad , \tag{3.36}$$

$$g_0 = \frac{D_x}{2} \quad . \tag{3.37}$$

Notice that here we are supposing that the initial state is $\mathbf{m} = \mathbf{e}_x$. Similarly to the derivation presented in section 2.4.3, in equations (3.31)-(3.33) the value of the parameters u_0, u_2 can be found by using parametric equations

$$m_x = -p\cos u \quad , \quad m_y = a_y + \frac{p}{k}\sin u \quad , \tag{3.38}$$

of the elliptic curve on which magnetization motion occurs:

$$m_x^2 + k^2(m_y - a_y)^2 = p^2 \quad , \tag{3.39}$$

to find the intersections with the unit circle $m_x^2 + m_y^2 = 1$. The value u_1 can be found from the intersection between the elliptical trajectory (3.39) with the ellipse $m_x^2 + k^2 m_y^2 = k^2$ delimiting the high energy region.

The above technique can be applied to whatever external field applied in the x, y plane. When the field is applied along one axis, as in our case, it is possible to carry out the integration of conservative LLG equation ($\alpha = 0$) where m_x, m_y are given in the parametric form (3.38):

$$\frac{du}{\sqrt{1 - p^2\cos^2 u - [a_y - (p/k)\sin u]^2}} = k(D_z - D_x)dt\,, \tag{3.40}$$

$h_a/h_{\rm SW}$	1.0	1.1	1.2	1.3	1.4	1.5
H_a [kA/m]	13.01	14.31	15.61	16.91	18.21	19.51
T_s [ns]	0.194	0.181	0.171	0.162	0.155	0.149

Table 3.1: Values of the switching times T_s, analytically computed with formula (3.33) and used in micromagnetic simulations (M_s = 795 kA/m, $A = 1.3 \times 10^{-11}$ J/m, $\alpha = 0.02$).

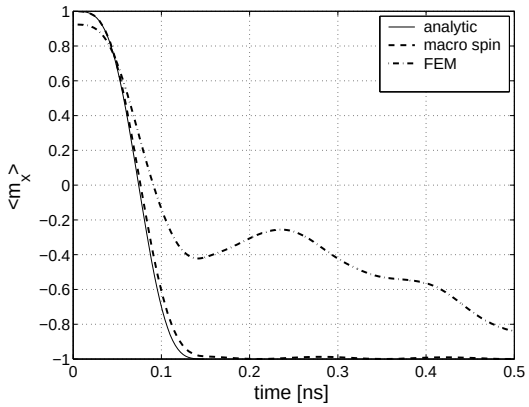

Figure 3.9: Analytical and numerical solutions of Landau-Lifshitz-Gilbert equation. Plot of $< m_x >$ vs time. $h_a = 1.5 \times h_{SW}$, $D_x = 1.2 \times 10^{-3}$, $D_y = 0.0175$, $D_z = 0.9763$.

which gives the relation between the parametric variable u and time. In fact it is possible [42, 50] to bring Eq. (3.40) in the canonical form which can be integrated by means of Jacobi elliptic[3] functions [72]. In this way one can obtain the magnetization dependance on time in exact analytical form and exact expression of the critical instants (3.31)-(3.33).

It is also shown in [42] that, in the case of $\mathbf{h}_{\rm a} = h_a \mathbf{e}_y$, the critical value of the external applied field for precessional switching is still one half of the Stoner-Wohlfarth field:

$$h_c = \frac{D_y - D_x}{2} = \frac{h_{\rm SW}}{2} \quad . \tag{3.41}$$

3.2.4 Numerical results

We performed a set of micromagnetic numerical simulations of the precessional switching process for the values of H_a and T_s specified in the table 3.1. This table reports the switching time T_s, analytically computed using Eq. (3.33), for different values of H_a. The simulations were started from both initial magnetization configurations which can be observed in the experiments on thin-film media: the S-state and C-state (see figure 3.4). In figure 3.9 a comparison between the

[3] See Appendix B

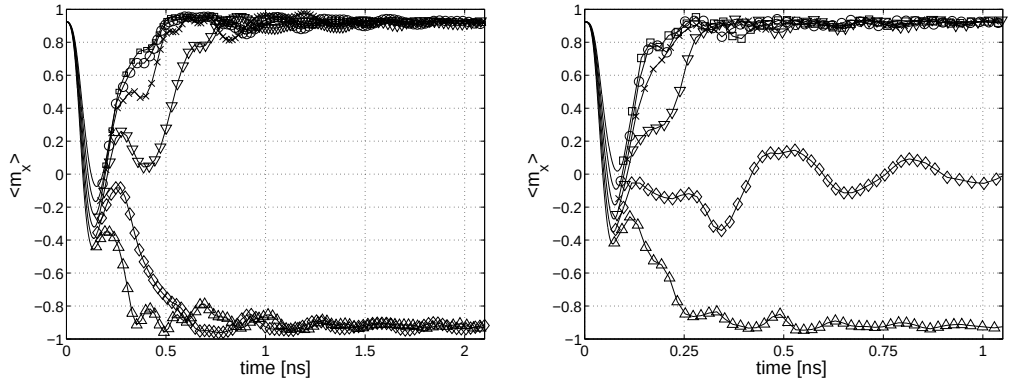

(a) (b)

Figure 3.10: Numerically computed $< m_x >$ as a function of time. S-state (a), C-state (b) initial condition. (In both figures) symbol "□" for $h_a = h_{\rm SW}$; "O" for $h_a = 1.1 \times h_{\rm SW}$; "X" for $h_a = 1.2 \times h_{\rm SW}$; "∇" for $h_a = 1.3 \times h_{\rm SW}$; "◇" for $h_a = 1.4 \times h_{\rm SW}$; "△" for $h_a = 1.5 \times h_{\rm SW}$.

analytical solution of LLG Eq. (2.18) with $\alpha = 0$, the numerical solution of LLG Eq. (2.18) with $\alpha = 0.02$ for a uniformly magnetized thin-film shaped ellipsoidal particle (macro-spin model) and the finite element solution of Eq. (3.20) is reported for an applied field strength $h_a = 1.5 \times h_{\rm SW}$.

In the undamped case, at time $t = T_s$ the magnetization is exactly in the reversed position. Therefore, when the external field is switched off, it remains definitely in this state. If the damping term is introduced, one can see that after $t = T_s$ there is a small oscillation of $< m_x >$ because the system is not yet in the minimum energy state. In the general nonuniform case one can easily see that the uniform mode theory provide anyway a reasonably good information about the duration of the field pulse, but the presence of nonuniform modes produces an oscillation that can bring magnetization back to the initial state as one can see in Figs. 3.10(a)-(b). For this reason, a field strength $h_a = 1.5 \times h_{\rm SW}$ is required to achieve successful switching starting from either an S-state or a C-state. We observe that this value is moderately larger than the critical value provided by uniform mode theory, $h_c = h_{\rm SW}/2$.

3.2.5 PRECESSIONAL SWITCHING: DEPENDANCE ON THE ANISOTROPY AND SWITCHING TIME TOLERANCE WINDOW

In this section we will demonstrate that the agreement with the analytical prediction increases for increasing values of the anisotropy constant. In this respect, we will verify that the time window tolerance (t_1, t_2) computed by Eqs. (3.31)-(3.32) gives very accurate information on the reliability of the switching.

In Fig. 3.11 the plot of the time instants t_1, T_s, t_2 is reported as a function

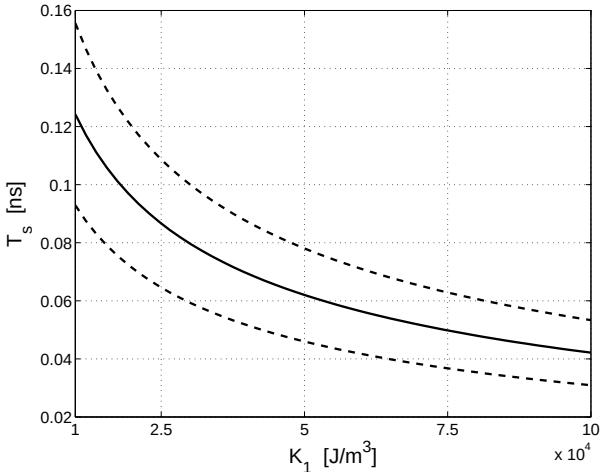

Figure 3.11: Plot of switching times T_s (solid line), t_1 and t_2 (dashed lines). $h_a = D_y - D_x$, $D_x = N_x - 2K_1/(\mu_0 M_s^2)$, $D_y = 0.0175$, $D_z = 0.9763$.

K_1 [10^4 J/m^3]	1.0	2.5	5.0	7.5	10
H_a [kA/m]	30.88	60.88	110.88	160.88	210.88
T_s [ps]	124.3	86.6	62.0	49.8	42.1
t_1 [ps]	92.9	64.6	46.0	36.7	30.9
t_2 [ps]	155.6	108.7	78.0	62.9	53.3

Table 3.2: Values of the parameters used in micromagnetic simulations (M_s = 795 kA/m, $A = 1.3 \times 10^{-11}$ J/m, $\alpha = 0.02$).

of the anisotropy constant K_1 when the applied field amplitude is chosen $H_a = M_s h_{\mathrm{SW}} = (D_y - D_x)M_s$. The normalized applied field $h_a = D_y - D_x$ is related to K_1 through Eq. (3.29). It is important to underline that the time window for switching the field off is reasonably wide because, in the analyzed interval of $K_1 \in [10^4, 10^5]$ J/m^3 (moderately soft materials used in magnetic recording technology), is $t_1 < 0.75 \times T_s$ and $t_2 > 1.25 \times T_s$, that is, a tolerance of at least $\pm 25\%$ on the switching pulse is allowed.

On the basis of the above analysis we performed a set of micromagnetic simulations of precessional switching experiments for the $500 \times 250 \times 5$ nm thin-film described at the beginning of section 3.2. Initially, the thin-film is saturated along the positive x-axis, then it is relaxed to the remanent state. At time $t = 0$ the rectangular external field pulse is applied $H_a = (D_y - D_x)M_s$ until time $t = T_s$ at which the field is switched off and the magnetization relaxes towards equilibrium. We performed different simulations for different values of K_1, reported in Table 3.2. The results are reported in Fig. 3.12. One can clearly see that for moderately low values of K_1 (Fig. 3.12a) at $t = T_s$ magnetization is not exactly

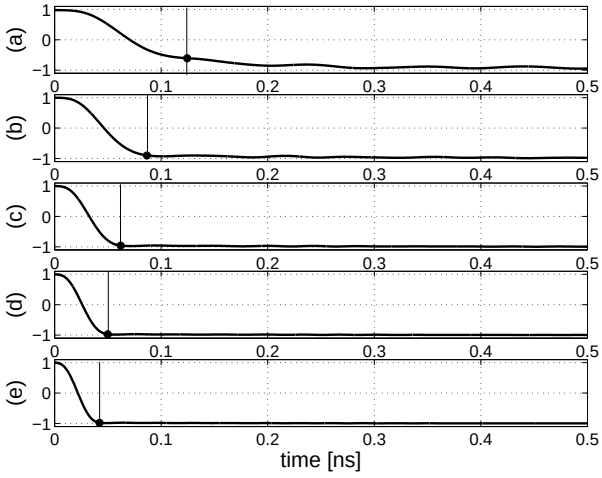

Figure 3.12: Micromagnetic simulations: plot of m_x vs time; (a) $K_1 = 10^4$ J/m^3; (b) $K_1 = 2.5 \times 10^4$ J/m^3; (c) $K_1 = 5 \times 10^4$ J/m^3; (d) $K_1 = 7.5 \times 10^4$ J/m^3; (e) $K_1 = 10 \times 10^4$ J/m^3. The switching time T_s is marked with a vertical line.

close to the reversed state, but micromagnetic simulations show that the higher the applied field strength is, the better is the agreement with the uniform mode theory. By moderately increasing the value of the anisotropy constant there is a very good agreement with the above prediction and the remaining oscillation after $t = T_s$ tends to be very close to the magnetization reversed state [Fig. 3.12(b)-(e)].

Next, we chose to verify the prediction of the uniform mode theory regarding the time window for switching the field off. We analyze, for sake of brevity, the case of anisotropy constant $K_1 = 2.5 \times 10^4$ J/m^3. The applied field is $H_a = (D_y - D_x)M_s = 60.88$ kA/m. The results (Fig. 3.13) show the accuracy of the uniform mode theory prediction. In fact, switching the applied field off just few picoseconds after time $t = t_2$ (Fig. 3.13b) or just a few picoseconds before time $t = t_1$ (Fig. 3.13d) leads to non-successful switching, while switching the applied field off just few picoseconds before time $t = t_2$ (Fig. 3.13a) or just a few picoseconds after time $t = t_1$ (Fig. 3.13c) leads to successful switching. Thus, we can conclude that, in precessional switching experiments on thin-film media constituted of moderately soft materials, the time window for switching the applied field off can be derived by using the uniform mode theory with a very high accuracy. Moreover, the knowledge of the time window $[t_1, t_2]$ can be used to find the switching diagrams proposed in Ref. [34] to design MRAM storage cells, in the case of short (rectangular) field pulse durations, without performing numerical simulations.

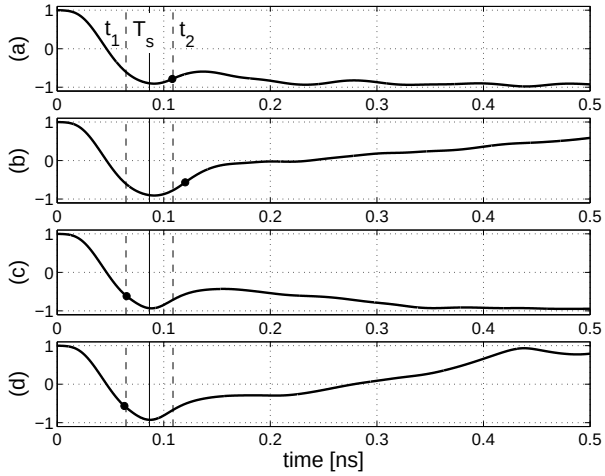

Figure 3.13: Micromagnetic simulations: plot of m_x vs time. $K_1 = 2.5 \times 10^4$ J/m^3, $H_a = (D_y - D_x)M_s = 60.88$ kA/m. The field is switched off at time (a) $t = 108$ ps; (b) $t = 120$ ps; (c) $t = 65$ ps; (d) $t = 63$ ps.

3.3 Fast switching of Tilted Media

In this section we present a very particular case of switching process in which it is possible to obtain magnetization reversal of a whole grain ensemble with external fields whose amplitude is below the Stoner-Wohlfarth limit. This kind of switching process has considerable applications in hard-disks realizations for several reasons that we will see below. Our purpose is to show that, although the medium is consisted of many weakly (exchange and magnetostatically coupled) interacting grains, it can be approximately treated as a collection of non-interacting grains. Therefore, the necessary conditions for the switching can be investigated with the uniform mode theory applied to a single grain.

3.3.1 Introduction

It has been recently underlined that tilted magnetic media can have considerable advantages in magnetic recording applications [74, 75, 76]. These media are usually realized as thin films constituted by grains with easy axis at an angle of approximately 45° with respect to the film plane (see for example Fig. 3.14). This leads to coercive fields smaller by a factor two compared to perpendicular media[4], and thus allows the use of high anisotropy magnetic materials, which in turn provide a better thermal stability or a higher areal density. Higher data rates can be also realized owing to the high torque that acts on the magnetization and

[4]Since the medium "sees" the external field as applied at 135° off the easy axis, this can be understood by looking at the Stoner-Wohlfarth astroid (see Fig. 3.16) in the direction at 135° off the x axis, where the critical field is about $h_{SW}/2$.

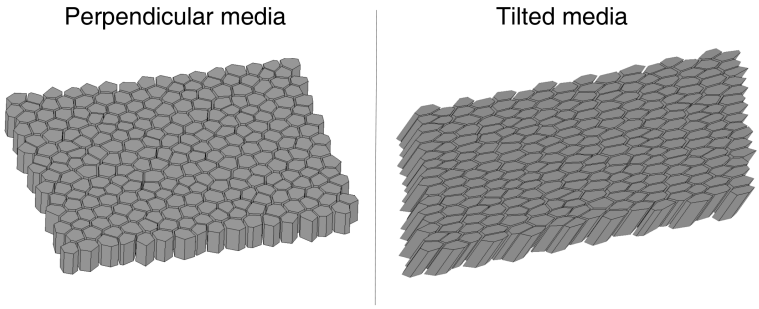

Figure 3.14: Granular structure of perpendicular and tilted media.

the high signal-to-noise ratio (SNR) related to the fact that grains with slightly different easy axes have almost the same switching field[5]. As mentioned before, in these media it is possible to realize switching for external fields below the Stoner-Wohlfarth (SW) limit [75], and, in the appropriate range of external field amplitude, it has been shown that the switching time decreases with decreasing amplitude of the external field pulse [76].

In the following we intend to analyze the switching process in weakly coupled granular tilted media. As first approximation we will analyze the case of noninteracting grains. Since the grains are usually almost uniformly magnetized, this case can be treated by using the uniform mode theory. In this respect, we consider a family of noninteracting grains with dispersion in the easy axis and initial magnetization directions. This analysis provides an estimate of the range of external field amplitude and directions required to realize switching. The parameter values predicted by the theory are then used in a 3D micromagnetic simulation of the switching process in which the interactions of the grains are taken into account.

3.3.2 UNIFORM MODE APPROXIMATION

To start the discussion, consider a uniformly magnetized Stoner-Wohlfarth (SW) particle, with easy axis along the x-axis of a cartesian reference system, characterized by the following normalized free energy $g(\mathbf{m})$:

$$g(\mathbf{m}) = \frac{1}{2}(D_x - N_\perp)m_x^2 - h_{ax}m_x - h_{ay}m_y \quad , \tag{3.42}$$

where $D_x = N_x - K_1/(\mu_0 M_s^2)$, K_1 is the uniaxial anisotropy constant, N_x and $N_\perp$ are demagnetizing factors along and perpendicular to the x-axis, respectively. Equilibria and switching of this particles can be analyzed by SW model which

[5]This can be inferred by observing that directions at about 135° off the x axis intersect the SW astroid at almost the same distance from the origin. This leads to very close values of critical fields.

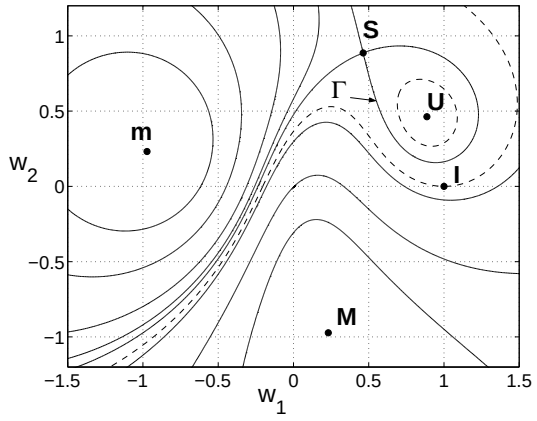

Figure 3.15: Phase portrait of LLG equation in the stereographic plane: M is a maximum, S is the saddle point, m is the target minimum. $N_\perp = 0.5$, $D_x = -3.0159$, $h_{\rm SW} = 3.5159$.

leads to the well-known asteroid curve in the applied field plane (see section 2.2 and Fig. 3.16) which separates the regions characterized by two minima of free energy (inside the asteroid) and one minimum (outside the asteroid). Within the static SW theory switching is attainable only for field above $h_{\rm SW} = N_\perp - D_x$. Nevertheless by using magnetization dynamics[6], it is possible to realize switching also below this limit. To investigate this circumstance, we will analyze magnetization dynamics by means of Landau-Lifshitz-Gilbert (LLG) equation:

$$\frac{d\mathbf{m}}{dt} = -\mathbf{m} \times \mathbf{h}_{\rm eff} + \alpha \left(\mathbf{m} \times \frac{d\mathbf{m}}{dt} \right) \quad , \tag{3.43}$$

where $\mathbf{h}_{\rm eff} = -\nabla_{\mathbf{m}} g$. In order to illustrate the main idea behind fast switching below SW limit, let us consider the conservative LLG equation, i.e. we put $\alpha = 0$ in Eq. (3.43). The qualitative features of LLG dynamics are conveniently represented on the plane by using the stereographic transformation introduced in section 2.3.

In Fig. 3.15 a portion of the conservative phase portrait of Eq. (3.43) is reported in the case of an external field with $h_a = 0.43 \times h_{\rm SW}$ and applied at an angle 45° off the x axis. The magnetization trajectories coincide with the contour lines of the energy function (3.42). Since $h_a < h_{\rm SW}$, there is still a minimum of the free energy in the point U near the initial state I which is assumed to be in the position $(1, 0)$ (positive easy axis direction). One can see that if the initial state is inside the homoclinic loop Γ around the minimum, the dynamics remains trapped around U, conversely when the initial magnetization state is

[6]We have already seen an example of switching below SW limit, namely the precessional switching analyzed in section 2.4.3.

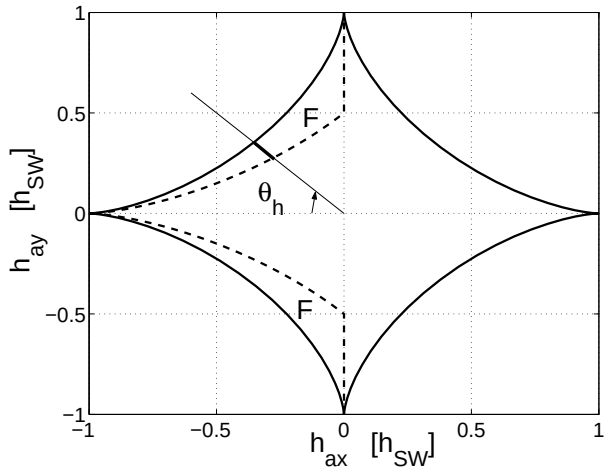

Figure 3.16: The solid line represents SW astroid, the dashed line represents the parametric curve defined by Eqs. (3.44).

outside Γ, the precessional oscillation brings magnetization far from the minimum U and this is instrumental to speed up the switching process. The dashed lines in Fig. 3.15 represent an example of these two possible trajectories. The critical case between the two behaviors occurs when the initial state I exactly lies on the homoclinic loop Γ. This situation is realized when the applied field is on a line in the $h_{ax} - h_{ay}$ plane which is inside the SW asteroid (see Fig.3.16). This curve can be expressed, in parametric form [28, 36] as:

$$h_{ax} = -h_{\rm SW} \cos u \cos^2 \frac{u}{2} \quad , \quad h_{ay} = h_{\rm SW} \sin u \sin^2 \frac{u}{2} \,, \tag{3.44}$$

where $|u| < \pi/2$ is the parameter. It turns out that it is necessary that the applied field is inside the region F between the dashed and the solid line to realize the switching. This region can be characterized by specifying for each angle θ_h the allowed applied field amplitude range $[h_{a1}, h_{a2}]$ (emphasized in Fig. 3.16). The upper limit h_{a2} is given by the SW theory [77]

$$h_{a2} = h_{\rm SW}[(\sin\theta_h)^{2/3} + (\cos\theta_h)^{2/3}]^{-3/2} \quad , \tag{3.45}$$

while h_{a1} can be found using Eqs. (3.44) once the applied field angle θ_h is connected with the corresponding parameter u^*, through the equation

$$h_{ay}(u^*)/h_{ax}(u^*) = -\tan\theta_h \quad . \tag{3.46}$$

Next we want to use the above uniform mode theory to study an ensemble of N noninteracting particles to take into account dispersion of anisotropy axis and initial magnetization. We assume that the nominal (average) easy axis direction of the media is along the unit vector $\mathbf{e}$ which is aligned with the x axis. The

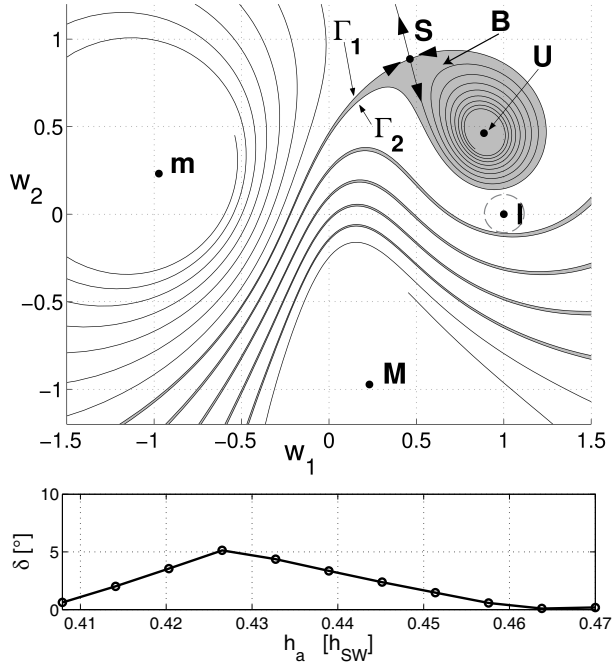

Figure 3.17: Up: phase portrait of LLG equation for $\alpha = 0.02$, $\theta_h = 45°$. Down: plots of the deviation angle δ as a function of h_a.

j-th particle is characterized by a magnetization direction $\mathbf{m}_j$ and an easy axis direction $\mathbf{e}_j$ forming an angle β_j with $\mathbf{e}$. We assume that the maximum β_j is less than a prescribed angle β.

We indicate by $\theta_{h,j}$ the angle between $\mathbf{h}_a$ and $-\mathbf{e}_j$ which satisfies the inequality

$$\theta_h - \beta < \theta_{h,j} < \theta_h + \beta \quad . \tag{3.47}$$

By assuming that the initial states are given by $\mathbf{m}_j = \mathbf{e}_j$, we find a family of applied field intervals $S_j = [h_{a1,j}, h_{a2,j}]$ which corresponds to the fast switching of each particle. Thus, we can determine the applied field interval S that allows the fast switching of all the particles by taking the intersection of the S_j:

$$S = \bigcap_{j=1}^{N} S_j \quad . \tag{3.48}$$

We computed this applied field interval for $\theta_h = 45°$ and $\beta = 5°$ and the result is $S = [0.401 \times h_{\mathrm{SW}}, 0.47 \times h_{\mathrm{SW}}]$.

The analysis above has been carried out by using the conservative dynamics. In the case of the actual dynamics with damping the study of switching is more complicated and a careful analysis of the phase portrait is required. Magnetization dynamics is now described by Eq. (3.43) with $\alpha > 0$. In Fig. 3.17 (up) one can see a portion of the phase portrait of the dynamical system for $\alpha = 0.02$,

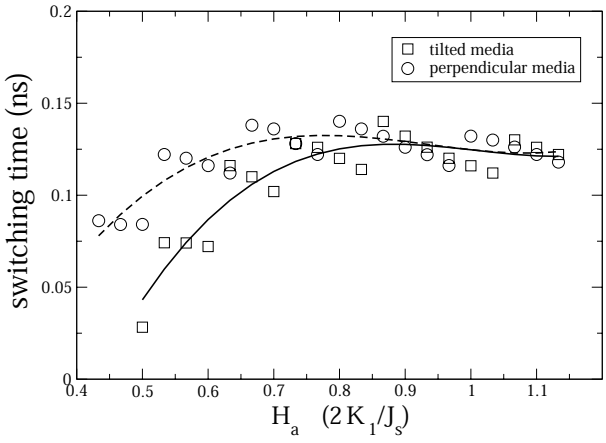

Figure 3.18: Comparison of the switching time for a perpendicular recording media and a tilted media.

$\theta_h = 45°$, $h_a = 0.43 \times h_{\mathrm{SW}}$. The shaded region B, enclosed in the separatrices Γ_1 and Γ_2, is the basin of attraction of the undesired minimum U. Magnetization trajectories spiral toward minima of the free energy and the phase portrait (see Fig. 3.17) is divided into the basins of attraction of the two minima m and U. A necessary condition for switching is that the initial position I is in the basin of attraction of the target minimum m.

In addition, it is desirable that a whole neighbor of the initial position is inside this basin of attraction. Indeed, in real granular materials the different grains, due to exchange and strayfield interactions with other grains, will have slightly different initial conditions with certain deviation from the easy axis. In this respect, by analyzing the phase portrait in Fig. 3.17 we can determine quantitatively what is the allowed deviation δ_j of the j-th particle magnetization $\mathbf{m}_j$ from the its easy axis $\mathbf{e}_j$, compatible with the requirement that the magnetization state is within the basin of attraction of the target minimum. This can be done by considering for each particle the circle of allowed initial conditions (see the dashed circle in Fig. 3.17). The analysis must be carried out for each particle in the ensemble and lead to the estimate of the maximum angular deviation δ. The results are summarized in Fig. 3.17 (down).

3.3.3 MICROMAGNETIC SIMULATIONS OF FAST SWITCHING PROCESS

The final steps in our analysis is to verify whether the indication of the theory above are still reasonable when we take into account the weak interactions among the grains. To this end we have performed finite element [78] calculations (FEM)

for weakly exchange and magnetostatically coupled granular media. The applied field is chosen within the range estimated with the uniform mode theory. Both perpendicular and tilted recording media with a weak exchange coupling between the grains ($A_{\text{inter}} = 3 \times 10^{-14}$ J/m) are investigated. The material parameters within the grains are: $J_s = \mu_0 M_s = 0.5$ T, $A = 10^{-11}$ J/m and $K_1 = 3.5 \times 10^5$ J/m^3. The thickness of the perpendicular media and the tilted media is 12 nm and 8.5 nm, respectively. The average grain diameter is 10 nm for both media. More than 45000 finite elements are used to provide an edge length smaller than the exchange length. A normal distribution of the easy axes directions with a maximum opening angle of 5° is assumed for both media. For the perpendicular media the average easy axis direction is parallel to the film normal. For the tilted media the angle between the average easy axis direction and the film normal is 45°. Thus, for both samples the average easy axis direction points parallel to the edges between the grains. The external field is applied 45° off the film normal and parallel to the film normal for the perpendicular media and the tilted media, respectively. The field rise time is 10 ps. The FEM simulations for granular structures verify that switching is possible for fields smaller than the SW switching field and within the range predicted by the uniform mode theory. The switching time is defined as the time until the average magnetization component parallel to the easy axis crosses zero the last time. Figure 3.18 compares the switching time as a function of the external field strength, for the perpendicular media and the tilted media, significantly different due to the different demagnetizing field. The jumps that can be observed in Fig. (3.18) are due to ringing of the magnetization. For tilted media, the FEM simulations also show that a change of the opening angle of the easy axes distribution from 5°to 1° changes the switching time by less than 0.1 %. Small switching field distributions lead to a high signal to noise ratio.

Chapter 4

Geometric integration of Landau-Lifshitz-Gilbert equation

4.1 Introduction

The purpose of this chapter is to address the general problem of the numerical integration of Landau-Lifshitz-Gilbert (LLG) equation. In fact, we have observed more than once, that due to the nonlinear nature of this equation, analytical solutions can be derived in very few particular cases, or by using linearization techniques (see chapter 2 and references therein). Consequently, the only general (and mostly used) method to study magnetization dynamics is to solve LLG equation by suitable numerical methods. In this respect, as mentioned in chapter 3, the most common procedure is to use a semi-discretization approach. First, the equation is only discretized in space by using finite difference or finite elements methods [52]. This leads to a discretized version of the micromagnetic free energy and a corresponding system of ordinary differential equations (ODEs). Second, this system of ODEs is numerically integrated by using appropriate time-stepping techniques. It is interesting to underline that, while the spatial discretization is generally carried out trying to preserve the main properties of the free energy functional $G(\mathbf{M};\mathbf{H}_a)$ introduced in chapter 1, little attention is generally paid to the preservation, after the time discretization, of the peculiar structure of LLG temporal evolution. This is probably due to the fact that, in the past, the main emphasis was on static micromagnetics and on reproducing accurate approximation of the free energy landscape associated to a magnetic system subject to quasi-static external fields. This goal has been generally achieved by using accurate spatial discretization of the free energy $G(\mathbf{M};\mathbf{H}_a)$. On the other hand, when dynamic magnetization processes have to be investigated, the issue of using appropriate numerical time integration technique becomes rather crucial. Nevertheless, this problem seems to have been substantially overlooked, and most workers in LLG numerical simulation use 'off-the-shelf' algorithms such

as Euler, linear multi-step methods (e.g. Adams-Bashforth, Adams-Moulton, Crank-Nicholson, Backward Differentiation Formulas (BDF)) or Runke-Kutta methods[79, 80]. We must underline here that these standard methods do not preserve structural properties of LLG time evolution. This equation has indeed peculiar dynamic properties, mentioned in section 1.3.5, which it is convenient to recall below.

a) First, the magnetization has constant magnitude in time at each spatial location, as indicated by Eq. (1.97). Equation (1.97) is a fundamental constraint on the LLG time evolution that should be respected in the time discretized version of LLG equation. Since, usual time stepping methods do not preserve this property, most researchers follows the naive approach of renormalizing the magnetization vector field at each time step or after a prescribed tolerance has been exceeded. This naive approach is actually a nonlinear numerical modification of the time evolution which in principle can have also relatively strong effect on the subsequent computation of magnetostatic field [86] and for this reason is not recommended, especially when long time regime have to be studied.

b) Second, for constant external field the LLG evolution has a Lyapunov structure [82], namely the free energy functional is a decreasing function of time along the trajectories of LLG equation, according to Eq. (1.102). This property is fundamental because it guarantees that the system tends toward stable equilibrium points, which are minima of free energy. Usual time-stepping techniques preserve this property only for sufficiently small time-step. Indeed, when the time-step is too large, instability phenomena can produce transient or even steady increase of energy. The stability constraint on the time step is usually rather severe and this generally leads to unnecessary long computational time.

c) Third, the LLG equation is obtained by adding a phenomenological damping term to an otherwise hamiltonian (conservative) equation and therefore one should expect that in the limit of $\alpha \to 0$, the numerical integration should preserve energy and, if possible, the hamiltonian structure. This is not only a mathematical requirement. In fact, in most experimental situations LLG evolution is not strongly dissipative and the damping effects can be considered as a perturbation of the conservative motion (see chapter 2, sections 2.4.3, 2.5, 2.6). In this respect, it is quite reasonable from the physical point of view, that the numerical integration scheme is able to reproduce

accurately the conservative motion. This is definitely the most challenging part in the numerical simulation since the conservative precession is generally much faster than the slow motion associated to dissipative processes. As it is well-known in hamiltonian dynamics studies, most standard numerical schemes do not preserve energy and/or hamiltonian structure, and particular care must by devoted to develop appropriate time stepping technique.

As matter of fact, it is generally very difficult to obtain the preservation of the above properties in the time discretization by using explicit methods (e.g. Euler, Adams-Bashforth). Implicit methods, on the other hand, have good performances in terms of stability, but do not preserve the amplitude of magnetization or the energy in the limit $\alpha \to 0$. However, the use of implicit methods generally makes it necessary to solve large system of coupled nonlinear equations at each time step which may lead to unacceptable computational cost. In this respect, most researchers generally try to avoid implicit methods by using appropriate semi-implicit techniques [81]. This has of course the drawback that accurate numerical time integration require stability upper bound for the time step. This in turn can be quite problematic since LLG dynamics, in many relevant cases, may exhibit dynamic processes with very different time scales.

In fact, the issue of developing time integrators for LLG equation that preserve relevant properties of the equation under discretization, has received lately some attention [25, 84, 85, 86]. The general point of view presented in these recent works is to use suitable geometric integrators[87] which are techniques designed to preserve geometrical properties of dynamics, namely symmetry, conservation of quantities, hamiltonian structure etc. In particular, the possibility of developing integrators for LLG equation based on Lie-group methods and Cayley transform have been investigated in Refs. [85, 86]. These methods preserve the magnetization amplitude, but they do not generally preserve the LLG Lyapunov structure and the energy in the limit of zero damping. The basic idea is to take into account the conservation of magnetization magnitude by an appropriate change of variable (lift of the problem in the Lie-algebra associated to the Lie-group of rotations). The problem is then solved with usual RK time-stepping algorithms. These methods are conditionally stable and the stability requirements are certainly affected by the choice of the new set of variables. This could lead to an increase of the temporal stiffness and, consequently, to an increase of the computational cost.

In this chapter, we will apply the (implicit) mid-point rule to the time integration of LLG equation. We shall demonstrate that the use of mid-point rule leads to a numerical time stepping that preserves the fundamental properties of LLG dynamics. This algorithm has been known for a long time and it has been applied extensively in the area of hamiltonian dynamics for its interesting preservation properties [83]. However, in its pure form, it has never been applied directly to the full 3D micromagnetics dynamical problem. A partial use of mid-point rule has been proposed in Ref. [25]. In this work, the mid point rule has been applied along with an appropriate explicit extrapolation formula (second order Adams-Bashforth) for the effective field. This method has the property of preserving magnetization magnitude and, due to the explicit extrapolation formula, does not require the inversion of a large system of coupled nonlinear equations (but just three by three linear system of equations at each location in space). However, the method does not in general preserve the Lyapunov structure of LLG equation neither the energy for zero damping. In addition, the semi-implicit nature of the scheme imposes stability restrictions to the time step.

Here we apply the implicit mid-point rule directly to the LLG equation in its pure form. With the use of the mid-point rule we can overcome the drawbacks of the standard methods. The methods is unconditionally stable, preserves exactly, independently from the time step, magnetization magnitude and, in the case of zero damping, free energy of the system. In addition, mid-point rule preserves unconditionally Lyapunov structure of LLG dynamics for constant applied field, namely in the discrete dynamics, the free energy is always decreasing regardless of the time step. The price we have to pay is that now we have to solve a large (generally full) system of nonlinear algebraic equations. As we will discuss in the following, this problem has been dealt with by using quasi-Newton algorithm which allows one to deal with sparse banded matrix inversions only.

4.2 THE MATHEMATICAL MODEL

It is very useful for the following discussion, to recall the dimensionless form (1.95) of LLG equation:

$$\frac{\partial \mathbf{m}}{\partial t} = -\mathbf{m} \times \left(\mathbf{h}_{\text{eff}}(\mathbf{m}, t) - \alpha \frac{\partial \mathbf{m}}{\partial t} \right) , \tag{4.1}$$

with the usual normalized quantities introduced in section 1.3.4.

The LLG equation (4.1) is implicit with respect to $\partial \mathbf{m}/\partial t$, and it can be transformed in the equivalent normalized Landau-Lifshitz form of Eq. (1.87):

$$\frac{\partial \mathbf{m}}{\partial t} = -\frac{1}{1+\alpha^2} \mathbf{m} \times \mathbf{h}_{\text{eff}}(\mathbf{m}, t) - \frac{\alpha}{1+\alpha^2} \mathbf{m} \times (\mathbf{m} \times \mathbf{h}_{\text{eff}}(\mathbf{m}, t)) , \tag{4.2}$$

where $\partial\mathbf{m}/\partial t$ is explicitly expressed. This form of LLG equation is the most commonly used for numerical integration.

As seen in chapter 1, the normalized effective field $\mathbf{h}_{\text{eff}}$ can be defined by the variational derivative $\mathbf{h}_{\text{eff}} = -\delta g/\delta\mathbf{m}$ of the normalized micromagnetic free energy functional, formed by the sum of normalized exchange, magnetostatic, anisotropy and Zeeman energy, respectively:

$$g(\mathbf{m};\mathbf{h}_{\text{a}}) = \int_{\Omega}\left[\frac{A}{\mu_0 M_s^2}\,(\nabla\mathbf{m})^2 - \frac{1}{2}\mathbf{h}_{\text{m}}\cdot\mathbf{m} + \frac{K_1}{\mu_0 M_s^2}\left[1-(\mathbf{m}\cdot\mathbf{e}_{\text{an}})^2\right] - \mathbf{h}_{\text{a}}\cdot\mathbf{m}\right] dv\,, \tag{4.3}$$

where A is the exchange constant, K_1 is the uniaxial anisotropy constant, $\mathbf{e}_{\text{an}}$ is the easy axis unit-vector and $\mathbf{h}_{\text{m}}$ is the magnetostatic (demagnetizing) field, which is the solution of the boundary value problem:

$$\nabla\cdot\mathbf{h}_{\text{m}} = -\nabla\cdot\mathbf{m} \qquad \text{in } \Omega\,, \tag{4.4}$$

$$\mathbf{n}\times[\mathbf{h}_{\text{m}}]_{\partial\Omega} = \mathbf{0}\,, \quad \mathbf{n}\cdot[\mathbf{h}_{\text{m}}]_{\partial\Omega} = \mathbf{n}\cdot\mathbf{m}\,. \tag{4.5}$$

In Eqs. (4.4)-(4.5), we have denoted with $\mathbf{n}$ the outward normal to the boundary $\partial\Omega$ of the magnetic body, and with $[\mathbf{h}_{\text{m}}]_{\partial\Omega}$ the jump of the vector field $\mathbf{h}_{\text{m}}$ across $\partial\Omega$.

The magnetization $\mathbf{m}(\mathbf{r},t)$ is also assumed to satisfy the following condition at the body surface:

$$\frac{\partial\mathbf{m}}{\partial\mathbf{n}} = \mathbf{0}\,, \tag{4.6}$$

which is related to the presence of first (laplacian) term in Eq. (4.3).

4.2.1 General properties of the effective field

By considering the variational derivative of Eq. (4.3) with respect to the vector field $\mathbf{m}$ and by using Eqs. (4.4)-(4.5) and the boundary condition (4.6), one can readily derive that the effective field is constituted by the sum of four terms: the exchange field $\mathbf{h}_{\text{ex}}$, the magnetostatic field $\mathbf{h}_{\text{m}}$, the anisotropy field $\mathbf{h}_{\text{an}}$ and the applied field $\mathbf{h}_{\text{a}}$:

$$\mathbf{h}_{\text{eff}}(\mathbf{m},t) = -\frac{\delta g}{\delta\mathbf{m}} = \mathbf{h}_{\text{ex}} + \mathbf{h}_{\text{m}} + \mathbf{h}_{\text{an}} + \mathbf{h}_{\text{a}}(t)\,, \tag{4.7}$$

where the explicit dependence of $\mathbf{h}_{\text{eff}}$ on time is related to the dependence on time of $\mathbf{h}_{\text{a}}$. The first three terms in Eq. (4.7) can be related to the vector field $\mathbf{m}$ through the following equations (sections 1.2.2 and 3.1):

$$\mathbf{h}_{\text{ex}} = \frac{2A}{\mu_0 M_s^2}\,\nabla^2\mathbf{m}\,, \tag{4.8}$$

$$\mathbf{h}_{\text{m}} = -\frac{1}{4\pi}\nabla\int_{\Omega}\nabla'\left(\frac{1}{|\mathbf{r}-\mathbf{r}'|}\right)\cdot\mathbf{m}(\mathbf{r}')\,dV_{\mathbf{r}'}\,, \tag{4.9}$$

$$\mathbf{h}_{\text{an}} = \frac{2K_1}{\mu_0 M_s^2}\,\mathbf{e}_{\text{an}}(\mathbf{r})(\mathbf{e}_{\text{an}}(\mathbf{r})\cdot\mathbf{m}(\mathbf{r}))\,, \tag{4.10}$$

From the Eqs. (4.4)-(4.5), (4.6) and (4.8)–(4.10), one can easily prove that the sum of the first three terms of the effective field (4.7) is a formally self-adjoint operator acting on the vector field $\mathbf{m}$ in a suitable subspace of $\mathbb{L}^2(\Omega)$ with respect to the usual scalar product in $\mathbb{L}^2(\Omega)$:

$$(\mathbf{v}, \mathbf{w})_{\mathbb{L}^2(\Omega)} = \int_\Omega \mathbf{v}(\mathbf{r}) \cdot \mathbf{w}(\mathbf{r}) dV \,. \tag{4.11}$$

In other terms the effective field (1.68) can be written in the following form

$$\mathbf{h}_{\text{eff}}(\mathbf{r}, t) = -\mathcal{C}\mathbf{m} + \mathbf{h}_{\text{a}}(t) \tag{4.12}$$

where $\mathcal{C}$ is a formally self-adjoint integro-differential operator in $\mathbb{L}^2(\Omega)$.

4.2.2 CONSTRAINTS FOR MAGNETIZATION DYNAMICS AND HAMILTONIAN STRUCTURE OF CONSERVATIVE DYNAMICS

Let us now summarize the fundamental properties of LLG dynamics in the normalized quantities introduced above.

The first property a) is expressed as

$$|\mathbf{m}(\mathbf{r}, t)| = |\mathbf{m}(\mathbf{r}, t_0)| \qquad \forall t \geq t_0 \,,\ \forall \mathbf{r} \in \Omega \,, \tag{4.13}$$

which can be easily derived as explained in section 1.3.5. In the typical micromagnetic problem it is assumed initially $|\mathbf{m}(\mathbf{r}, t_0)| = 1$ which is the normalized version of the micromagnetic constraint $|\mathbf{M}| = \mathrm{M_s}$.

The second fundamental property b) is related to the nature of the energy balance in LLG dynamics:

$$\frac{d}{dt} g(t) = -\int_\Omega \alpha \left| \frac{\partial \mathbf{m}}{\partial t} \right|^2 dv - \int_\Omega \mathbf{m} \cdot \frac{\partial \mathbf{h}_a}{\partial t} \, dv \tag{4.14}$$

which has very important implications. For constant applied field, Eq. (4.14) reduces to

$$\frac{d}{dt} g(t) = -\int_\Omega \alpha \left| \frac{\partial \mathbf{m}}{\partial t} \right|^2 dv \,, \tag{4.15}$$

This equation reveals the role of the damping and shows that LLG dynamics has a Lyapunov structure, namely, for constant external field, the free energy is always a decreasing function of time. In addition, it also demonstrates the nature of the Gilbert phenomenological damping: the dissipation is proportional to the square of the velocity of variation of magnetization. This is connected to the fact that the Gilbert damping term can be introduced by using the Rayleigh approach described in section 1.3.5.

This property is very important because it guarantees that the system tends toward minima of free energy (i.e. meta-stable equilibrium points).

Third, for $\alpha = 0$ the LLG equation becomes an Hamiltonian dynamical system for the vector field $\mathbf{m}$ defined as

$$\frac{\partial \mathbf{m}}{\partial t} = \mathbf{m} \times \frac{\delta g}{\delta \mathbf{m}} \,. \tag{4.16}$$

The LLG hamiltonian form (4.16) is related to the following LLG Poisson bracket

$$\{f(\mathbf{m}), h(\mathbf{m})\} = \mathbf{m} \cdot \frac{\delta f}{\delta \mathbf{m}} \times \frac{\delta h}{\delta \mathbf{m}} \tag{4.17}$$

where $f(\mathbf{m})$ and $h(\mathbf{m})$ are two generic functionals of $\mathbf{m}$. In Eq. (4.16), the role of the hamiltonian is played by $g(\mathbf{m}; \mathbf{h}_\mathrm{a})$. It should be underlined that, although the LLG dynamics is always dissipative, it is interesting to consider the conservative case as in most experimental situations the dissipative effect are quite small (typically $\alpha \sim 10^{-2}$). In other terms, the LLG dynamics, on relatively short time scale, is a perturbation of the conservative (hamiltonian) precessional dynamics. In this respect, many interesting conclusions on the nature of dynamics can be also derived from the conservative[1] Eq. (4.16).

4.3 Spatially semi-discretized LLG equation

We now introduce a spatially discretized version of the mathematical model. The discussion presented below is considerably general and thus applicable to all the usual spatial discretization techniques [52].

To start the discussion, let us assume that the magnetic body has been subdivided in N cells or finite elements. We denote the magnetization vector associated to the l-th cell or node by $\mathbf{m}_l(t) \in \mathbb{R}^3$. Analogously, the effective and the applied fields at each cell will be denoted by the vector $\mathbf{h}_{\mathrm{eff},l}(t)$, $\mathbf{h}_{a,l}(t)$. In addition to the cell-vectors, we introduce another notation for the mesh vectors which include the information of all cells of the mesh. In this respect, we will indicate with $\underline{\mathbf{m}}$, $\underline{\mathbf{h}}_\mathrm{eff}$, $\underline{\mathbf{h}}_\mathrm{a}$ the vectors in $\mathbb{R}^{3N}$ given by:

$$\underline{\mathbf{m}} = \begin{pmatrix} \mathbf{m}_1 \\ \vdots \\ \mathbf{m}_N \end{pmatrix} \qquad \underline{\mathbf{h}}_\mathrm{eff} = \begin{pmatrix} \mathbf{h}_{\mathrm{eff},1} \\ \vdots \\ \mathbf{h}_{\mathrm{eff,N}} \end{pmatrix} \qquad \underline{\mathbf{h}}_\mathrm{a} = \begin{pmatrix} \mathbf{h}_{\mathrm{a},1} \\ \vdots \\ \mathbf{h}_{\mathrm{a,N}} \end{pmatrix} \quad . \tag{4.18}$$

4.3.1 Discretized free energy and effective field

Usual spatial discretization techniques [52] (e.g. finite elements and finite differences) quite naturally lead to a discretized version of the free energy (4.3) which has generally the form

$$\underline{\mathrm{g}}(\underline{\mathbf{m}}, \underline{\mathbf{h}}_a) = \frac{1}{2}\, \underline{\mathbf{m}}^T \cdot \underline{\mathrm{C}} \cdot \underline{\mathbf{m}} - \underline{\mathbf{h}}_a \cdot \underline{\mathbf{m}} \quad . \tag{4.19}$$

[1] We have seen examples of this in chapter 2, for uniformly magnetized particles.

where $\underline{\mathrm{C}}$ is now a $3N \times 3N$ symmetric matrix [80] which describes exchange, anisotropy and magnetostatic interactions. Once the free energy has been discretized, the corresponding spatially discretized effective field $\underline{\mathbf{h}}_{\mathrm{eff}}(\underline{\mathbf{m}}, t)$ can be obtained as

$$\underline{\mathbf{h}}_{\mathrm{eff}}(\underline{\mathbf{m}}, t) = -\frac{\partial \underline{\mathrm{g}}}{\partial \underline{\mathbf{m}}} = -\underline{\mathrm{C}} \cdot \underline{\mathbf{m}} + \underline{\mathbf{h}}_a(t)\,. \tag{4.20}$$

We notice that the effective field mathematical structure (4.12) is formally preserved after the spatial discretization, and the matrix $\underline{\mathrm{C}}$ is the discretized version of the formally self-adjoint integro-differential operator $\mathcal{C}$.

The matrix $\underline{\mathrm{C}}$ can be naturally decomposed into the sum of the three terms $\underline{\mathrm{C}}_{\mathrm{ex}}$, $\underline{\mathrm{C}}_{\mathrm{m}}$, $\underline{\mathrm{C}}_{\mathrm{an}}$ which correspond to discretized exchange, magnetostatic and anisotropy interactions:

$$\underline{\mathrm{C}} = \underline{\mathrm{C}}_{\mathrm{ex}} + \underline{\mathrm{C}}_{\mathrm{m}} + \underline{\mathrm{C}}_{\mathrm{an}} \quad . \tag{4.21}$$

It is important to observe that $\underline{\mathrm{C}}_{\mathrm{ex}}$ and $\underline{\mathrm{C}}_{\mathrm{an}}$ are sparse matrices since the exchange and anisotropy interactions have a local character, whereas $\underline{\mathrm{C}}_{\mathrm{m}}$ is a full matrix owing to the long-range magnetostatic interactions.

4.3.2 Semi-discretized LLG equation properties

By using the above notations, the spatially semi-discretized LLG equation consists in a system of $3N$ ODEs which, for the generic $l-$th cell, can be written in the following form :

$$\frac{d}{dt}\mathbf{m}_l = -\mathbf{m}_l \times \left[\mathbf{h}_{\mathrm{eff},l}(\underline{\mathbf{m}}, t) - \alpha \frac{d}{dt}\mathbf{m}_l\right] \quad , \tag{4.22}$$

and for the whole collection of cells as:

$$\frac{d}{dt}\underline{\mathbf{m}} = -\underline{\Lambda}(\underline{\mathbf{m}}) \cdot \left[\underline{\mathbf{h}}_{\mathrm{eff}}(\underline{\mathbf{m}}, t) - \alpha \frac{d}{dt}\underline{\mathbf{m}}\right] \quad , \tag{4.23}$$

where $\underline{\Lambda}(\underline{\mathbf{m}})$ is a block-diagonal matrix

$$\underline{\Lambda}(\underline{\mathbf{m}}) = \mathrm{diag}(\Lambda(\mathbf{m}_1), \ldots, \Lambda(\mathbf{m}_N)) \tag{4.24}$$

with blocks $\Lambda(\,\cdot\,) \in \mathbb{R}^{3\times 3}$ such that $\Lambda(\mathbf{v})\cdot\mathbf{w} = \mathbf{v}\times\mathbf{w}$, $\forall\, \mathbf{v},\ \mathbf{w} \in \mathbb{R}^3$. We also observe that $\underline{\Lambda}(\underline{\mathbf{m}})$ is linearly dependent on $\underline{\mathbf{m}}$ through an appropriate third order tensor $\underline{\Gamma}$ as

$$\underline{\Lambda} = \underline{\Gamma} \cdot \underline{\mathbf{m}} \tag{4.25}$$

where $\underline{\Gamma}$ is block diagonal with N diagonal $3 \times 3 \times 3$ blocks constituted by third order permutation tensors and the dot product in Eq. (4.25) represent an index contraction. The meaning of this contraction can be inferred by the considering

that the component of the vector $\underline{\mathbf{v}} \cdot (\underline{\Gamma} \cdot \underline{\mathbf{w}})$ corresponding to the l-th cell is given by

$$(\underline{\mathbf{v}} \cdot (\underline{\Gamma} \cdot \underline{\mathbf{w}}))_l = \mathbf{v}_l \times \mathbf{w}_l \,, \tag{4.26}$$

where we have used the notation introduced above for mesh vectors ($\underline{\mathbf{v}}$, $\underline{\mathbf{w}}$) and cell vectors ($\mathbf{v}_l$, $\mathbf{w}_l$).

Now, we briefly summarize the properties of the semi-discretized LLG. These properties are completely analogous to the properties (4.13)-(4.17) and the demonstration can be obtained by following the very same line of reasoning. Indeed, we can easily prove that

$$|\mathbf{m}_l(t)| = |\mathbf{m}_l(t_0)| \qquad \forall t \geq t_0 \,,\ l = 1, \ldots, N \ , \tag{4.27}$$

$$\frac{d}{dt}\underline{\mathrm{g}}(t) = -\alpha \left| \frac{d\underline{\mathbf{m}}}{dt} \right|^2 - \underline{\mathbf{m}} \cdot \frac{d\underline{\mathbf{h}}_a}{dt} = -\sum_{l=1}^{N} \alpha \left| \frac{d\mathbf{m}_l}{dt} \right|^2 - \sum_{l=1}^{N} \mathbf{m}_l \cdot \frac{d\underline{\mathbf{h}}_{a,l}}{dt} \,, \tag{4.28}$$

and, in the case of constant applied field, that:

$$\frac{d}{dt}\underline{\mathrm{g}}(t) = -\alpha \left| \frac{d\underline{\mathbf{m}}}{dt} \right|^2 = -\sum_{l=1}^{N} \alpha \left| \frac{d\mathbf{m}_l}{dt} \right|^2 \,. \tag{4.29}$$

Finally, in the case $\alpha = 0$, the semi-discretized LLG (4.23) takes the form

$$\frac{d\underline{\mathbf{m}}}{dt} = \underline{\Lambda}(\underline{\mathbf{m}}) \cdot \frac{\partial g}{\partial \underline{\mathbf{m}}} \,, \tag{4.30}$$

which is related to the semi-discretized version of Poisson bracket (4.17)

$$\{f(\underline{\mathbf{m}}), h(\underline{\mathbf{m}})\} = \frac{\partial f}{\partial \underline{\mathbf{m}}} \cdot \underline{\Lambda}(\underline{\mathbf{m}}) \cdot \left(\frac{\partial h}{\partial \underline{\mathbf{m}}} \right)^T \tag{4.31}$$

where T indicate the matrix transpose, $f(\underline{\mathbf{m}})$ and $h(\underline{\mathbf{m}})$ are two generic functions of $\underline{\mathbf{m}}$, and $\partial f/\partial \underline{\mathbf{m}}$, $\partial h/\partial \underline{\mathbf{m}}$ are the corresponding gradients.

In connection with the hamiltonian structure (4.30), it is interesting to mention that when the matrix $\underline{\Lambda}(\underline{\mathbf{m}})$ has the linear form (4.25), the related hamiltonian system (4.30) is said to have a Lie-Poisson structure [88]. As we will discuss in the sequel, this structure affects the nature of mid-point approximation of LLG equation.

4.4 Mid-point LLG discrete dynamics

We now proceed to derive the full discretization of LLG equation by applying the mid-point rule (see Appendix C) to the spatially semi-discretized system of ODEs given by Eq. (4.22). In the following, we will denote the value of physical

quantities at the n-th time step with the suffix n. The mid-point rule consists in the following time-stepping scheme, written for the for the generic $l-$th cell:

$$\frac{\mathbf{m}_l^{n+1}-\mathbf{m}_l^n}{\Delta t} = -\left(\frac{\mathbf{m}_l^{n+1}+\mathbf{m}_l^n}{2}\right)\times\left[\mathbf{h}_{\mathrm{eff},l}\left(\frac{\underline{\mathbf{m}}^{n+1}+\underline{\mathbf{m}}^n}{2},\, t^n+\frac{\Delta t}{2}\right)-\alpha\frac{\mathbf{m}_l^{n+1}-\mathbf{m}_l^n}{\Delta t}\right], \tag{4.32}$$

where Δt is the time step which, for the sake of simplicity, is assumed here constant. Nevertheless, due to the single-step nature of mid-point rule, most considerations in the following can be generalized to nonconstant time steps. Equation (4.32) can be rewritten in terms of mesh vectors as follows

$$\frac{\underline{\mathbf{m}}^{n+1}-\underline{\mathbf{m}}^n}{\Delta t} = -\underline{\Lambda}\left(\frac{\underline{\mathbf{m}}^{n+1}+\underline{\mathbf{m}}^n}{2}\right)\cdot\left[\underline{\mathbf{h}}_{\mathrm{eff}}\left(\frac{\underline{\mathbf{m}}^{n+1}+\underline{\mathbf{m}}^n}{2},\, t^n+\frac{\Delta t}{2}\right)-\alpha\frac{\underline{\mathbf{m}}^{n+1}-\underline{\mathbf{m}}^n}{\Delta t}\right]. \tag{4.33}$$

Equation (4.33) defines $\underline{\mathbf{m}}^{n+1}$ in terms of $\underline{\mathbf{m}}^n$ implicitly. By solving this equation for $\underline{\mathbf{m}}^{n+1}$, we generate a map

$$\underline{\mathbf{m}}^{n+1} = \Phi(\underline{\mathbf{m}}^n, \Delta t) \tag{4.34}$$

which describe the LLG discrete dynamics. We will discuss the technique for solving the implicit equation (4.33) in the following section. In this section, instead, we will focus on the properties of the map (4.34) defined implicitly by Eq. (4.32) or equivalently by Eq. (4.33).

As a preliminary consideration, we notice that, in most LLG numerical investigations, numerical discretization of LLG equation is carried out starting from the Landau-Lifshitz form (4.2) which has the advantage of explicitly expressing the time derivative of $\mathbf{m}$. Conversely, in the approach we propose, we directly discretized the original LLG equation in which the time derivative is implicitly contained. In fact, since the mid-point scheme is already implicit, the implicit nature of LLG equation does not introduce any further complication, but rather it drastically simplifies the treatment and the algorithm.

4.4.1 PROPERTIES OF MID-POINT RULE INDUCED DYNAMICS

Point-wise magnitude conservation

The first important property of the discrete dynamics can be readily obtained from Eq. (4.32) by scalar multiplying both sides of the equation by $(\mathbf{m}_l^{n+1}+\mathbf{m}_l^n)$. This leads immediately to

$$(\mathbf{m}_l^{n+1}-\mathbf{m}_l^n)\cdot(\mathbf{m}_l^{n+1}+\mathbf{m}_l^n) = |\mathbf{m}_l^{n+1}|^2-|\mathbf{m}_l^n|^2 = 0\ ,\ l=1\dots N\,, \tag{4.35}$$

which means that the magnitude of the magnetization vector remains constant in each cell. Thus, the mid-point rule preserves exactly the magnitude preservation property (4.27), regardless of the time step.

Energy balance and discrete Lyapunov structure

Next, we analyze the energy balance properties of the discrete dynamics. The derivation of the main equation can be carried out by scalar multiplying both members of Eq. (4.33) by the quantity

$$\left[\underline{\mathbf{h}}_{\text{eff}}\left(\frac{\underline{\mathbf{m}}^{n+1}+\underline{\mathbf{m}}^{n}}{2},\, t^{n}+\frac{\Delta t}{2}\right)-\alpha\frac{\underline{\mathbf{m}}^{n+1}-\underline{\mathbf{m}}^{n}}{\Delta t}\right]. \tag{4.36}$$

It is clear that, due to the antisymmetry of the matrix $\underline{\Lambda}(\underline{\mathbf{m}})$ (which in turn is related to the antisymmetry of its 3×3 diagonal blocks), the dot multiplication of (4.36) and the right-hand-side of Eq. (4.33) gives zero. As far as the left-hand side is concerned, by using the expression of the discretized effective field (4.20), one obtains:

$$\frac{\underline{\mathbf{m}}^{n+1}-\underline{\mathbf{m}}^{n}}{\Delta t}\cdot\left[-\underline{\mathrm{C}}\cdot\left(\frac{\underline{\mathbf{m}}^{n+1}+\underline{\mathbf{m}}^{n}}{2}\right)+\underline{\mathbf{h}}_{a}\left(t^{n}+\frac{\Delta t}{2}\right)-\alpha\frac{\underline{\mathbf{m}}^{n+1}-\underline{\mathbf{m}}^{n}}{\Delta t}\right]=\mathbf{0}\,. \tag{4.37}$$

Then, by using the symmetry of the matrix $\underline{\mathrm{C}}$ and the following mid-point approximation for the mid-point value of the applied field:

$$\underline{\mathbf{h}}_{a}\left(t^{n}+\frac{\Delta t}{2}\right)=\frac{\underline{\mathbf{h}}_{a}^{n+1}+\underline{\mathbf{h}}_{a}^{n}}{2}+\frac{\Delta t^{2}}{4}\left.\frac{d^{2}\underline{\mathbf{h}}_{a}}{dt^{2}}\right|_{t^{n}+\frac{\Delta t}{2}}, \tag{4.38}$$

one can readily derive the following equation

$$\begin{aligned}\frac{\underline{\mathrm{g}}(\underline{\mathbf{m}}^{n+1};\underline{\mathbf{h}}_{a}^{n+1})-\underline{\mathrm{g}}(\underline{\mathbf{m}}^{n};\underline{\mathbf{h}}_{a}^{n})}{\Delta t}&=-\alpha\left|\frac{\underline{\mathbf{m}}^{n+1}-\underline{\mathbf{m}}^{n}}{\Delta t}\right|^{2}+\\ -\frac{(\underline{\mathbf{m}}^{n+1}+\underline{\mathbf{m}}^{n})}{2}\cdot\frac{\underline{\mathbf{h}}_{a}^{n+1}-\underline{\mathbf{h}}_{a}^{n}}{\Delta t}&+\frac{\Delta t}{4}(\underline{\mathbf{m}}^{n+1}-\underline{\mathbf{m}}^{n})\cdot\left.\frac{d^{2}\underline{\mathbf{h}}_{a}}{dt^{2}}\right|_{t^{n}+\frac{\Delta t}{2}}.\end{aligned} \tag{4.39}$$

Notice that since $(\underline{\mathbf{m}}^{n+1}-\underline{\mathbf{m}}^{n})$ is of the order $\mathcal{O}(\Delta t)$ then the last term at the right hand side of the equation is $\mathcal{O}(\Delta t^{2})$ and thus, as we expected, up to this second order term, the discrete dynamics reproduce the energy balance for semi-discretized equation (4.28).

In fact, very interesting properties of the scheme can be inferred from Eq. (4.39). First we notice that, if the applied field $\underline{\mathbf{h}}_{a}$ is piece-wise linear with respect to time, in each time interval $[t^{n},t^{n+1}]$, then the last term in right hand side vanishes and the energy balance is exactly reproduced in its mid-point time discretized version. In addition, in the case of constant applied field, the last two terms in Eq. (4.39) vanish and the energy balance reduces to the following form

$$\frac{\underline{\mathrm{g}}(\underline{\mathbf{m}}^{n+1};\underline{\mathbf{h}}_{a})-\underline{\mathrm{g}}(\underline{\mathbf{m}}^{n};\underline{\mathbf{h}}_{a})}{\Delta t}=-\alpha\left|\frac{\underline{\mathbf{m}}^{n+1}-\underline{\mathbf{m}}^{n}}{\Delta t}\right|^{2}. \tag{4.40}$$

Equation (4.40) has very important consequences. First, independently of the time step, the discretized energy $\underline{\mathrm{g}}(\underline{\mathbf{m}}^{n};\underline{\mathbf{h}}_{a})$ is decreasing. This confirms that

the mid-point rule is an unconditionally stable algorithm which reproduce the relaxation behavior in LLG discrete dynamics for any choice of the time step. Notice also that the rate of variation of energy in the discrete dynamics is coherent the mid-point version of Eq. (4.29).

Second, for $\alpha = 0$ the energy is exactly preserved regardless of the time steps. These two properties confirms the unconditional stability of mid-point rule, but more importantly they indicate that, in the short time scale, the mid-point rule will tend to reproduce correctly the most important part in the LLG dynamics, i.e. the precessional magnetization motion.

Preservation of Hamiltonian structure

Finally, it is also important to address the issue of the preservation of the hamiltonian structure [89] (in the case $\alpha = 0$) given by Eq. (4.30). Let us indicate by $\underline{\mathbf{m}}(t) = \phi(t, \underline{\mathbf{m}}_0)$ the flow of Eq. (4.30), namely the solution of the Cauchy problem for the system of ODEs (4.30) with the initial condition $\underline{\mathbf{m}}(t = t_0) = \underline{\mathbf{m}}_0$. It is well known that the map $\phi(t, \underline{\mathbf{m}}_0)$ mapping $\underline{\mathbf{m}}_0$ into $\underline{\mathbf{m}}(t)$ satisfies the following symplecticity condition

$$\frac{\partial \phi(t, \underline{\mathbf{m}})}{\partial \underline{\mathbf{m}}} \cdot \underline{\Lambda}(\underline{\mathbf{m}}) \cdot \left(\frac{\partial \phi(t, \underline{\mathbf{m}})}{\partial \underline{\mathbf{m}}} \right)^T = \underline{\Lambda}(\phi(t, \underline{\mathbf{m}})) \,. \tag{4.41}$$

A numerical scheme is said to preserve the hamiltonian structure if the associated map, which connects one step to the following (in the case of mid-point rule the map $\Phi(\underline{\mathbf{m}}^n, \Delta t)$ introduced in Eq. (4.34)), fulfills the condition (4.41). In this respect, by using the fact that the LLG equation has a Lie-Poisson structure (i.e. the matrix $\underline{\Lambda}(\underline{\mathbf{m}})$ is linear with respect to $\underline{\mathbf{m}}$ as expressed in Eq. (4.25)), it is possible to prove the following error formula [83]

$$\frac{\partial \Phi(\Delta t, \underline{\mathbf{m}})}{\partial \underline{\mathbf{m}}} \cdot \underline{\Lambda}(\underline{\mathbf{m}}) \cdot \left(\frac{\partial \Phi(\Delta t, \underline{\mathbf{m}})}{\partial \underline{\mathbf{m}}} \right)^T - \underline{\Lambda}(\Phi(\Delta t, \underline{\mathbf{m}})) = \mathcal{O}(\Delta t^3) \tag{4.42}$$

which means that, the mid-point rule applied to LLG equation preserves hamiltonian structure up to the third order term in Δt.

It is also interesting to underline that the preservation of hamiltonian structure would be exact for an hamiltonian system defined by a Poisson bracket of the type $\{f(\underline{\mathbf{m}}), h(\underline{\mathbf{m}})\} = (\partial f / \partial \underline{\mathbf{m}}) \cdot \underline{\mathrm{J}} \cdot (\partial h / \partial \underline{\mathbf{m}})^T$ where the matrix $\underline{\mathrm{J}}$ does not depend on $\underline{\mathbf{m}}$. In LLG studies this situation is encountered in all those problems in which LLG equation is linearized around a given magnetization state as it is generally done in Spin-wave analysis [4] and nucleation problems [5]. In this respect, it must be underlined that, although these problems are linear in nature, analytical solutions are obtainable only under quite restrictive assumptions about

the geometry of the magnetic body. General geometries can be treated only by numerical techniques.

4.5 Solution of the time-stepping equation

The properties we have just discussed are strongly related to the implicit nature of mid-point rule. As consequence of this implicit nature, we have to solve the time-stepping Eq. (4.33) for the unknown $\underline{\mathbf{m}}^{n+1}$ at each time step which amounts to solve the following system of $3N$ nonlinear equations in the $3N$ unknowns $\underline{\mathbf{m}}^{n+1}$:

$$\mathbf{F}(\underline{\mathbf{m}}^{n+1}) = \mathbf{0} \quad , \tag{4.43}$$

where $\mathbf{F}(\underline{\mathbf{y}}) : \mathbb{R}^{3N} \rightarrow \mathbb{R}^{3N}$ is the following vector function:

$$\mathbf{F}(\underline{\mathbf{y}}) = \left[\underline{\mathrm{I}} - \alpha\underline{\Lambda}\left(\frac{\underline{\mathbf{y}} + \underline{\mathbf{m}}^n}{2}\right)\right]\left(\underline{\mathbf{y}} - \underline{\mathbf{m}}^n\right) - \Delta t\ \mathbf{f}\left(\frac{\underline{\mathbf{y}} + \underline{\mathbf{m}}^n}{2}\right) , \tag{4.44}$$

and where

$$\mathbf{f}(\underline{\mathbf{m}}) = -\underline{\Lambda}(\underline{\mathbf{m}}) \cdot \underline{\mathbf{h}}_{\mathrm{eff}}(\underline{\mathbf{m}}) = \underline{\Lambda}(\underline{\mathbf{m}}) \cdot \frac{\partial \underline{\mathrm{g}}}{\partial \underline{\mathbf{m}}} , \tag{4.45}$$

is the right-hand-side of the conservative LLG equation. It is interesting to notice that the damping is present in only one term in the function $\mathbf{F}(\underline{\mathbf{y}})$ and it introduce only a slight modification of the function.

The solution of the system of equation (4.43) can be obtained by using Newton-Raphson (NR) algorithm. To this end, we derive the jacobian matrix $\underline{\mathrm{J}}_{\mathrm{F}}(\underline{\mathbf{y}})$ of the vector function $\mathbf{F}(\underline{\mathbf{y}})$ which, after simple algebraic manipulations, can be written in the following form

$$\underline{\mathrm{J}}_{\mathrm{F}}(\underline{\mathbf{y}}) = \underline{\mathrm{I}} - \alpha\underline{\Lambda}(\underline{\mathbf{m}}^n) - \frac{\Delta t}{2}\ \underline{\mathrm{J}}_{\mathrm{f}}\left(\frac{\underline{\mathbf{y}} + \underline{\mathbf{m}}^n}{2}\right) \tag{4.46}$$

where $\underline{\mathrm{J}}_{\mathrm{f}}$ is the jacobian matrix associated to $\mathbf{f}(\underline{\mathbf{m}})$. By using the Eqs.(4.25), (4.45), one obtains:

$$\underline{\mathrm{J}}_{\mathrm{f}}(\underline{\mathbf{m}}) = \frac{\partial \mathbf{f}}{\partial \underline{\mathbf{m}}}(\underline{\mathbf{m}}) = \underline{\Lambda}(\underline{\mathbf{m}}) \cdot \underline{\mathrm{C}} + \underline{\Gamma} \cdot (-\underline{\mathrm{C}} \cdot \underline{\mathbf{m}} + \underline{\mathbf{h}}_a) \ . \tag{4.47}$$

The main difficulty in applying NR method is that the Jacobian $\underline{\mathrm{J}}_{\mathrm{F}}(\underline{\mathbf{y}})$ of $\mathbf{F}(\underline{\mathbf{y}})$ is a full matrix, due to the long-range character of magnetostatic interactions which reflects in the full nature of the matrix $\underline{\mathrm{C}}$. In this connection, let us observe that the damping term affect only a small sparse component of the jacobian $\underline{\mathrm{J}}_{\mathrm{F}}(\underline{\mathbf{y}})$ and thus does not introduce any basic difficulty.

Anyhow, due to the full nature of $\underline{\mathrm{J}}_{\mathrm{F}}(\underline{\mathbf{y}})$, the use of the plain NR method would require an unpractical computational cost. However, as it is usual in solving field problems with implicit time stepping, we can use a quasi-Newton

method by considering a reasonable approximation of the Jacobian. In order to have a sparse Jacobian one can consider the following expression $\underline{\tilde{\mathrm{J}}}_{\mathrm{F}}$ in which magnetostatic interactions are not included:

$$\underline{\tilde{\mathrm{J}}}_{\mathrm{F}}(\underline{\mathbf{y}}) = \underline{\mathrm{I}} - \alpha\underline{\Lambda}(\underline{\mathbf{m}}^n) - \frac{\Delta t}{2}\,\underline{\tilde{\mathrm{J}}}_{\mathrm{f}}\left(\frac{\underline{\mathbf{y}} + \underline{\mathbf{m}}^n}{2}\right) \quad , \tag{4.48}$$

where the matrix $\underline{\tilde{\mathrm{J}}}_{\mathrm{f}}$ is

$$\underline{\tilde{\mathrm{J}}}_{\mathrm{f}}(\underline{\mathbf{m}}) = -\underline{\Lambda}(\underline{\mathbf{m}}) \cdot (-(\underline{\mathrm{C}}_{\mathrm{ex}} + \underline{\mathrm{C}}_{\mathrm{an}})) + \underline{\Gamma} \cdot [-(\underline{\mathrm{C}}_{\mathrm{ex}} + \underline{\mathrm{C}}_{\mathrm{an}}) \cdot \underline{\mathbf{m}} + \underline{\mathbf{h}}_a] \quad . \tag{4.49}$$

Basically, the latter equation is obtained by substituting the full matrix $\underline{\mathrm{C}}$ with its sparse component $\underline{\mathrm{C}}_{\mathrm{ex}} + \underline{\mathrm{C}}_{\mathrm{an}}$ in Eq. (4.47). Thus, the iterative procedure can be summarized as follows:

$$\underline{\mathbf{y}}_0 = \underline{\mathbf{m}}^n\,, \quad \underline{\mathbf{y}}_{k+1} = \underline{\mathbf{y}}_k + \Delta\underline{\mathbf{y}}_{k+1} \quad \text{with} \quad \underline{\tilde{\mathrm{J}}}_{\mathrm{F}}(\underline{\mathbf{y}}_k)\Delta\underline{\mathbf{y}}_{k+1} = -\mathbf{F}(\underline{\mathbf{y}}_k)\,. \tag{4.50}$$

At each iteration, the linear system defined by the matrix (4.49) has to be inverted. Since this matrix is non-symmetric, we have found appropriate to use generalized minimum residual (GMRES) method [91]. The iteration (4.50) is repeated until the norm $\|\mathbf{F}(\underline{\mathbf{y}}_k)\|$ is under a prescribed tolerance.

The iterative technique we developed to solve Eq. (4.43) belongs to the main category of quasi-Newton methods. In this respect, it has been proven [92] that this kind of iterative procedure is convergent and the order of convergency is the first order, provided that the initial guess is sufficiently close to the 'true' solution of the system.

4.6 ACCURACY TESTS FOR LLG DISCRETE DYNAMICS

We have shown that mid-point rule time-stepping preserves magnetization magnitude conservation and Lyapunov structure of LLG equation. Nevertheless, since the time-stepping equations (4.33) are solved through an iterative procedure, the properties of mid-point rule we have demonstrated in Sec. 4.4 are fulfilled only within a certain accuracy related to the tolerance which we imposed on the quasi-NR technique. In this respect, it is important to test the accuracy of the preservation of LLG properties during the computation.

To this end, as far as magnetization magnitude conservation, we will check the accuracy with the following quantities:

$$\mathrm{m}_{\mathrm{av}} = \frac{1}{N}\sum_{l=1}^{N}|\mathbf{m}_l| \quad , \quad \sigma_{\mathrm{m}}^2 = \frac{1}{N}\sum_{l=1}^{N}(|\mathbf{m}_l| - \mathrm{m}_{\mathrm{av}})^2 \quad , \tag{4.51}$$

which are, respectively, mean value and variance of the magnetization magnitude over the cells of the mesh.

As far as the energy balance equation is concerned, we use the self-consistency criterion proposed by Albuquerque and coworkers [94]. This criterion is based on Eq. (4.28) rewritten in the following form

$$\alpha = \left(\frac{d}{dt} \underline{\mathrm{g}}(t) \right) \Big/ \left| \frac{d\underline{\mathbf{m}}}{dt} \right|^2 \quad . \tag{4.52}$$

which is valid for constant applied field. It is quite natural, to test the preservation of energy dynamics in numerical computation, to compute

$$\hat{\alpha}^n = - \left(\frac{\underline{\mathrm{g}}(\underline{\mathbf{m}}^{n+1}; \underline{\mathbf{h}}_a) - \underline{\mathrm{g}}(\underline{\mathbf{m}}^{n}; \underline{\mathbf{h}}_a)}{\Delta t} \right) \Big/ \left| \frac{\underline{\mathbf{m}}^{n+1} - \underline{\mathbf{m}}^{n}}{\Delta t} \right|^2 \quad . \tag{4.53}$$

at each time step, and compare the value of the sequence $\hat{\alpha}^n$ with the constant α. In this respect, we observe that if we could exactly invert the nonlinear system of equations (4.43), then the sequence $\hat{\alpha}^n$ would be constant coincident with α. This can be immediately derived from the property (4.40) of the mid-point rule. However, since we determine the new time step by an iterative procedure, the sequence will be in fact nonconstant and it will usually exhibit an oscillatory behavior. It has been shown in Ref. [94] that numerical instabilities can be detected from the observation of the behavior of the values $\hat{\alpha}^n$.

For the case of conservative dynamics, the discretized energy is conserved according to Eq. (4.29) for $\alpha = 0$:

$$\underline{\mathrm{g}}(t) = \underline{\mathrm{g}}(t_0) \quad \forall\, t \geq t_0 \quad . \tag{4.54}$$

With mid-point rule time discretization, this property becomes (see Eq. (4.40)):

$$\underline{\mathrm{g}}(\underline{\mathbf{m}}^{n+1}; \underline{\mathbf{h}}_a) = \underline{\mathrm{g}}(\underline{\mathbf{m}}^{n}; \underline{\mathbf{h}}_a) \quad , \tag{4.55}$$

which holds regardless of the time step. One can test the accuracy of the scheme by recording the deviation of the total energy from its initial value. Again, one cannot expect that this property will be exactly fulfilled as far as we solve the time stepping algorithm with an iterative procedure. In this respect, we will verify a-posteriori that the energy conservation is guaranteed with sufficient precision by computing the relative error e_{g} of $\underline{\mathrm{g}}(\underline{\mathbf{m}}^{n}; \underline{\mathbf{h}}_a)$ with respect to the initial energy $\underline{\mathrm{g}}(\underline{\mathbf{m}}^{0}; \underline{\mathbf{h}}_a)$:

$$e_{\mathrm{g}}^n = \frac{\underline{\mathrm{g}}(\underline{\mathbf{m}}^{0}; \underline{\mathbf{h}}_a) - \underline{\mathrm{g}}(\underline{\mathbf{m}}^{n}; \underline{\mathbf{h}}_a)}{\underline{\mathrm{g}}(\underline{\mathbf{m}}^{0}; \underline{\mathbf{h}}_a)} \quad , \tag{4.56}$$

and checking that the sequence e_{g}^n remains within prescribed tolerance.

4.7 FINITE DIFFERENCES SPATIAL DISCRETIZATION OF LLG EQUATION

Up to this point the considerations we made about the properties and the implementation of mid-point rule were rather independent from the spatial discretization used. In the following, to test the method we have chosen a specific technique based on finite-differences method. The magnetic body is subdivided into a collection of rectangular prisms with edges parallel to the coordinate axes. The edge lengths are d_x, d_y, d_z. In this framework, it is convenient to identify each cell by three indices i, j, k instead of using the index l as we did before. The magnetization $\mathbf{m}_{i,j,k}$ is assumed to be uniform within the generic (i, j, k) cell. With this notation, the effective field in the generic (i, j, k) cell can be expressed as

$$\mathbf{h}_{\mathrm{eff;i,j,k}} = \mathbf{h}_{\mathrm{ex;i,j,k}} + \mathbf{h}_{\mathrm{m;i,j,k}} + \mathbf{h}_{\mathrm{an;i,j,k}} + \mathbf{h}_{\mathrm{a;i,j,k}} \tag{4.57}$$

The exchange field (4.8) is computed by means of a 7-point laplacian discretization, which is second order accurate in space. In the generic "internal" cell (i, j, k), the exchange field can be expressed as follows:

$$\begin{aligned}\mathbf{h}_{\mathrm{ex;i,j,k}} = \frac{2A}{\mu_0 M_s^2}\Bigg[&\frac{\mathbf{m}_{i+1,j,k} + \mathbf{m}_{i-1,j,k}}{d_y^2} + \frac{\mathbf{m}_{i,j+1,k} + \mathbf{m}_{i,j-1,k}}{d_x^2} + \\ &+ \frac{\mathbf{m}_{i,j,k+1} + \mathbf{m}_{i,j,k-1}}{d_z^2} - \left(\frac{2}{d_y^2} + \frac{2}{d_x^2} + \frac{2}{d_z^2}\right)\mathbf{m}_{i,j,k}\Bigg]\end{aligned} \tag{4.58}$$

A similar expression holds for the boundary cells where the Neumann boundary condition (4.6) has to be taken into account. Since the exchange interaction is a first-neighbors interaction, one can easily observe that the matrix $\underline{\mathrm{C}}_{\mathrm{ex}}$ is a block-diagonal matrix.

As seen in section 3.1, the magnetostatic field (4.9) can be expressed as discrete convolution:

$$\mathbf{h}_{\mathrm{m;i,j,k}} = \sum_{i' \neq i} \sum_{j' \neq j} \sum_{k' \neq k} N_{i-i',j-j',k-k'} \cdot \mathbf{m}_{i',j',k'}\, d_x d_y d_z \tag{4.59}$$

where $N_{i-i',j-j',k-k'}$ is the 3×3 block of the magnetostatic interaction matrix $\underline{\mathrm{C}}_{\mathrm{m}}$ which describes the magnetostatic interaction between the cells i, j, k and i', j', k'. The discrete convolution (4.59) is computed by means of 3D Fast Fourier Transform (FFT) using the zero-padding algorithm [64]. The kernel of the convolution is obtained in exact analytical form by means of a slight generalization of the one proposed in Ref. [93] for cubic cells. As far as anisotropy is concerned, we assume that the body has uniaxial anisotropy defined by the anisotropy constant K_1. Therefore, the anisotropy field is

$$\mathbf{h}_{\mathrm{an;i,j,k}} = \frac{2K_1}{\mu_0 M_s^2}\,(\mathbf{m}_{i,j,k} \cdot \mathbf{e}_x)\mathbf{e}_x \quad . \tag{4.60}$$

and the matrix $\underline{\mathrm{C}}_{\mathrm{an}}$ is a diagonal matrix.

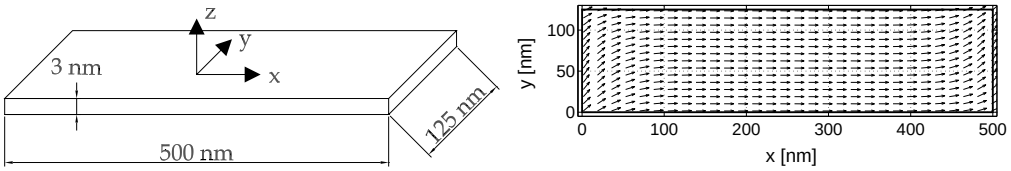

Figure 4.1: (Left) Thin-film geometry for μ-mag standard problem n. 4. (Right) Initial equilibrium S-state.

4.8 Numerical Simulations of μ-mag standard problem n. 4

4.8.1 Definition of the problem

We apply the above numerical technique to solve the μ-mag standard problem n. 4 (see Ref. [79]). This problem concerns the study of magnetization reversal dynamics in a thin-film subject to a constant and spatially uniform external field, applied almost antiparallel to the initial magnetization. The geometry of the medium is sketched in Fig. 4.1. The material parameters are $A = 1.3\times10^{-11}$ J/m, $M_s = 8.0 \times 10^5$ A/m, $K_1 = 0$ J/m^3 and $\alpha = 0.02$ (permalloy). The initial state is an equilibrium s-state (see Fig. 4.1, right) such as is obtained after applying and slowly reducing a saturating field along the $[1, 1, 1]$ direction to zero. In all the numerical simulations the equilibrium condition has been chosen such that:

$$\max_{l=1\ldots N} \left| \frac{\mathbf{m}_l^{n+1} - \mathbf{m}_l^n}{\Delta t} \right| < 10^{-5} \quad , \tag{4.61}$$

i.e. the maximum of the (normalized) torque across the body has been checked for equilibrium. Moreover, the stopping criterion of the quasi-Newton iterative procedure has been chosen

$$\max |\mathrm{F}_q(\mathbf{y}_k)| < 10^{-14} \quad , \quad q = 1, \ldots, 3N \quad . \tag{4.62}$$

where $\mathrm{F}_q(\mathbf{y}_k)$ is the q-th components of the vector $\mathbf{F}(\mathbf{y}_k)$, and the index k indicates the number of quasi-Newton iterations.

Two switching events will be calculated using fields applied in the x-y plane of different magnitude and direction. In the first case the external field is applied at an angle of 170° off the x axis with $x - y$ components such that $\mu_0\mathrm{M_s h}_{ax} = -24.6$ mT, $\mu_0\mathrm{M_s h}_{ay} = 4.3$ mT and $\mu_0\mathrm{h}_a = 25$ mT. In the second case the external field is applied at an angle of 190° off the x axis with $x - y$ components such that $\mu_0\mathrm{M_s h}_{ax} = -35.5$ mT, $\mu_0\mathrm{M_s h}_{ay} = -6.3$ mT, and $\mu_0\mathrm{M_s h}_a = 36$ mT. In both cases the cell edges are $d_x = 3.125$ nm, $d_y = 3.125$ nm, $d_z = 3$ nm and therefore the number of cells is $N = 160 \times 40 \times 1 = 6400$.

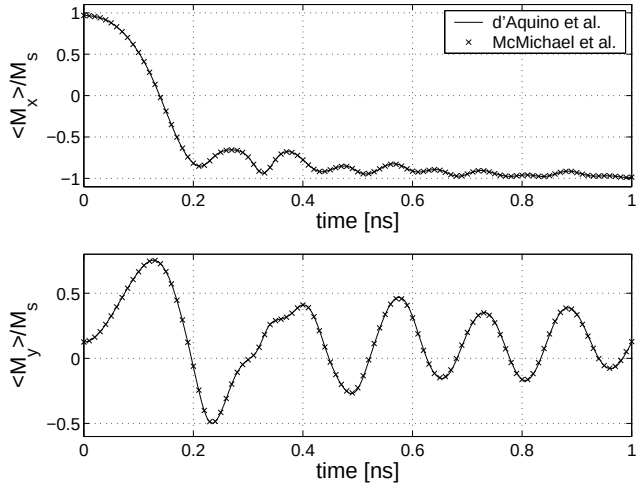

Figure 4.2: Comparison between solutions of μ-mag standard problem no. 4. Plots of $< m_x >=< M_x > /M_s$ and $< m_y >=< M_y > /M_s$ versus time. The external field is applied at an angle of 170° off the x-axis.

4.8.2 NUMERICAL RESULTS

Next we report the comparison between the solution obtained using the above numerical technique and the solutions submitted by other researchers [79] to the μ-mag website. The time step of the mid-point numerical algorithm is fixed and has been chosen such that $(|\gamma|M_s)^{-1}\,\Delta t = 2.5$ ps. We observe that the time steps related to the other solutions (see Ref. [79]) are considerably smaller (less then 0.2 ps) to fulfill numerical stability requirements. In Figs. 4.2 and 4.3 plots of $< m_y >$ ($< \cdot >$ means spatial average) as a function of time are reported. We observe that in the first case (Fig. 4.2) there is substantial agreement between the submitted solutions (see Ref. [79]) and for this reason we report, for comparison purposes, only the solution proposed by McMichael and coworkers. In Fig. 4.4 the plots of magnetization vector field when $< m_x >$ crosses zero for the first time are reported. Numerical simulations of the same problem were performed with a smaller cell edge (2.5 nm, number of cells $N = 10000$). The results, reported in Fig. 4.5, show that the computed magnetization dynamics does not depend on the mesh size. As far as accuracy is concerned, the self-consistency conditions mentioned in section 4.6 have been verified by means of the computation of the values $\mathrm{m_{av}}$, σ^2_{m} and $\hat{\alpha}^n$. The result of this computations is reported in Figs. 4.6-4.8.3. One can observe from Fig. 4.6 that the magnetization magnitude is very well preserved, since the mean value $\mathrm{m_{av}} \sim 1 \pm 10^{-16}$ and the variance σ^2_{m} is in the order of 10^{-30}. Moreover, one can see from Fig. 4.8.3 that the relative error $e^n_\alpha = (\hat{\alpha}^n - \alpha)/\alpha$ is in the order of 10^{-7}. As far as conservative dynamics is

concerned, the same problem has been simulated with $\alpha = 0$. The results, shown in Fig. 4.8.3 show that the reversal of the thin-film occurs, in the sense that the average magnetization exhibits a persistent oscillation around the reversed state. This means that the precessional effects are prevalent with respect to the damping effects. The free energy is conserved as one can see from Fig. 4.8 where exchange, magnetostatic, anisotropy, Zeeman energy and the total free energy are reported as functions of time. Quantitatively speaking, the relative error e_{g} of the free energy with respect to its initial value is in the order of 10^{-8} as one can see from Fig. 4.9.

4.8.3 Discussion about computational cost

As far as computational effort is concerned, numerical simulations for different number of cells and different time steps have been performed beyond the previous ones, with the only purpose of performance evaluation of the code. Some indicators, such as the average number of quasi-Newton iterations per time step (NR), the average number of GMRES iterations in one quasi-Newton iteration (LIN), the simulated time T, the simulation time T_s and the ratio between them, the maximum relative error $e_{\alpha,\max} = \max|(\hat{\alpha}^n - \alpha)/\alpha|$, the angle of the applied field δ, the number of cells N and the time step are reported in Table 4.1. In this respect, some considerations can be drawn. First, one can observe that the total number of cells N does not affect the quasi-Newton procedure in both the cases $\delta = 170°$ and $\delta = 190°$, whereas it affects the solution of the linear systems by increasing the average number of GMRES iterations. Second, one can clearly see that the minimum and maximum values of quasi-Newton and GMRES iterations are close to the average values, meaning that the iterative procedure weakly depends on magnetization dynamics; in fact, as seen before, the approximate jacobian matrix $\underline{\tilde{\mathbf{J}}}_{\mathrm{F}}$ depends on the particular value of magnetization vector $\underline{\mathbf{m}}$. Third, some considerations on computational cost can be made. We expect that the computational cost function $C(N)$ of the algorithm can be reasonably expressed by the sum of two terms. In fact, at each quasi-Newton iteration the cost of the evaluation of magnetostatic field (3D FFT convolution [64]) is proportional to $N \log N$. On the other hand, within each quasi-Newton iteration, the cost of LIN iterations of GMRES is proportional to N, since basically is the cost of LIN sparse matrix-vector products. Thus, we can express the overall cost function $C(N)$ as:

$$C(N) = T_s(N)/T = c_1\,\mathrm{NR}\,N\log N + c_2\,\mathrm{NR}\,\mathrm{LIN}\,N \quad , \tag{4.63}$$

δ	N	$\frac{\Delta t}{\lvert\gamma\rvert M_s}$ [ps]	NR	LIN	$e_{\alpha,\max}$	T [ns]	T_s [s]	T_s/T [s/ns]
170°	1000	2.5	11/14/17	4/5/5	1.5×10^{-8}	5.7700	648.05	112
170°	2500	2.5	11/14/17	6/7/7	2.0×10^{-7}	5.8450	1976.47	338
170°	6400	2.5	11/14/18	11/13/15	3.0×10^{-7}	5.8400	5631.23	964
170°	10000	2.5	11/14/18	17/19/22	1.3×10^{-7}	5.8425	12152.74	2080
190°	1000	2.5	11/14/17	4/5/5	1.4×10^{-8}	5.5800	632.34	113
190°	2500	2.5	11/14/18	6/7/8	0.7×10^{-7}	6.4100	2183.36	341
190°	6400	2.5	11/14/18	12/13/15	6.2×10^{-7}	6.4100	6257.13	976
190°	10000	2.5	11/14/18	18/20/23	7.0×10^{-7}	6.4100	13546.79	2113
170°	6400	1.0	9/12/14	6/6/7	3.7×10^{-7}	5.8420	10145.46	1737
170°	6400	2.5	11/14/18	11/13/15	3.0×10^{-7}	5.8400	5631.23	964
170°	6400	5.0	14/18/25	24/26/28	3.5×10^{-7}	5.9400	4624.31	779
190°	6400	1.0	9/12/14	6/6/7	1.3×10^{-7}	6.4150	11163.490	1740
190°	6400	2.5	11/14/18	12/13/15	6.2×10^{-7}	6.4100	6257.13	976
190°	6400	5.0	14/18/27	23/26/30	1.1×10^{-7}	7.4950	5705.520	761

Table 4.1: Numerical results. Indicators of computational effort for the proposed mid-point rule numerical technique. δ is the angle of the applied field, N is the number of cells, Δt is the time step, column NR reports minimum/average/maximum number of quasi-Newton iterations per time step, column LIN reports minimum/average/maximum number of GMRES iterations for one quasi-Newton iteration, $e_{\alpha,\max} = \max|(\hat{\alpha}^n - \alpha)/\alpha|$ is the maximum relative error with respect to the assigned damping parameter α, T is the simulated time, T_s the simulation time. $N = 1000$ refers to a prism cell of size $12.5 \times 5 \times 3$ nm. $N = 2500$ refers to a prism cell of size $5 \times 5 \times 3$ nm. $N = 6400$ refers to a prism cell of size $3.125 \times 3.125 \times 3$ nm. $N = 10000$ refers to a prism cell of size $2.5 \times 2.5 \times 3$ nm. The simulations have been performed with a Pentium 4 processor workstation (3 GHz), 1 GB RAM under RedHat Linux 9.

where c_1 and c_2 are fitting parameters. One can see from Fig. 4.10 that for moderately large number of cells, the ratio T_s/T increases according to the $\mathcal{O}(N \log N)$ scaling expected for the computation of the demagnetizing field by the 3D FFT convolution, whereas, for larger number of cells, the computational cost of the GMRES iterations becomes prevalent. Finally, it is important to underline that by increasing the time step Δt, the numerical algorithm exhibits a considerable speed-up, as one can see comparing the ratios T_s/T obtained in both the cases for a given number of cells $N = 6400$ and time steps such that $(|\gamma|M_s)^{-1}\,\Delta t$ =1, 2.5, 5 ps. In all the simulations it has been observed that the relative error $e_{\alpha,\max}$ is in the order of 10^{-7}.

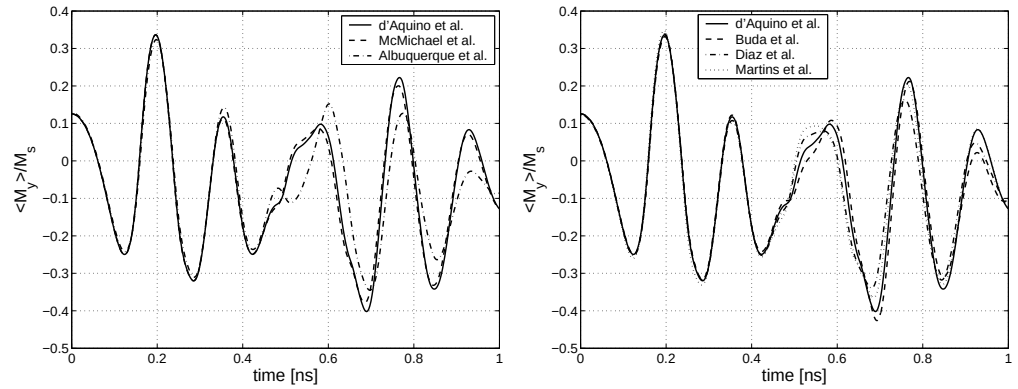

Figure 4.3: Comparison between solutions of μ-mag standard problem no. 4. Plots of $< m_y >=< M_y > /M_s$ versus time. The external field is applied at an angle of 190° off the x-axis.

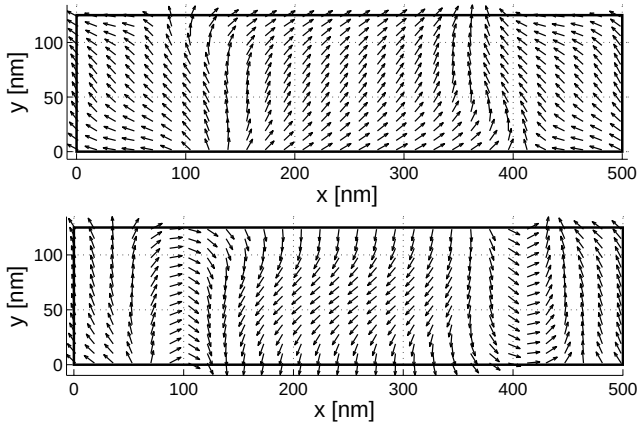

Figure 4.4: Numerical results for μ-mag standard problem no. 4. Snapshot of magnetization vector field when the average $< m_x >$ crosses zero for the first time. The external field is applied at an angle of 170° (up) and 190° (down) off the x-axis.

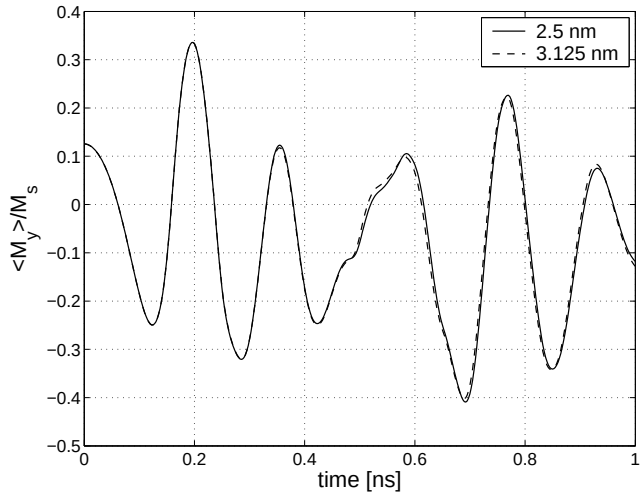

Figure 4.5: Numerical results for μ-mag standard problem no. 4. Plots of $< m_y >=< M_y > /M_s$ versus time for two different sizes of the mesh edge length. The external field is applied at an angle of 190° off the x-axis.

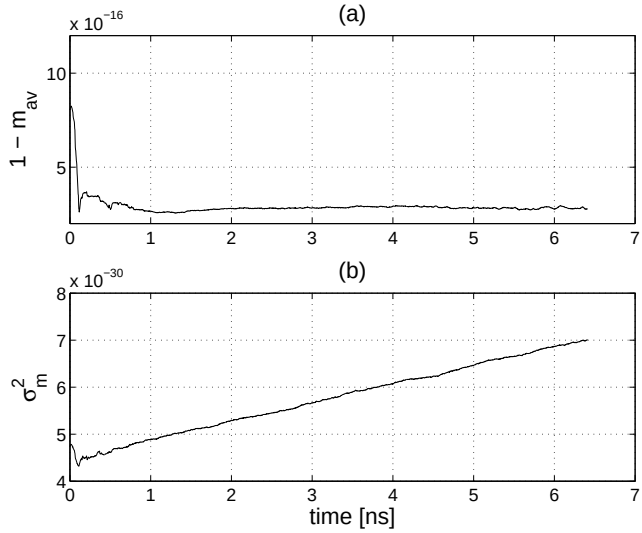

Figure 4.6: Numerical results for μ-mag standard problem no. 4. (a) Plot of $1 - \mathrm{m_{av}}$ as a function of time. (b) Plot of the variance σ^2_{m} as a function of time. In both plots $\delta = 190°$, $N = 6400$.

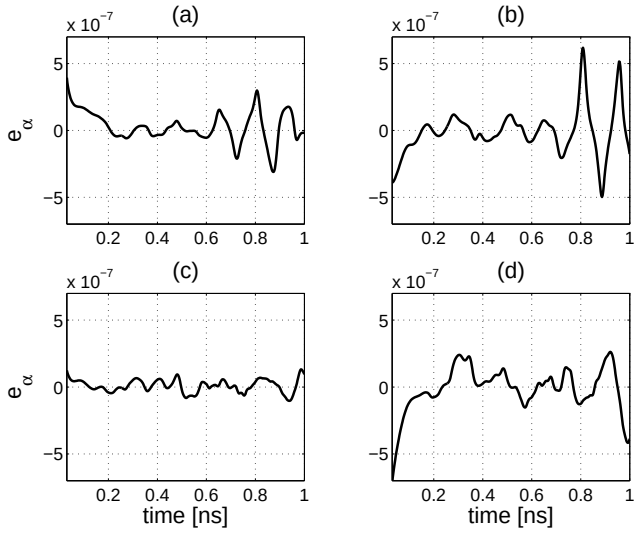

Figure 4.7: Numerical results for μ-mag standard problem no. 4. Plot of the relative error $e_\alpha^n = (\hat{\alpha}^n - \alpha)/\alpha$ as a function of time. (a) $\delta = 170°$, $N = 6400$. (b) $\delta = 170°$, $N = 10000$. (c) $\delta = 190°$, $N = 6400$. (d) $\delta = 190°$, $N = 10000$.

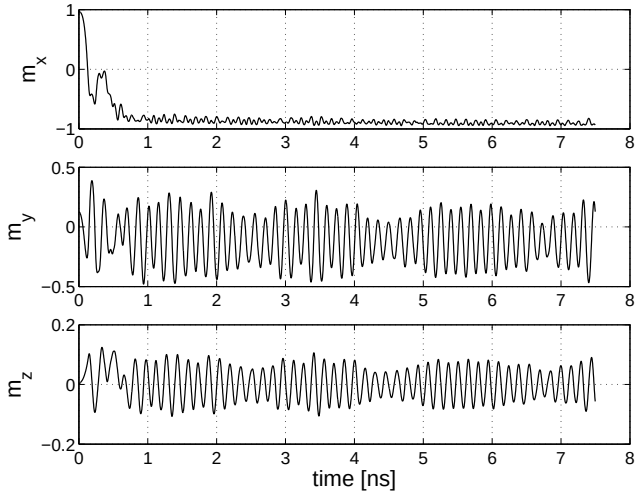

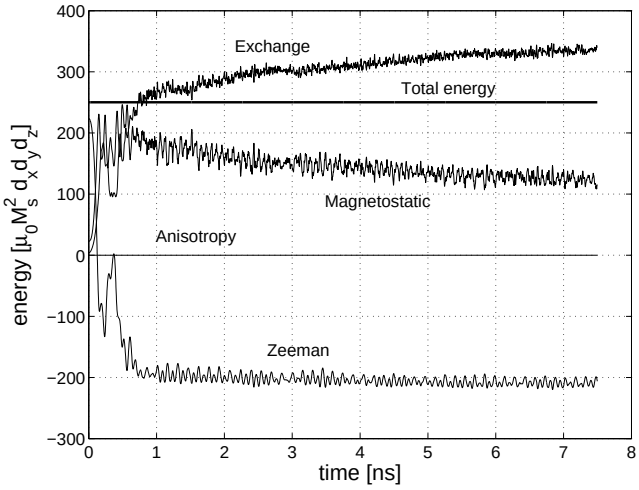

Figure 4.8: Numerical results for μ-mag standard problem no. 4 in the conservative case $\alpha = 0$. Plot of exchange, anisotropy, magnetostatic, Zeeman and total free energy as functions of time. $\delta = 190°$, $N = 6400$.

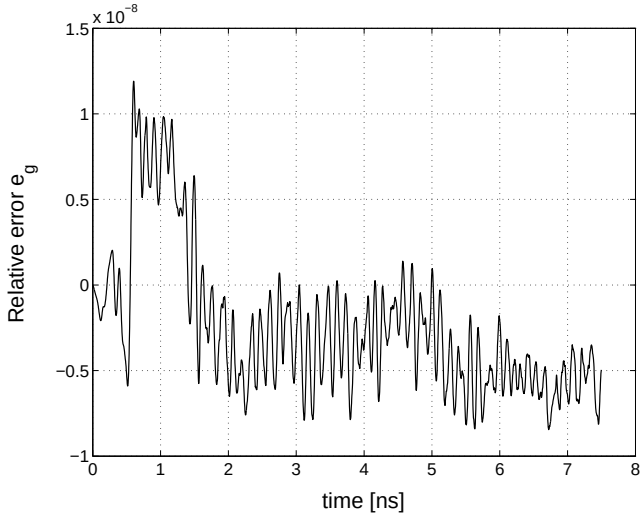

Figure 4.9: Numerical results for μ-mag standard problem no. 4 in the conservative case $\alpha = 0$. Plot of the relative error $e_{\mathrm{g}}^n = (\underline{\mathrm{g}}(\underline{\mathbf{m}}^0; \underline{\mathbf{h}}_a) - \underline{\mathrm{g}}(\underline{\mathbf{m}}^n; \underline{\mathbf{h}}_a))/\underline{\mathrm{g}}(\underline{\mathbf{m}}^0; \underline{\mathbf{h}}_a)$ as function of time. $\delta = 190°$, $N = 6400$.

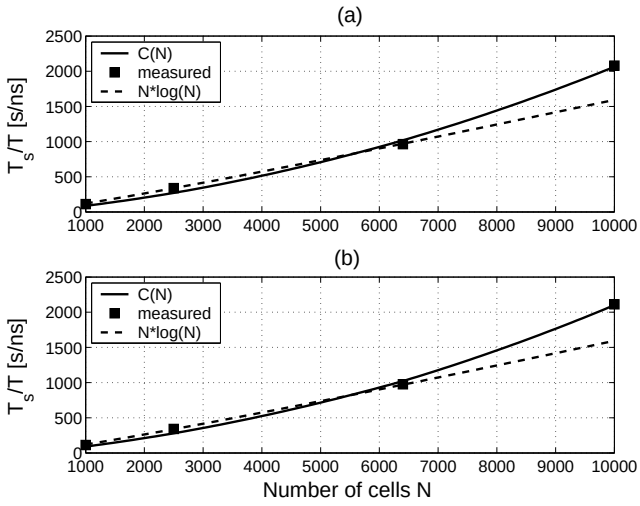

Figure 4.10: Numerical results for μ-mag standard problem no. 4. Plots of the ratio T_s/T between simulation time T_s [s] and simulated time T [ns] for different number of cells N. The theoretical computational cost function $C(N)$ and $N \log N$ scaling are also reported. The time step is such that $(|\gamma|M_s)^{-1}\,\Delta t = 2.5$ ps. (a) $\delta = 170°$; $c_1 = 5 \times 10^{-4}$, $c_2 = 5.2 \times 10^{-4}$ (b) $\delta = 190°$; $c_1 = 6 \times 10^{-4}$, $c_2 = 4.8 \times 10^{-4}$

Conclusions and Outlook

In this thesis some categories of magnetization phenomena, connected with high-end technological applications have been investigated. The followed approach has its foundations in micromagnetics, which is capable of properly describing magnetic phenomena on sub-micron scale. A first step has been done by studying magnetization dynamics under the hypothesis that the particles were uniformly magnetized. In this framework, it has been recalled that magnetization dynamical processes of technological interest, like damping switching and precessional switching, can be treated with analytical approaches present in literature, which provide critical design parameters like critical fields, as well as switching time and, for precessional switching, the time tolerance allowed in order to have successful switching. A slightly different context in the framework of uniform mode theory, has been touched, regarding some aspects of the LLG dynamics under circularly polarized fields, which arises in typical ferromagnetic resonance experiments. In particular, a special perturbative technique, based on mathematical background in the framework of dynamical systems theory, has been developed for the study of quasiperiodic solutions of LLG equation under circularly polarized field. In this respect, the problem of finding quasiperiodic solutions has been turned into the determination of limit cycles of a suitable modification of LLG equation, obtained by introducing the appropriate rotating reference frame. Basically, the result is that the study of the existence, the number, the stability of limit cycles of the dissipative LLG dynamics can be performed, at first order, on the conservative dynamics. The analytical results have been confirmed by numerical simulations that indeed show the accuracy of the predictions.

In addition, this technique, which permits also to study the (global) bifurcations of the limit cycles, has been applied to the study of LLG dynamics driven by spin-transfer torque. This subject is currently the focus of considerable research for its applications to current-driven switching of MRAMs cells. In particular, by using the above perturbative technique, and on the other hand the analytical treatment of the conservative dynamics, it is possible to predict analytically the critical values of the electric current and magnetic fields that rule complicated

behaviors, like the onset of self-oscillations and the current-driven switching, observed in recent experiments on spin-injection. Moreover, with this technique characteristics of the self-oscillations like frequency and amplitude can be analytically computed from the knowledge of the conservative dynamics.

As soon as the hypothesis of uniformly magnetized particles has been abandoned, the problem of the numerical computation of the magnetostatic field, which has been recognized to be the bottleneck of micromagnetic computations, has been analyzed. The two most used methods, respectively for finite differences and finite elements discretizations, have been described. Afterwards it has been shown with micromagnetic simulations of damping and precessional switching, that the former is an intrinsically non-uniform process, whereas the latter can be reasonably considered quasi-uniform also for dimensions of hundreds of nanometers (half micron) and moderately low anisotropy. In this respect, by computing the switching time with the uniform mode analysis, reliable switching can be obtained. It has been demonstrated that the accuracy of the prediction increases for increasing anisotropy of the material. Moreover, for moderately soft materials, with K_1 in the order of $10^4 \div 10^5$ J/m^3, a tolerance of $\pm 25\%$ on the pulse amplitude is allowed. The predicted time window agree with micromagnetic simulations with a precision of few picoseconds.

Then the fast switching of tilted granular media has been analyzed by means of a uniform mode approximation. The medium has been considered as a collection of noninteracting grains with dispersion of easy axes and initial conditions. In this framework, the necessary condition for the switching of the whole granular medium, i.e. the applied field amplitude range which makes fast switching possible, has been derived by analyzing the single grain dynamics, first conservative and then dissipative. A set of micromagnetic simulations have confirmed the predictions made with the uniform mode analysis.

Thus, the main result of this study is the fact that the uniform mode theory can be applied to study processes of technological interest, and in some cases it provides critical design parameters.

Beside the above analysis, the problem of geometrical integration of LLG equation has been addressed. In fact, the mostly used numerical time-stepping techniques do not preserve the fundamental properties of LLG dynamics, namely magnetization magnitude conservation, Lyapunov structure for constant in time applied field and hamiltonian structure in the conservative case. There is an interesting example in literature of how the missed fulfillment of magnitude conservation leads to inaccurate computation of magnetostatic field. Moreover, the quantitative discordance arising in the solution of micromagnetic standard prob-

lems suggests that the particular choice of numerical methods may affect the results of the computations. Therefore, we are convinced that a numerical model has to qualitatively reproduce the properties of the continuous model as best as possible, but, nevertheless it must have a feasible computational cost. In this respect, the proposed implicit mid-point rule technique has revealed very efficient from both points of view. First of all, it can be applied to any spatial discretization, like finite differences and finite elements, which preserves the formal structure of the effective field. Then, we have shown that the mid-point discretized LLG equation exactly fulfills magnetization magnitude conservation regardless of the time step. In addition, in case of constant applied field, the discrete dynamics has itself a Lyapunov structure regardless of the time step, and in the case of conservative dynamics ($\alpha = 0$) the discretized free energy is preserved regardless of the time step and the hamiltonian structure is preserved up to third order in the time step.

The implicit nature of the mid-point time-stepping leads to the solution of a nonlinear system of equations at each time step. Therefore, special and reasonably fast quasi-Newton iterative procedure has been developed to solve this system. Since the solution is approximate depending on the tolerance of the quasi-Newton procedure, the precision in the fulfillment of the LLG dynamics properties has been checked a posteriori. In particular, for finite differences spatial discretization, we have solved the micromagnetic standard problem no. 4. As far as the accuracy tests are concerned, the magnitude has been preserved within machine precision for each cell and the Lyapunov structure is preserved with a relative error in the order of 10^{-8}. Conservative simulations of the same problem show that the free energy is preserved with relative error also in the order of 10^{-8}. As far as computational effort is concerned, the use of quasi-Newton technique which approximates the full jacobian matrix of the nonlinear system of equations as a sparse matrix, allows the use of fast iterative methods (GMRES) for the inversion of the linear systems arising in the single quasi-Newton iteration. The moderately low measured simulation times, together with the fact that the time step can be chosen much larger than explicit methods due to mid-point rule unconditional stability, make this method a good candidate for accurate micromagnetic simulations.

Future work in this framework could be made by developing a finite element code with mid-point rule time-stepping, which would permit to treat magnetic bodies with in principle arbitrary shape. Moreover the computational cost could be lowered by implementing suitable preconditioning for the GMRES method. In addition, the inclusion of the spin-transfer torque term in the code would permit

to investigate non-uniform spin-injection phenomena in multi-layers structures.

Finally, the inclusion of thermal effects in magnetization dynamics model and, consequently in micromagnetic simulations, would be a considerable improvement of the investigation. This direction will be pursued in future activities.

Appendix A

A.1 Main Properties of Ferromagnetic Materials

Some material properties of typical ferromagnetic materials are listed in the table below:

Material	T_c	$\mu_0 M_s$	A	K_1	l_{ex}	$(\gamma M_s)^{-1}$
Unit	[K]	[T]	10^{-11} [J/m]	10^5 [J/m^3]	[nm]	[ps]
Fe	1044	2.16	1.5	0.48	2.8	2.6
Co	1398	1.82	1.5	5	3.4	3.1
Ni	627	0.62	1.5	-0.057	9.9	9.2
Permalloy	720	1.0	1.3	0	5.7	5.7
CrO_2		0.5	0.1	0.22	3.2	11.4
$SmCo_5$	993	1.05	2.4	170	7.4	5.4

T_c is the Curie temperature of the material, M_s is the saturation magnetization, A is the exchange constant, K_1 is the uniaxial magneto-crystalline anisotropy constant, l_{ex} is the exchange length (see Eq. (1.92)) of the material, $(\gamma M_s)^{-1}$ is the value of the normalized time unit for a given material.

Appendix B

B.1 Elliptic Functions

The Jacobi elliptic functions are standard forms of elliptic functions [72]. The three basic functions are denoted by $\mathrm{sn}(u,k), \mathrm{cn}(u,k)$ and $\mathrm{sn}(u,k)$, where k is the modulus such that $0 < k^2 < 1$. They arise from the inversion of the incomplete elliptic integral of the first kind:

$$u = F(\phi, k) = \int_0^{\phi} \frac{d\varphi}{\sqrt{1 - k^2 \sin^2 \varphi}} \quad . \tag{B.1}$$

The inverse function of $F(u,k)$ is given by the Jacobi amplitude $\mathrm{am}(u,k)$

$$\phi = \mathrm{am}(u,k) = F^{-1}(u,k) \quad . \tag{B.2}$$

The Jacobi elliptic functions can be defined as follows:

$$\mathrm{sn}(u,k) = \sin\phi = \sin\left(F^{-1}(u,k)\right) = \sin\left(\mathrm{am}(u,k)\right) \tag{B.3}$$

$$\mathrm{cn}(u,k) = \cos\phi = \cos\left(F^{-1}(u,k)\right) = \cos\left(\mathrm{am}(u,k)\right) \tag{B.4}$$

$$\mathrm{dn}(u,k) = \sqrt{1 - \sin^2\phi} = \sqrt{1 - \sin^2\left(\mathrm{am}(u,k)\right)} \quad . \tag{B.5}$$

By introducing $x = \sin\varphi$ as new integration variable in Eq. (B.1), one obtains the following new expression of the incomplete elliptic integral of the first kind:

$$u = \int_0^{s} \frac{dx}{\sqrt{(1 - k^2x^2)(1 - x^2)}} \quad , \tag{B.6}$$

where $s = \sin\phi$. By taking into account that $u = \mathrm{sn}^{-1}(\sin\phi, k)$ we may also write the last equation as

$$\int_0^{s} \frac{dx}{\sqrt{(1 - k^2x^2)(1 - x^2)}} = \mathrm{sn}^{-1}(s,k) \quad . \tag{B.7}$$

Similar formulas can be written for $\mathrm{cn}(u,k)$ and $\mathrm{dn}(u,k)$. The Jacobi elliptic function are doubly periodic in K and K' in the following sense:

$$\mathrm{sn}(u + 2mK + i2nK', k) = (-1)^m \mathrm{sn}(u,k) \tag{B.8}$$

$$\mathrm{cn}(u + 2mK + i2nK', k) = (-1)^{m+n} \mathrm{cn}(u,k) \tag{B.9}$$

$$\mathrm{dn}(u + 2mK + i2nK', k) = (-1)^n \mathrm{dn}(u,k) \quad , \tag{B.10}$$

where $m, n \in \mathbb{Z}$, $i = \sqrt{-1}$, $K(k)$ is the complete elliptic integral of the first kind:

$$K(k) = F(\pi/2, k) = \int_0^{\pi/2} \frac{d\varphi}{\sqrt{1 - k^2 \sin^2 \varphi}} = \int_0^1 \frac{dx}{\sqrt{(1 - k^2 x^2)(1 - x^2)}} \quad , \tag{B.11}$$

$K'(k) = K(k')$ and $k' = \sqrt{1 - k^2}$ is the complementary modulus. The Jacobi elliptic functions $\mathrm{sn}(u, k), \mathrm{cn}(u, k), \mathrm{dn}(u, k)$ can be seen as doubly periodic generalizations of the trigonometric function satisfying the conditions:

$$\mathrm{sn}(u, 0) = \sin u \tag{B.12}$$

$$\mathrm{cn}(u, 0) = \cos u \tag{B.13}$$

$$\mathrm{dn}(u, 0) = 1 \quad . \tag{B.14}$$

In addition, they are related through the following identities:

$$\mathrm{sn}^2(u, k) + \mathrm{cn}^2(u, k) = 1 \tag{B.15}$$

$$k^2 \mathrm{sn}^2(u, k) + \mathrm{dn}^2(i, k) = 1 \tag{B.16}$$

$$k^2 \mathrm{cn}^2(u, k) + k'^2 = \mathrm{dn}^2(u, k) \tag{B.17}$$

$$\mathrm{cn}^2(u, k) + k'^2 \mathrm{sn}^2(u, k) = \mathrm{dn}^2(u, k) \quad . \tag{B.18}$$

B.2 PERTURBATIVE ANALYSIS OF LIMIT CYCLES IN 2D DYNAMICAL SYSTEMS

Here we present the Poincaré-Melnikov perturbative technique to analyze limit cycles in dynamical systems defined on a 2D manifold Σ. We follow the approach proposed by Perko in Ref. [43].

Let us consider an autonomous dynamical system:

$$\frac{d\mathbf{x}}{dt} = \mathbf{f}_0(\mathbf{x}) \quad , \tag{B.19}$$

with $\mathbf{x} = (x_1, x_2) \in \mathbb{R}^2$ and $\mathbf{f}_0(\mathbf{x})$ analytical in $\mathbb{R}^2$. Let us suppose to perturbe the system in the following way:

$$\frac{d\mathbf{x}}{dt} = \mathbf{f}_0(\mathbf{x}) + \varepsilon \mathbf{f}_1(\mathbf{x}, \varepsilon) \quad , \tag{B.20}$$

where ε is the amplitude of the perturbation and $\mathbf{f}_1(\mathbf{x}, \varepsilon)$ is an analytical function in $\mathbb{R}^2$. We assume now that the unperturbed system (B.19) has a continuous family of periodic trajectories:

$$\Gamma_{\mathbf{x}_0} : \mathbf{x}(t) = \gamma(\mathbf{x}_0, t) \quad . \tag{B.21}$$

These trajectories can be determined by the initial condition $\mathbf{x}_0$ chosen on a Poincaré section S (see Fig. B.1 and Ref. [43]) normal to the family of periodic

trajectories. Conversely, the generic trajectory of the perturbed system (B.20) will be, in general

$$\mathbf{x}(t) = \varphi(t, \mathbf{x}_0, \varepsilon) \quad , \tag{B.22}$$

where we have indicated with $\varphi(t, \mathbf{x}_0, \varepsilon)$ the flow of the dynamical system (B.20) From Eq. (B.22) it follows that:

$$\gamma(t) = \varphi(t, \mathbf{x}_0, \varepsilon = 0) \quad , \tag{B.23}$$

where, for sake of brevity, the dependance on $\mathbf{x}_0$ has been not indicated. The flow (B.22) can be developed in Taylor series with respect to the perturbation parameter ε:

$$\mathbf{x}(t) = \varphi(t, \mathbf{x}_0, 0) + \frac{\partial \varphi}{\partial \varepsilon}(t, \mathbf{x}_0, 0)\varepsilon + \mathcal{O}(\varepsilon^2) \quad . \tag{B.24}$$

By remembering Eq. (B.23) and by setting

$$\frac{\partial \varphi}{\partial \varepsilon}(t, \mathbf{x}_0, 0) = \Delta\mathbf{x} \quad , \tag{B.25}$$

one obtains

$$\mathbf{x}(t) = \varphi(t, \mathbf{x}_0, 0) + \varepsilon\Delta\mathbf{x} + \mathcal{O}(\varepsilon^2) \quad . \tag{B.26}$$

By using the latter equation in the perturbed dynamical system (B.20), we end up with:

$$\frac{d}{dt}\gamma(t) + \varepsilon\frac{d\Delta\mathbf{x}}{dt} = \mathbf{f}_0(\gamma(t) + \varepsilon\Delta\mathbf{x}) + \varepsilon\mathbf{f}_1(\gamma(t) + \varepsilon\Delta\mathbf{x}, \varepsilon) \quad . \tag{B.27}$$

By developing in Taylor series the right-hand side of the latter equation with respect to the variables $\mathbf{x}, \varepsilon$, one has:

$$\begin{aligned}\frac{d}{dt}\gamma(t) + \varepsilon\frac{d\Delta\mathbf{x}}{dt} = \mathbf{f}_0(\gamma(t)) + \frac{\partial \varphi}{\partial \mathbf{x}}(\gamma(t))\varepsilon\Delta\mathbf{x} + \varepsilon\Bigg(\mathbf{f}_1(\gamma(t), 0) + \\ + \frac{\partial \mathbf{f}_1}{\partial \mathbf{x}}(\gamma(t), 0)\varepsilon\Delta\mathbf{x} + \frac{\partial \mathbf{f}_1}{\partial \varepsilon}(\gamma(t), 0)\varepsilon)\Bigg) \quad .\end{aligned} \tag{B.28}$$

By remembering that $\frac{d}{dt}\gamma(t) = \mathbf{f}_0(\gamma(t))$ and by neglecting second order terms, one ends up with the following equation:

$$\frac{d\Delta\mathbf{x}}{dt} = \frac{\partial \varphi}{\partial \mathbf{x}}(\gamma(t))\Delta\mathbf{x} + \mathbf{f}_1(\gamma(t), 0) \quad , \tag{B.29}$$

which we call first variational equation with respect to ε. Equation (B.29) defines a 2D dynamical system which can be used, in principle to study how the perturbation affects the displacement $\Delta\mathbf{x}$ of the perturbed trajectory with respect to the unperturbed orbit in one period. We notice that the dynamical system (B.29) has periodic coefficients and, therefore it is not possible to solve it in exact analytical form. Nevertheless, we observe that we are interested only on

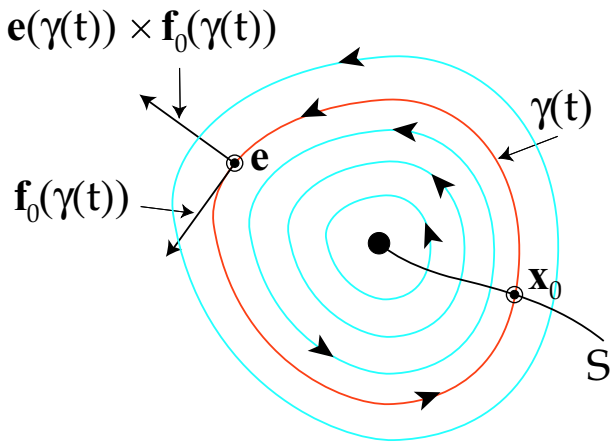

Figure B.1: Planar sketch of a portion of the phase portrait of the unperturbed dynamical system (B.19). S is the Poincaré section normal to the family of continuous trajectories.

the component of $\Delta\mathbf{x}$ normal to the unperturbed trajectory $\gamma(t)$:

$$\Delta x_n = \Delta\mathbf{x} \cdot \mathbf{n} \quad , \tag{B.30}$$

where $\mathbf{n}$ is the unit-vector normal to $\gamma(t)$ and tangential to the manifold Σ. The unit-vector $\mathbf{n}$ is proportional to the following vector:

$$\mathbf{f}_0(\gamma(t)) \times \mathbf{e}(\gamma(t)) \quad , \tag{B.31}$$

where $\mathbf{e}$ is the unit-vector normal to Σ. Therefore, we can express Δx_n as

$$\Delta x_n = \Delta\mathbf{x} \cdot \mathbf{f}_0(\gamma(t)) \times \mathbf{e}(\gamma(t)) = \Delta\mathbf{x} \wedge \mathbf{f}_0(\gamma(t)) \quad , \tag{B.32}$$

where the *wedge product* $\mathbf{v} \wedge \mathbf{w}$, with $\mathbf{v} = (v_1, v_2), \mathbf{w} = (w_1, w_2) \in \mathbb{R}^2$, is defined as

$$\mathbf{v} \wedge \mathbf{w} = v_1 w_2 - v_2 w_1 \quad . \tag{B.33}$$

By differentiating both members of Eq. (B.32) with respect to time, remembering Eq. (B.29), and using straightforward algebra, one ends up with the following one-dimensional differential equation, with periodic coefficients, for Δx_n:

$$\frac{d}{dt}\Delta x_n = \mathbf{f}_1(\gamma(t), 0) \wedge \mathbf{f}_0(\gamma(t)) + \nabla_\Sigma \cdot \mathbf{f}_0(\gamma(t))\Delta x_n \quad , \tag{B.34}$$

where $\nabla_\Sigma \cdot \mathbf{f}_0 = \mathrm{tr}\left[\frac{\partial \mathbf{f}_0}{\partial \mathbf{x}}(\gamma(t))\right]$ is the divergence of the 2D vector field $\mathbf{f}_0(\gamma(t))$. It can be shown [43] that

$$\int_0^{T_{\mathbf{x}_0}} \nabla_\Sigma \cdot \mathbf{f}_0(\gamma(t))\, dt = 0 \quad . \tag{B.35}$$

Equation (B.34) can be analytically integrated over one period of the unperturbed solution $T_{\mathbf{x}_0}$. By taking into account the latter equation, the solution can be written as:

$$\Delta x_n(T_{\mathbf{x}_0}) = \int_0^{T_{\mathbf{x}_0}} \exp\left[-\int_0^t \nabla_\Sigma \cdot \mathbf{f}_0(\gamma(\tau))\, d\tau\right] [\mathbf{f}_1(\gamma(t),0) \wedge \mathbf{f}_0(\gamma(t))]\; dt \quad . \tag{B.36}$$

In addition, if $\mathbf{f}_0(\mathbf{x})$ is a conservative vector field it happens that:

$$\nabla_\Sigma \cdot \mathbf{f}_0 = 0 \quad . \tag{B.37}$$

Thus, Eq. (B.36) reduces to the following simpler form:

$$\Delta x_n(T_{\mathbf{x}_0}) = \int_0^{T_{\mathbf{x}_0}} \mathbf{f}_1(\gamma(t),0) \wedge \mathbf{f}_0(\gamma(t))\, dt \quad . \tag{B.38}$$

Let us suppose now that the generic unperturbed trajectory, determined by the initial condition $\mathbf{x}_0$, can be univocally determined by a scalar parameter g_0 through a correspondence $g_0 = g(\mathbf{x}_0)$. From Eq. (B.36) one can define the Melnikov function $M(g_0)$:

$$M(g_0) = \int_0^{T_{g_0}} \exp\left[-\int_0^t \nabla_\Sigma \cdot \mathbf{f}_0(\gamma(\tau))\, d\tau\right] [\mathbf{f}_1(\gamma(t),0) \wedge \mathbf{f}_0(\gamma(t))]\; dt \quad , \tag{B.39}$$

where $T_{g_0} = T_{g(\mathbf{x}_0)}$. Therefore, to summarize, the Melnikov function, computed on the value g_0, determines the one period displacement of the unperturbed trajectory, determined by g_0, in the direction normal to that unperturbed trajectory. Intuitively, it can be inferred that when $M(g_0) = 0$, the unperturbed trajectory corresponding to g_0 becomes a limit cycle when the perturbation is introduced. This can be rigorously proven (see Ref. [43]) for finite (but small) values of the perturbation parameter ε. Thus, the zeros of the Melnikov function correspond to limit cycles of the perturbed dynamical system (B.20). Moreover, the sign of the derivative of the Melnikov function at the zero determines the stability of the corresponding limit cycle. In particular, positive derivative implies that the limit cycle is stable, whereas negative sign corresponds to an unstable limit cycle. By using this technique, also bifurcations of limit cycles can be studied. In particular, it is possible to find algebraic conditions which corresponds to suitable bifurcation conditions [43]. For instance, the condition for the *Andronov-Hopf bifurcation* is given by:

$$M(g_0) = 0 \quad , \quad \frac{dM}{dg_0} = 0 \quad , \tag{B.40}$$

and the condition for *homoclinic connection bifurcation* is obtained by imposing that the Melnikov function vanishes in correspondence of an unperturbed homoclinic trajectory.

Appendix C

C.1 Brief remarks on the mid-point rule numerical technique

Let us consider the generic ordinary differential equation:

$$\frac{d}{dt}x(t) = f(x(t), t) \quad , \tag{C.1}$$

with $f(x,t) : \mathbb{R}^2 \to \mathbb{R}$. Let us consider the time interval $[t, t+\Delta t]$ where Δt is the time step. The latter equation can be written at the time instant $t + \Delta t/2$:

$$\frac{dx}{dt}\Big|_{t+\Delta t/2} = f(x(t+\Delta t/2), t+\Delta t/2) \quad , \tag{C.2}$$

Let us develop the function $x(t)$ in Taylor series with respect to the initial point t:

$$x(t+\Delta t) = x(t+\Delta t/2) + \frac{dx}{dt}\Big|_{t+\Delta t/2}\frac{\Delta t}{2} + \frac{d^2x}{dt^2}\Big|_{t+\Delta t/2}\frac{\Delta t^2}{4} + \mathcal{O}(\Delta t^3) \quad , \tag{C.3}$$

$$x(t) = x(t+\Delta t/2) - \frac{dx}{dt}\Big|_{t+\Delta t/2}\frac{\Delta t}{2} + \frac{d^2x}{dt^2}\Big|_{t+\Delta t/2}\frac{\Delta t^2}{4} + \mathcal{O}(\Delta t^3) \quad , \tag{C.4}$$

where the symbol $\mathcal{O}(\Delta t^3)$ indicates the terms of the third order and greater in Δt. By subtracting the latter expressions, one obtains:

$$\frac{x(t+\Delta t) - x(t)}{\Delta t} = \frac{dx}{dt}\Big|_{t+\Delta t/2} + \mathcal{O}(\Delta t^2) \quad , \tag{C.5}$$

meaning that the substitution in Eq. (C.2) of the derivative in the mid-point of the interval $[t, t+\Delta t]$ with the left-hand side of Eq. (C.5), leads to a truncation error of the second order with respect to the time step.

By summing Eqs. (C.3)-(C.4) and using simple algebra the following mid-point formula can be derived:

$$x(t+\Delta t/2) = \frac{x(t+\Delta t) + x(t)}{2} + \mathcal{O}(\Delta t^2) \quad . \tag{C.6}$$

In addition, by using Eq. (C.6), it can be shown with the very same line of reasoning that:

$$f\left(x(t+\Delta t/2), t+\frac{\Delta t}{2}\right) = f\left(\frac{x(t+\Delta t)+x(t)}{2}, t+\frac{\Delta t}{2}\right) + \mathcal{O}(\Delta t^2) \quad . \tag{C.7}$$

Therefore, the numerical scheme obtained from Eq. (C.2) with the second-order approximations (C.5) and (C.7)

$$\left.\frac{dx}{dt}\right|_{t+\Delta t/2} = \frac{x(t+\Delta t) - x(t)}{\Delta t} + \mathcal{O}(\Delta t^2) \tag{C.8}$$

$$\frac{x(t+\Delta t) + x(t)}{2} = x(t + \Delta t/2) + \mathcal{O}(\Delta t^2) \tag{C.9}$$

with the position $t_n = t_0 + n\Delta t$ and $x_n = x(t_n)$, can be written in the following way:

$$\frac{x_{n+1} - x_n}{\Delta t} = f\left(\frac{x_{n+1} + x_n}{2}, t_n + \frac{\Delta t}{2}\right) \quad . \tag{C.10}$$

This scheme is commonly refereed to as *mid-point rule* numerical technique and is second-order accurate with respect to the time step Δt.

Now we want to investigate the stability property of the mid-point rule scheme (C.10). We refer, for sake of simplicity, to the scalar initial value problem:

$$\frac{dx}{dt} = \lambda x \quad , \quad x(t_0) = x_0 \quad , \quad \lambda \in \mathbb{C} : \mathrm{Re}[\lambda] < 0 \quad . \tag{C.11}$$

The latter equation can be discretized according to the mid-point rule:

$$x_{n+1} - x_n = \frac{\lambda \Delta t}{2}(x_{n+1} + x_n) \quad . \tag{C.12}$$

With some straightforward algebra, one can obtain the following time-stepping algorithm:

$$x_{n+1} = \frac{1 - \frac{\lambda \Delta t}{2}}{1 + \frac{\lambda \Delta t}{2}} x_n \quad . \tag{C.13}$$

Now, if we study the evolution of two solutions of Eq. (C.11), one starting from the initial condition x_0 and the other starting from $y_0 = x_0 + e_0$, the evolution of the perturbation $e_n = y_n - x_n$ can be found with the same time-stepping as Eq. (C.13):

$$e_{n+1} = \frac{1 - \frac{\lambda \Delta t}{2}}{1 + \frac{\lambda \Delta t}{2}} e_n \quad , \tag{C.14}$$

which can be rewritten with respect to the initial perturbation e_0:

$$e_n = \left[\frac{1 - \frac{\lambda \Delta t}{2}}{1 + \frac{\lambda \Delta t}{2}}\right]^n e_0 \quad . \tag{C.15}$$

In particular, the modulus of the perturbation evolves according to the following equation:

$$|e_n| = \left|\frac{1 - \frac{\lambda \Delta t}{2}}{1 + \frac{\lambda \Delta t}{2}}\right|^n |e_0| \quad . \tag{C.16}$$

It turns out that, in order that the error vanishes for $n \to \infty$, the following constraint is required:

$$\left|\frac{1 - \frac{z}{2}}{1 + \frac{z}{2}}\right| < 1 \quad . \tag{C.17}$$

where the complex variable $z = \lambda \Delta t$ has been defined. It can be shown that the complex function

$$g(z) = \frac{1 - \frac{z}{2}}{1 + \frac{z}{2}} \tag{C.18}$$

fulfills the constraint (C.17) $\forall z \in \mathbb{C} : \mathrm{Re}[z] < 0$. Therefore, the mid-point rule numerical scheme is stable for any $\lambda \in \mathbb{C} : \mathrm{Re}[\lambda] < 0$ and for any time step Δt, namely is unconditionally stable. In particular, this property is referred in literature [95] to as *A-stability* of the mid-point rule numerical method.

Bibliography

[1] IBM Research website,
http://www.research.ibm.com/research/gmr/basics.html

[2] T. Yamashita, *Magnetic Recording Disk Technology: Practical Challenges in Delivering the Areal Density Performance*, abstract submitted to the Eighth International Symposium on Magnetic, Materials, Processes, and Devices, october 2004.

[3] L.D. Landau, E.M. Lifshitz, *Theory of the dispersion of magnetic permeability in ferromagnetic bodies*. Phys. Z. Sowietunion **8**, 153 (1935)

[4] W.F. Brown Jr, *Micromagnetics*, Interscience Publishers (1963).

[5] A. Aharoni, Introduction to the Theory of Ferromagnetism, Oxford University Press (2001).

[6] H.B. Callen, *Thermodynamics and an Introduction to Thermostatistics*, 2nd edition, Wiley, (1985).

[7] E. Fermi, *Termodinamica*, Boringhieri, Torino (1958).

[8] P. Weiss, *L'Hypothese du champ Moleculaire et de la Propriete Ferromagnetique*, J. de Phys. **6**, (1907) pp. 661-690.

[9] C. Kittel, *Theory of the Structure of Ferromagnetic Domains in Films and Small Particles*, Phys. Rev. 70 (1946), pp 965-971.

[10] W. Heisenberg, Z. Physik 69 (1931), pp. 287-297.

[11] L.D. Landau, E.M. Lifshitz, *Electrodynamics of continuous media*, MIR, Moskow (1986).

[12] W.F. Brown Jr, *Magnetostatic Principles in Ferromagnetism*, North-Holland Publishing Company (1962).

[13] J.D. Jackson, *Classical Electrodynamics*, Wiley (1962).

[14] S. Bobbio, *Electrodynamics of Materials*, Academic Press, San Diego (1999).

[15] F. Barozzi, F. Gasparini, *Fondamenti di Elettrotecnica: Elettromagnetismo*, UTET Torino (1989).

[16] G. Bertotti, *Tutorial Session Notes: Micromagnetics and Nonlinear Magnetization Dynamics*, 10th Biennal Conference on Electromagnetic Fields Computation, Perugia (2002).

[17] A. Arrott, *Plenary Lecture: Progress in Micromagnetics*, Moscow International Symposium on Magnetism, Moscow (2002).

[18] T.L. Gilbert, Physical Review, **100** (1955), p. 1243.

[19] W.F. Brown Jr, *Magnetoelastic interactions*, Springer-Verlag (1966).

[20] G. Bertotti, *Hysteresis in magnetism*, Academic Press, San Diego (1998).

[21] W.F. Brown Jr, *Thermal fluctuations of a single-domain particle*, Physical Review, **130**, p. 16771686 (1963).

[22] S. Wiggins, *Introduction to Applied Nonlinear Dynamical Systems and Chaos*, Springer-Verlag, New York (1990).

[23] J. H. Hubbard and B. H. West, *Differential Equations: A Dynamical System Approach. Part II*, Springer-Verlag, New York (1995).

[24] L. F. Àlvarez, O. Pla, and O. Chubykalo, Phys. Rev. B **61**, p. 613 (2000)

[25] C. Serpico, I.D. Mayergoyz, G. Bertotti, *Numerical technique for integration of the LandauLifshitz equation*, Journal of Applied Physics, **89**, p. 6991 (2001).

[26] J.C. Mallinson, *Damped gyromagnetic switching*, IEEE Transactions on Magnetics, **36**, p. 1976 (2000).

[27] G. Bertotti, I.D. Mayergoyz, C. Serpico, M. Dimian, *Comparison of analytical solutions of Landau-Lifshitz equation for "damping" and "precessional" switchings*, Journal of Applied Physics, **93**, p. 6811 (2003).

[28] G. Bertotti, I.D. Mayergoyz, C. Serpico, *Critical fields and pulse durations for precessional switching of thin magnetic films*, IEEE Transactions on Magnetics, **39**, p. 2504 (2003).

[29] J.C. Mallinson, *On damped gyromagnetic precession*, IEEE Transactions on Magnetics, **23**, p. 2003 (1987).

[30] R. Kikuchi, *On the Minimum of Magnetization Reversal Time*, Journal of Applied Physics, **27**, 1352 (1956).

[31] R.F.M. Thornley, *Pulse response of recording media*, IEEE Tansactions on Magnetics, **11**, p. 1197 (1975).

[32] W.D. Doyle and L. He, Flanders P. J, *Measurement of the switching speed limit in high coercivity magnetic media*, IEEE Transactions on Magnetics, **29**, p. 3634 (1993).

[33] N.D. Rizzo, T.J. Silva and A.B. Kos, IEEE Transactions on Magnetics, *Nanosecond magnetization reversal in high coercivity thin films*, **36**, p. 159 (2000).

[34] M. Bauer, J. Fassbender, B. Hillebrands, R.L Stamps, *Switching behavior of a Stoner particle beyond the relaxation time limit*, Physical Review B, **61**, p. 3410 (2000).

[35] G. Bertotti, I.D. Mayergoyz, C. Serpico, and M. dAquino, *Geometrical Analysis of Precessional Switching and Relaxation in Uniformly Magnetized Bodies*, IEEE Transaction on Magnetics, **39**, p. 2501 (2003).

[36] D.G. Porter, *Analytical Determination of the LLG Zero-Damping Critical Switching Field*, IEEE Transactions Magnetics, **34**, p. 1663 (1998).

[37] S. Kaka, S.E. Russek, *Precessional switching of submicrometer spin valves*, Applied Physics Letters, **80**, p. 2958 (2002).

[38] J.H.E. Griffiths, *Anomalous high frequency resistance of ferromagnetic metals*, Nature **158**, p. 670 (1946).

[39] C. Kittel, *On the theory of ferromagnetic resonance absorption*, Pysical Review, **73** (1948).

[40] G. Bertotti, C. Serpico, I.D. Mayergoyz, *Nonlinear Magnetization Dynamics under Circularly Polarized Field*, Physical Review Letters, **86**, p. 724 (2001).

[41] C.Serpico, M. d'Aquino, G. Bertotti, I.D. Mayergoyz, *Analysis of quasiperiodic LandauLifshitzGilbert dynamics*, Journal of Magnetism and Magnetic Materials, **272-276**, p. 734 (2004).

[42] C. Serpico, I.D. Mayergoyz, G. Bertotti, *Analytical solutions of Landau-Lifshitz equation for precessional switching*,Journal of Applied Physics, **93**, p. 6909 (2003).

[43] L.Perko, *Differential Equations and Dynamical Systems*, Springer, 1996.

[44] J.C. Slonczewski, *Current-driven excitation of magnetic multilayers*, Journal of Magnetism and Magnetic Materials, **159** (1996), L1-L7.

[45] J.Z. Sun, *Current-driven magnetic switching in manganite trilayer junctions*, Journal of Magnetism and Magnetic Materials, **202** p. 157 (1999).

[46] S.I. Kiselev, J.C. Sankey, I.N. Krivorotov, N.C. Emley, R.J. Schoelkopf, R.A. Buhrman, D. C. Ralph, *Microwave oscillations of a nanomagnet driven by a spin-polarized current*, Letters to Nature **425**, p. 380 (2003).

[47] C. Serpico, private communication.

[48] J. Grollier, V. Cros, H. Jaffrés, A. Hamzic, J.M. George, G. Faini, J. Ben Youssef, H. Le Gall, A. Fert, *Field dependence of magnetization reversal by spin transfer*, Physical Review B, **67**, p. 174402 (2003).

[49] G. Bertotti, C. Serpico, I.D. Mayergoyz, A. Magni, M. dAquino, R. Bonin, *Magnetization Switching and Microwave Oscillations in Nanomagnets Driven by Spin-Polarized Currents*, submitted to Physcal Review Letters.

[50] G. Bertotti, I.D. Mayergoyz, C. Serpico, *Analytical solutions of LandauLifshitz equation for precessional dynamics*, Physica B, **343**, p. 325 (2004).

[51] A. Aharoni, *Micromagnetics: past, present and future*, Physica B, **309**, p. 1 (2001).

[52] J. Fidler and T. Schrefl, *Micromagnetic modellingThe current state of the art*, Journal of Physics D: Applied Physics, **33**, R135 (2000).

[53] R.D. McMichael, M.J. Donahue, and D.G. Porter, *Comparison of magnetostatic field calculation methods on two-dimensional square grids as applied to a micromagnetic standard problem*, Journal of Applied Physics, **85**, p. 5816 (1999).

[54] Q. Chen and A. Conrad, *A review of finite element open boundary techniques for static and quasi-static electromagnetic field problems*, IEEE Transactions on Magnetics **33**, p. 663 (1997).

[55] B. Yang and D.R. Fredkin, *Dynamical micromagnetics by finite element method*, IEEE Transactions on Magnetics, **43**, p. 3842 (1998).

[56] A. Khebir, A.B. Kouki and R. Mittra, *Asymptotic boundary for finite element analysis of three-dimensional transmission line discontinuities*, IEEE Transactions on Microwave Theory Techniques, **38**, p. 1427 (1990).

[57] X. Brunotte, G. Meunier and J.F. Imhoff, *Finite element modelling of unbounded problems using transformations: rigorous, powerful and easy solutions*, IEEE Transactions on Magnetics, **28**, p. 1663 (1992).

[58] T. Schrefl and J. Fidler, *Modelling of exchange spring permanent magnets*, Journal of Magnetism and Magnetic Materials **177**, p. 970 (1998).

[59] R. Fischer and H. Kronmueller, *Importance of ideal grain boundaries of high remanent composite permanent magnets*, Journal of Applied Physics, **83**, p. 3271 (1998).

[60] J. W. Cooley and J. W. Tukey, *An algorithm for the machine computation of the complex Fourier series*, Mathematics of Computation, **19**, p. 297 (1965).

[61] J.G. Zhu, N.H. Bertram, *Micromagnetic studies of thin metallic films*, Journal of Applied Physics, **63**, p. 3248 (1988).

[62] H.N. Bertram, *Monte-Carlo calculation of magnetic anhysteresis*, Journal de Physique, **32**, p. 684 (1971).

[63] J.J. Miles, B.K. Middleton, *A hierarchical micromagnetic model of longitudinal thin-film recording media*, Journal of Magnetism and Magnetic Materials, **95**, p. 99 (1991).

[64] D.V. Berkov, K. Ramstck, A. Hubert, Solving Micromagnetic Problems, Physica Status Solidi A, **137**, p. 207 (1993).

[65] S.W. Yuan, H.N. Bertram, *Fast adaptive algorithms for Micromagnetics*, IEEE Transaction on Magnetics, **28**, p. 2031 (1992).

[66] O.D. Kellogg, *Foundations of potential theory*, Dover, New York (1953).

[67] D.A. Lindholm, *Three-dimensional magnetostatic fields from point-matched integral equations with linearly varying scalar sources*, IEEE Transaction on Magnetics, **20**, p. 2025 (1984).

[68] H.W. Schumacher, C. Chappert, R.C. Sousa, P.P. Freitas, J. Miltat, *Quasi ballistic magnetization reversal*, Physical Review Letters, **90**, p. 17204 (2003).

[69] P.N. Brown, A.C. Hindmarsh, *Reduced Storage Matrix Methods in Stiff ODE Systems*, Journal of Applied Mathematics and Computation, **31**, p. 40 (1989).

[70] D.R. Friedkin, T.R. Koehler, *Hybrid Method for Computing Magnetostatic Fields*, IEEE Transactions on Magnetics, **26**, p. 415 (1990).

[71] D. C. Cronemeyer, *Demagnetizing factors for general ellipsoids*, Journal of Applied Physics, **70**, p. 7660 (1991).

[72] H. Hancock, *Elliptic integrals*, Wiley, New York (1917).

[73] W. Scholz, MAGPAR parallel micromagnetic code, Vienna University of Technology, website http://magnet.atp.tuwien.ac.at/scholz/magpar.

[74] C.H. Hee, Y.Y. Zou, and J.P. Wang, *Tilted media by micromagnetic simulation: A possibility for the extension of longitudinal magnetic recording?* Journal of Applied Physics, **91**, p. 8004 (2002).

[75] L. He, W.D. Doyle, H. Fujiwara, *High speed coherent switching below the Stoner-Wohlfarth limit*, IEEE Transactions on Magnetics, **30**, p. 4086 (1994).

[76] D. Suess, T. Schrefl, W. Scholz, J. Fidler, *Fast switching of small magnetic particles*, Journal of Magnetism and Magnetic Materials, **242**, p. 426 (2002).

[77] E.C. Stoner, E.P. Wohlfarth, *A mechanism of magnetic hysteresis in heterogeneous alloys*, Philos. Trans. R. Soc. London Ser., A240 (1949).

[78] D. Suess, V. Tsiantos, T. Schrefl, J. Fidler, W. Scholz, H. Forster, R. Dittrich, and J.J. Miles, *Time resolved micromagnetics using a preconditioned finite element method*, Journal of Magnetism and Magnetic Materials, **248**, p. 298 (2002).

[79] μ-mag group website, http://www.ctcms.nist.gov/~rdm/mumag.org.html

[80] W. Scholz, *Scalable Parallel Micromagnetic Solvers for Magnetic Nanostructures*, PhD Thesis (2003), http://magnet.atp.tuwien.ac.at/scholz/

[81] X. Wang, C.J. García-Cervera, Weinan E, *A GaussSeidel Projection Method for Micromagnetics Simulations*, Journal of Computational Physics **171**, p. 357 (2001).

[82] P. Podio-Guidugli, *On dissipation mechanisms in micromagnetics*, The European Physical Journal B, **19**, p. 417 (2001).

[83] M.A. Austin, P.S. Krishnaprasad, *Almost Poisson Integration of Rigid Body Systems*, Journal of Computational Physics, **107**, p. 105 (1993).

[84] A. W. Spargo, P. H. W. Ridley, G. W. Roberts, *Geometric integration of the Gilbert equation*, Journal of Applied Physics, **93**, p. 6805 (2003).

[85] P.S. Krishnaprasad, X. Tan, *Cayley transforms in micromagnetics*, Physica B, **306**, p.195 (2001).

[86] D. Lewis, N. Nigam, *Geometric integration on spheres and some interesting applications*, Journal of Computational and Applied Mathematics, **151**, p. 141 (2003).

[87] C.J. Budd, M.D. Piggott, *Geometric integration and its applications*, http://www.maths.bath.ac.uk/~cjb/ (2001).

[88] J.E. Marsden, T.S. Ratiu, *Introduction to Mechanics and Symmetry*, Springer Verlag, New York, 1999.

[89] P.J. Channell and J.C. Scovel, *Integrators for Lie-Poisson dynamical systems*, Physica D **50**, p. 80 (1991).

[90] S.W. Yuan, H. Neal, Bertram, *Fast Adaptive Algorithms for Micromagnetics*, IEEE Transactions on Magnetics, **28**, p. 2031 (1992).

[91] Y. Saad and M.H. Schultz, *GMRES: A Generalized Minimal Residual Algorithm for Solving Nonsymmetric Linear Systems*, SIAM Journal of Scientific and Statistical Computation, **7**, p. 856 (1986).

[92] J.M. Ortega, W. C. Rheinboldt, *Iterative solution of nonlinear equations in several variables*, SIAM Philadelphia (2000).

[93] M. E. Schabes and A. Aharoni, *Magnetostatic Interaction Fields for a Three-Dimensional Array of Ferromagnetic Cubes*, IEEE Transaction On Magnetics, **23**, p. 3882 (1987).

[94] G. Albuquerque, J. Miltat, A. Thiaville, *Self-consistency based control scheme for magnetization dynamics* Journal of Applied Physics, **89**, p. 6719 (2001).

[95] V. Comincioli, *Analisi numerica*, McGraw-Hill, Milano (1995).